

Modern computational approaches for quantifying inter- and intramolecular interactions

THÈSE N° 5988 (2013)

PRÉSENTÉE LE 6 DÉCEMBRE 2013

À LA FACULTÉ DES SCIENCES DE BASE

LABORATOIRE DE DESIGN MOLÉCULAIRE COMPUTATIONNEL

PROGRAMME DOCTORAL EN CHIMIE ET GÉNIE CHIMIQUE

ÉCOLE POLYTECHNIQUE FÉDÉRALE DE LAUSANNE

POUR L'OBTENTION DU GRADE DE DOCTEUR ÈS SCIENCES

PAR

Jérôme Florian GONTHIER

acceptée sur proposition du jury:

Prof. B. Fierz, président du jury
Prof. A.-C. Corminboeuf, directrice de thèse
Prof. A. Genoni, rapporteur
Prof. K. Patkowski, rapporteur
Dr F. Rotzinger, rapporteur



ÉCOLE POLYTECHNIQUE
FÉDÉRALE DE LAUSANNE

Suisse
2013

Lourd est le parpaing de la réalité
sur la tartelette aux fraises de nos illusions
— Boulet

Pourquoi, pourquoi j'ai pris la pilule bleue ?
— Matrix

À mes grands-parents

Acknowledgements

First of all, I would like to thank my advisor, Clémence Corminboeuf, for giving me the freedom to carry a difficult and risky project in her group. Her great optimism on the projects we conducted together was always encouraging, and her high-quality english writing inspires me to improve my own. I thank her for carefully proof-reading the present thesis and providing corrections promptly. I am grateful to her husband Matt for his clear grammar and english vocabulary corrections. Being the last representative of the first generation of Ph.D. students in the lab, I had numerous labmates. Thank you Fabrice for getting me started in the lab, for your constant jokes, your happiness and your taste for good food ! Sorry for all the others, but the lab has been a little less funny since you left ! Daniel, I thank you as well for getting me started in this lab and for your help in dominating computers from these early times until now, dear sysadmin ! Stephan, thank you for the numerous discussions we had. Your critical mind, your anticipation of difficulties arising in scientific projects and your rigor should inspire all Ph.D. students ! Having to fight against your constant pessimism helped me construct a critical look on my own work, and it was a pleasure to travel with you to conferences. In the next generation of Ph.D. students, I thank Riccardo for his jokes and his great observation skills, and for making me phone to real estate agencies for him... Thank you also to Shanshan, I wish you plenty of success in the UK ! Antonio and Laurent, I wish you both a successful Ph.D. I thank the post-docs as well, first Tanya for her constant smile, for making us laugh in the lab and for her ability to make a story out of almost nothing. Laetitia, I appreciated all our conversations, you were always there to cheer me up in difficult times. Eric, thanks for your pink short and your amazing shirts, and for your sense of freely interpreting reality for the sake of humour. Peter and Hongguang, I wish you all the best for the future !

I am very grateful to my jury members, Konrad Patkowski who traveled from the United States to evaluate my work and provided detailed corrections, Alessandro Genoni who came from Nancy and François Rotzinger from the EPFL. Thank you all for the useful corrections you provided, you helped make this thesis better.

Durant ces quatre années, j'ai aussi bénéficié de beaucoup de soutien depuis l'extérieur du laboratoire. Basile et Julie, je vous remercie beaucoup pour vos nombreuses invitations à piller vos victuailles et à regarder un film le dimanche soir ! Ces distractions étaient les bienvenues lorsque les ordinateurs persistaient à s'opposer à ma thèse. J'ai aussi passé de très bons moments avec Pascal et Sibyl, par exemple en Ecosse à manger du hareng fumé et du haggis au petit déjeuner... Marine, merci pour le sirop de framboises ! Jérémy, John, François et Ksénia, nos séjours au "chalet" m'ont fait beaucoup de bien malgré le temps souvent détestable, surtout

Acknowledgements

la tartiflette au petit déjeuner et dans les sandwiches à la mousse de canard. Jérémy, merci aussi pour tout le temps que tu passes à trouver des concerts toute l'année, ça m'a permis de découvrir énormément de choses !

Jeanne, je te remercie pour tous les moments que nous avons partagés, notamment lors de nos voyages. Et merci aussi pour le sirop de framboises ! Très très bon ! Je te souhaite beaucoup de réussite dans tes projets.

Je remercie également ici le club de vo-vietnam de Morges, notamment Patrick, Alban et Tristan, pour tout ce qu'ils m'ont apporté non seulement à travers le Son Long Quyen Thuat, qui a pris une grande importance dans ma vie, mais aussi à travers l'organisation de la vie de ce club. Merci aussi à Annie pour les nombreuses soirées jeux, pour m'avoir fait découvrir de super séries et pour ton soutien lors de mon passage d'élève-professeur !

Finalement, je remercie mes parents pour m'avoir soutenu et m'avoir permis d'entreprendre mes études de chimie dans les meilleures conditions. Grâce à vous, j'ai la chance d'être payé pour faire quelque chose qui me passionne.

The EPFL and the Swiss NSF Grant 200021_121577/1 EPFL are of course acknowledged for financial support.

Abstract

This thesis introduces modern computational approaches for quantifying and analyzing both intra- and intermolecular interactions. An original formalism to quantify intramolecular interactions *ab initio* is first introduced. Inspired from intermolecular Symmetry-Adapted Perturbation Theory (SAPT), we derive a zeroth-order wavefunction, $\Psi^{(0)}$, suitable for development of an intramolecular variant of SAPT. $\Psi^{(0)}$ is constructed based upon the Chemical Hamiltonian concept and uses strictly localized orbitals to suppress the interactions between two intramolecular fragments. As a result, the total zeroth-order energy corresponds to a relaxed wavefunction that excludes interactions between relevant intramolecular fragments. Numerical tests on propane and halogenated derivatives yield both reasonable energy convergence and intuitive chemical trends. Moreover, the proposed scheme provides a promising description of intramolecular hydrogen bonds and energy profiles. Thus, $\Psi^{(0)}$ delivers the relevant information necessary to the prospected derivation of intramolecular SAPT.

Besides our quest for a rigorous *ab initio* intramolecular energy scheme, we also propose a simpler method based on bond separation reactions to assess (de)stabilizing interactions associated with various 1,3-nonbonded substituent patterns within highly branched alkanes. While *n*- and singly methylated alkanes show positive bond separation energies (BSE) (*i.e.*, stabilization), which increase systematically along the series, permethylated alkanes are characterized by decreasing BSEs (*i.e.*, destabilizing interactions). Our quantitative analysis shows that singly methylated alkanes are more stabilized than linear alkane chains and that the unique destabilizing feature of permethylated alkanes arises from the close proximity of bulky methyl groups causing highly distorted geometries along the carbon backbone.

The enhancement of intermolecular interactions constitutes yet another objective of this thesis. We demonstrate that π -depleted polyaromatic molecules present superior π -stacking ability. This somewhat counterintuitive realization is quantified using a novel computational criterion, LOLIPOP, that identifies π -conjugated frameworks presenting the desired electronic features. The screening of molecular targets benefits greatly from such a rational design criteria, which can detect the most promising candidates. The utility of the LOLIPOP criterion is thus demonstrated by identifying chemosensors presenting enhanced π -stacking ability. In particular, we have designed tailored chemosensors, which display remarkable sensitivity and selectivity towards caffeine relying upon the formation of π - π stacked complexes. Finally, the importance of weak intermolecular interactions was also shown to be essential when considering an assembly of four tetrathiafulvalene (TTF) molecules as a potential metal-free molecular catalyst for the four-electron reduction of O_2 to H_2O . Based on experimental evidence, we demonstrated that

Acknowledgements

the formation of a non-covalently bond helical tetramer $[\text{TTF}_4\text{H}_2]^{2+}$ is able to deliver the needed four electrons and protons to convert O_2 into water.

Keywords: symmetry-adapted perturbation theory, intramolecular interactions, strictly localized orbitals, chemical hamiltonian, intermolecular interactions, zeroth-order wavefunction, bond separation energies, hydrocarbon, LOLIPOP, fluorescent sensors, π -stacking, π -depletion, four-electron reduction, tetrathiafulvalene

Résumé

Cette thèse introduit des approches computationnelles modernes pour la quantification et l'analyse des interactions intra- et intermoléculaires. Un formalisme original pour la quantification *ab initio* des interactions intramoléculaires est présenté pour la première fois. Inspirés par la théorie des perturbations intermoléculaire adaptée à la symétrie (Symmetry-Adapted Perturbation Theory, SAPT), nous dérivons une fonction d'onde d'ordre zéro, $\Psi^{(0)}$, convenable pour le développement futur d'une version intramoléculaire de la SAPT. $\Psi^{(0)}$ est construite en se basant sur les concepts de l'Hamiltonien Chimique (Chemical Hamiltonian, CHA) et fait usage d'orbitales strictement localisées pour supprimer les interactions entre deux fragments intramoléculaires. De ce fait, l'énergie totale d'ordre zéro correspond à une fonction d'onde optimisée excluant toute interaction entre les fragments intramoléculaires en question. Des tests numériques sur le propane et ses dérivés halogénés démontrent à la fois une convergence de l'énergie raisonnable et des tendances chimiques intuitives. De plus, le schéma proposé offre une description prometteuse des liaisons hydrogènes intramoléculaires et des profils d'énergie. Ainsi, $\Psi^{(0)}$ fournit des informations pertinentes, condition nécessaire à la dérivation recherchée de la SAPT intramoléculaire.

En parallèle à notre quête pour une méthode *ab initio* rigoureuse d'énergie intramoléculaire, nous proposons également un schéma plus simple basé sur les réactions de séparation de liaisons pour évaluer les interactions (dé)stabilisantes associées avec divers substituants non-liés en position 1,3 au sein d'alcanes hautement ramifiés. Tandis que les alcanes linéaires et à méthylation simple donnent des énergies de séparation de liaisons (bond separation energies, BSE) positives (*i.e.*, stabilisantes) qui croissent systématiquement le long de la série, les alcanes perméthylés sont caractérisés par des BSE décroissantes (*i.e.*, des interactions déstabilisantes). Notre analyse quantitative démontre que les alcanes à simple méthylation sont plus stabilisés que les alcanes linéaires et que la déstabilisation particulière aux alcanes perméthylés provient de la grande proximité de groupes méthyles encombrés, causant par là même d'importantes distortions le long du squelette carboné.

Le renforcement des interactions intermoléculaires constitue encore un autre objectif de cette thèse. Nous démontrons que les molécules polyaromatiques π -appauvries présentent des capacités supérieures d'empilement π . Cette prise de conscience quelque peu contre-intuitive est quantifiée au moyen d'un nouveau critère computationnel, LOLIPOP, qui identifie les structures π -conjuguées présentant les particularités électroniques désirées. Le filtrage de cibles moléculaires bénéficie grandement d'un tel critère de conception qui peut détecter les candidats les plus prometteurs. L'utilité du critère LOLIPOP est ainsi démontrée par l'identification de

Acknowledgements

enseurs chimiques présentant des capacités supérieures d'empilement π . En particulier, nous avons conçu des senseurs chimiques sur mesure qui démontrent une sensibilité et une sélectivité remarquables pour la caféine grâce à la formation de complexes empilés π - π . Finalement, l'importance des interactions intermoléculaires faibles est démontrée dans la considération d'un assemblage de quatre molécules de tétrathiafulvalène (TTF) en tant que catalyseur potentiel sans métal pour la réduction à quatre électrons de O_2 en H_2O . En nous basant sur des preuves expérimentales, nous avons démontré que la formation sans liaisons covalentes du tétramère hélicoïdal $[TTF_4H_2]^{2+}$ est capable de fournir les quatre électrons et les protons nécessaires à la conversion de O_2 en eau.

Mots-clefs : théorie des perturbations adaptée à la symétrie, interactions intramoléculaires, orbitales strictement localisées, Hamiltonien chimique, interactions intermoléculaires, fonction d'onde d'ordre zéro, énergies de séparation de liaisons, hydrocarbures, LOLIPOP, senseurs fluorescents, empilement π , π -appauvrissement, réduction à quatre électrons, tétrathiafulvalène

Contents

Acknowledgements	v
Abstract	vii
Résumé	ix
1 Introduction	1
2 Theoretical methods	7
2.1 Symmetry-Adapted Perturbation Theory	7
2.1.1 Polarization theory	8
2.1.2 Symmetry-Adapted Perturbation Theory	10
2.2 The Chemical Hamiltonian	12
2.2.1 Application to the BSSE problem	13
2.2.2 Energy partitioning schemes	15
2.3 Strict orbital localization	18
2.3.1 Fundamental equations	18
2.3.2 Applications of SLOs	20
3 Exploration of Zeroth-Order Wavefunctions and Energies for Intramolecular Symmetry-Adapted Perturbation Theory	23
3.1 Introduction	23
3.2 Zeroth-order wavefunction from non-hermitian operators	26
3.2.1 Chemical Hamiltonian partitioning	26
3.2.2 Electron localization	29
3.2.3 Relevance of the non-hermitian formalism	30
3.3 Results and discussion	32
3.3.1 Basis set dependence	33
3.3.2 Chemical trends	34
3.3.3 Geometry dependence	37
3.4 Conclusion	38

4	Branched Alkanes Have Contrasting Stabilities	41
4.1	Introduction	41
4.2	Computational details	42
4.3	Determination of Heats of Formation of Branched Alkanes	43
4.4	Quantifying Nonbonded Group Interactions in Branched Alkanes	44
4.5	Conclusion	47
5	π-Depletion as a Criterion to predict π-stacking Ability	49
5.1	Introduction	49
5.2	Computational details and methods	50
5.3	The LOLIPOP index	51
5.4	The interplay between LOLIPOP and π -stacking energies	53
5.5	Caffeine sensors	56
5.6	Conclusion	59
6	Four-Electron Oxygen Reduction by Tetrathiafulvalene	61
6.1	Introduction	61
6.2	Computational details	61
6.3	Summary of experimental results	62
6.4	Computational mechanistic investigation	64
6.4.1	Conformational study	64
6.4.2	Reaction barriers	65
6.5	Conclusion	68
7	General Conclusions and Outlook	69
A	Supplementary Tables and Figures	73
A.1	Branched Alkanes Have Contrasting Stabilities	73
A.2	π -Depletion as a Criterion to predict π -stacking Ability	76
A.3	Four-Electron Oxygen Reduction by Tetrathiafulvalene	77
	Bibliography	94
	Glossary	95
	Curriculum Vitae	98

1 Introduction

According to Moore's law,¹ originally published in 1965, the number of transistors on integrated circuits doubles approximately every two years. Although merely an empirical observation, 50 years later this law still holds true, meaning there are now approximately 2^{25} times more transistors on integrated circuits than in 1965, and a similar increase in computational power. This exponential increase was accompanied by increased importance of computers in all aspects of our lives, both personal and professional. Likewise, computers continue to gain importance in science, permitting previously impossible computations to now be accomplished in minutes. In the field of chemistry, the theoretical foundation of computations is the Schrödinger equation (SE), first published in 1926.² The SE describes the electrons within a molecule through a wavefunction, linked to the probability of finding an electron in some region of space. This first paper succeeds in reproducing the measured energy levels of the hydrogen atom, which was the first hint that the Schrödinger equation had the power to reproduce and predict experimental outcomes. Although the SE does not include relativistic effects originally, it can only be solved analytically for the simplest systems. Thus, approximate methods were devised to obtain useful information from the SE in an efficient way.

Prior to the availability of computers, when only pen and paper could be used, simple Molecular Orbital theories such as Hückel theory³⁻⁶ were powerful models to rationalize chemical trends for aromatic and conjugated molecules. As the first computers appeared, better models could be applied to small molecules. The Hartree-Fock method⁷⁻¹¹ was the first non-empirical approximate solution to the SE, and its solution for small polyatomic molecules was only possible¹²⁻¹⁴ on the best available machines in the 1960s.

As computers evolved, so did programming languages. From the original machine language directly using binary codes, programmers went to Assembly where all elementary operations had to be specified, and then to the more evolved FORTRAN language, allowing to code efficiently more and more complex and accurate approximations to the solution of the SE. Electron correlation was approximately included by perturbation theory¹⁵ and configuration interaction methods.^{16,17}

Later, coupled-cluster methods were imported from physics¹⁸⁻²² and allowed excellent accuracies to be reached for comparison with experiment. Relativistic corrections were added to the SE, which attained impressive accuracy for small systems, even revealing experimental errors.²³

In parallel, density functional theory (DFT) was developed and used essentially for solid state physics. Density functional theory departs from the traditional approach based on the SE, in that the wavefunction is not formally needed. All properties of the system, in principle, can be described from the electronic density,²⁴ a much simpler quantity. The functional connecting the electronic density to the energy is not known and today's computations rely on approximate functionals. The power of density functional theory was realized only recently in chemistry, as efficient and accurate approximations for molecular computations were developed.²⁵

Though extremely powerful and applicable now to quite large molecules, the methods used in computational chemistry nowadays rely on complex quantities, either the electronic density or the massively multidimensional wavefunction. As a result, chemical insight is often lost in the complexity of the method and results are sometimes less easy to rationalize than if using the very simple Hückel theory. The fundamental comprehension of phenomena governing the intermolecular and intramolecular interactions is of utmost importance to experimental and theoretical chemists. Intermolecular interactions play fundamental roles in the formation of pre-reactive complexes in reaction mechanisms, in determining the shapes of supermolecular assemblies, in the design of drugs which should interact with specific targets, in the interactions between proteins or between an enzyme and its substrate.^{26,27} Intramolecular interactions are equally important and determine the shape of proteins, the conformational preferences of simple molecules, the preferred transition states in enantiomeric reactions or the relative energetics of isomers. To allow for the design of better chemical systems, an identification and rationalization of chemical trends is needed, either in terms of physical phenomena or in terms of simple and informative indices. In order to access unprecedented trends, this thesis is concerned with the development of quantum chemical approaches, which probe the effect of intra- and intermolecular interactions on molecular properties.

Although intermolecular interactions have been extensively analyzed since the first years of quantum chemistry,^{28,29} their intramolecular counterparts remain much more elusive. The existing methods to compute these energies often perturb the system considerably or do not allow for separating the interaction into different, physically meaningful energy components. The theoretical framework necessary for the development of a method to evaluate intramolecular interactions is introduced in **Chapter 2**. First, Symmetry-Adapted Perturbation Theory (SAPT) will be described.^{30–32} SAPT not only allows for the accurate computation of intermolecular interactions, but also decomposes them in physically meaningful terms such as electrostatics, exchange, induction and dispersion. SAPT is thus a method providing both accurate energetics and rationalization, a feature which would be most useful for further understanding intramolecular interactions, and will be used as our primary workhorse. The derivation of intramolecular SAPT energetic terms is, however, not the topic of this thesis, which is rather to devise a suitable wavefunction that could be used as a basis for such intramolecular perturbation theory. For this purpose, the concepts developed in the Chemical Hamiltonian (CHA)³³ approach will prove to be useful and are thus detailed next. Although unusual, the formalism associated with CHA was successfully applied to derive a SCF method for interaction energies naturally free from the basis set superposition error (BSSE).³⁴ Chemically meaningful energy partitioning schemes

were also derived from the CHA approach.³⁵ Both aspects will be presented and their results are briefly discussed. Finally, the inherently delocalized nature of electrons may hinder proper computation of interaction energy between different molecular fragments. The localization of electrons within the molecule thus may be desirable, and can be achieved through strictly localized orbitals,^{36–38} *i.e.*, orbitals that are expressed only in a subspace of the entire basis describing the molecular wavefunction. The method to optimize these orbitals and some of their applications^{37,39–42} to gain insight in intra- or intermolecular phenomena will be presented.

Chapter 3 exploits the theoretical tools previously introduced by devising a method to compute intramolecular interactions. As previously stated, the development of SAPT³⁰ will be our guide. Intramolecular perturbation theory is not derived in this thesis, since the primary objective is to obtain a suitable zeroth-order wavefunction $\Psi^{(0)}$. $\Psi^{(0)}$ should be constructed such that the two intramolecular fragments of interest are not interacting. Upon optimization of the corresponding energy expression, variational collapse of the orbitals could only be avoided through the previously introduced chemical hamiltonian formalism.³³ $\Psi^{(0)}$ then yields reasonable total energies, which can be directly compared with the corresponding fully interacting system. This formalism was also combined with strictly localized orbitals³⁶ to constrain electrons in specific molecular regions. Comparison of the zeroth-order energy with the full molecular energy then allows total intramolecular interaction energies to be computed. Applications on small test systems revealed that computed interaction energies are likely to be shifted by an approximately constant amount between similar systems, but still reveal useful chemical and geometrical trends. These results are gathered in an article that will be submitted to *The Journal of Chemical Physics*.

Rigorous derivation and computation of intramolecular interaction energies is, of course, desirable. However, information about intramolecular interactions may be obtained by much simpler means. In **Chapter 4** thermodynamic quantities are exploited to gain insight into the nature of intramolecular interactions in alkanes. Three series of molecules were considered: linear alkanes $\text{CH}_3(\text{CH}_2)_n\text{CH}_3$, singly-methylated alkanes $\text{CH}_3(\text{CH}(\text{CH}_3))_n\text{CH}_3$ and permethylated alkanes $\text{CH}_3(\text{C}(\text{CH}_3)_2)_n\text{CH}_3$, $n=3-5$. Experimental heats of formation were unavailable for some species, hence accurate thermochemistry had to be computed with an efficient *ansatz* for large molecules. This was achieved through the use of hyperhomodesmotic reactions,⁴³ which maximize error compensation by conserving bonds and their environment between reactants and products. Reaction energies could then be computed both efficiently and accurately by DFT methods and combined with experimental values to obtain heats of formation. Accuracy of the method was confirmed by comparison with experimental numbers, where available. Examination of bond separation energies (BSE) of the three alkane series revealed a linear trend for each one as the alkane is extended. Since BSE reflect 1,3-interactions and further, it was possible to attribute an energetic value to the interactions between carbon centers bearing different numbers of methyl substituents by fitting to the obtained BSEs, based on reasonable assumptions. Results revealed that interactions are mostly attractive, explaining the greater stability of branched alkanes over their linear counterparts. However, permethylation of alkanes results in

a strong repulsion dominating the attractive interaction, explaining the lower heat of formation of these systems. Thus, despite the simplified picture of branched alkane stability commonly accepted, these species show widely varying stability trends based on number and location of added methyl groups. Excessive branching actually results in strongly destabilizing interactions. The simple fitting method used in this case proves useful when associated to accurate thermochemical numbers to describe the repulsive or attractive nature of intramolecular interactions. This study was published in *Organic Letters*.⁴⁴

Information about specific types of intermolecular interactions may also be deduced from properties of a monomer alone. As an example, in **Chapter 5** we design an index reflecting the π -stacking ability of aromatic molecules only from their electronic structure. In order to visualize characteristics of the π electron density, the Localized Orbital Locator (LOL)⁴⁵ function was employed. LOL has a value proportional to the local kinetic energy of the electrons, and indicates whether electrons are localized or delocalized. Electron localization was proposed to increase exchange repulsion and induce less favorable π -stacking. Careful visualization of π LOL isosurfaces⁴⁶ and the corresponding interaction energies confirmed this hypothesis and allowed the design of an index to reflect the LOL values - and hence the electronic localization content - of aromatic systems. This index was used to distinguish candidates for π - π interactions with caffeine in the context of the design of a fluorescent sensor. Experimental binding affinities with caffeine confirmed that the best sensor was also revealed by having a favorable LOL-based index. Thus, a link was established between characteristics of the π electron localization in aromatic rings and the π -stacking ability. The results presented in this chapter have been published in *Chemical Communications*.⁴⁷

As previously underlined, intermolecular interactions are of importance in reaction mechanisms. This is illustrated by the collaborative experimental and theoretical study of the four-electron reduction of O_2 by tetrathiafulvalene (TTF) described in **Chapter 6**. Reduction of O_2 to H_2O is a key point for the development of efficient fuel cells.⁴⁸ The absence of any metal catalyst for the reduction of oxygen considered above makes it a very unusual reaction, whose mechanism may be of interest. Tetrathiafulvalene is known to be an excellent electron donor, but it is unable to give four electrons at once. Four molecules of TTF should thus be involved in the reaction, hence a correct description of intermolecular interactions is essential for describing the system. Because of the size of the reaction system, DFT methods were used to compute the energies and optimize geometries of the reacting molecules. To ensure a correct description of the important dispersion interactions, two different functionals were used. First, B3LYP-dDsC,^{25,49-52} which appends a density-dependent dispersion correction developed in our laboratory onto the B3LYP functional which fails to describe weak interactions. The second functional, M06-2X,^{53,54} includes medium range correlation contributions by a flexible functional form and extensive parametrization. Owing to their description of weak interactions during geometry optimizations, these functionals revealed the existence of stacked assemblies of four TTF molecules, two of which were protonated. This assembly may be able to transfer the four electrons and the two protons needed for the O_2 reduction. The first H radical transfer

reaction barrier was computed and found to be possible under experimental conditions, opening the way for further reduction. This finding indicates that a proper description of intermolecular interactions is essential for understanding of reaction mechanisms. Results presented in this chapter were published in the *Journal of the American Chemical Society*.⁵⁵

Finally, **Chapter 7** concludes this thesis and summarizes the main findings, placing emphasis on the importance of inter- and intramolecular interactions in the field of chemistry. Future directions for the development of a reliable intramolecular interaction decomposition are outlined.

2 Theoretical methods

This chapter summarizes the different theoretical methods and mathematical tools used throughout this thesis. The first section is devoted to Symmetry-Adapted Perturbation Theory (SAPT),³⁰ designed to compute intermolecular interactions and decompose them into physically meaningful energy terms. The next chapter introduces a zeroth-order wavefunction $\Psi^{(0)}$ for the derivation of intramolecular SAPT. Consequently, emphasis is placed on both the underlying philosophy to define the zeroth-order wavefunction and on the convergence properties rather than on the detailed expressions of the physical terms. Section 2.2 details the Chemical Hamiltonian (CHA)³³ formalism and the subsequent energy decomposition analysis. These concepts inspired our definition of the zeroth-order energy allowing optimization of $\Psi^{(0)}$. The Chemical Hamiltonian Approach with Conventional Energy (CHA/CE) method³⁴ to suppress basis-set superposition error (BSSE) in intermolecular interactions is also presented. Our zeroth-order wavefunction $\Psi^{(0)}$ relies on formulae similar to the non-hermitian formalism employed in CHA/CE, hence we benefit from the developments in this field. Finally, the strictly localized orbitals³⁶ (SLOs) and their applications are summarized. These orbitals localize electrons into specific molecular regions and will serve to clearly define the interacting molecular fragments in the next chapter.

2.1 Symmetry-Adapted Perturbation Theory

Intermolecular interaction energies of two monomers A and B can be obtained according to two different approaches. The most common, the *supermolecular approach*, consists of subtracting the total energies of the monomers from the total energy of the dimer: $\Delta E = E_{AB} - E_A - E_B$. If each energy is computed in the basis set of the corresponding system, an error arises from the imbalance in the description of the dimer and the monomers. In the dimer, each monomer can lower its energy by borrowing basis functions from the other, irrespectively of the actual interaction taking place in the system. This BSSE can be corrected if each energy is obtained in the dimer basis set,⁵⁶ although some argue this is only a partial correction,^{57,58} and the cases with more than two monomers are more difficult to handle. Other corrections resort to variants of the original method,⁵⁹ to a perturbative approach^{37,60} or to semi-empirical pairwise atomic corrections.⁶¹ The second way to obtain interaction energies is to compute them directly from the monomer wavefunctions using perturbation theory. In this case, the dimer is never explicitly computed, which reduces computational cost and eliminates the BSSE problem. The devel-

opment of perturbation theory for intermolecular interactions now spans more than 80 years since being first suggested by London in the 1930s. The main steps of this development are summarized in the next section.

2.1.1 Polarization theory

Perturbation theory for the computation of intermolecular interactions was first developed in the 1930s by London.^{28,30} In this flavor of perturbation theory, the zeroth order Hamiltonian $\hat{H}^{(0)} = \hat{H}_A + \hat{H}_B$ is simply the sum of the monomer Hamiltonians, and the perturbation operator $\hat{V} = \hat{H}_{tot} - \hat{H}^{(0)}$ is the difference of the full and zeroth-order Hamiltonians. \hat{V} contains all interaction terms between the two monomers, *i.e.*, the nuclei-nuclei and electron-electron repulsion, and the nuclei-electron attraction. From \hat{V} and the zeroth-order wavefunction, the interaction energy can be derived, as shown below. Instead of using the full interaction energy operator \hat{V} , London replaced it by a multipole expansion,^{28,29} which was shown to converge only at large intermolecular separations.⁶² Later, the perturbation expansion of London was improved by using the exact form of the interaction operator \hat{V} , resulting in *polarization theory*.⁶³ The energetic components present in polarization theory, but absent in London formulations, are defined as charge penetration effects, which cannot be described by a multipole expansion and appear as the electron densities of the monomers overlap.^{64,65} Polarization theory is a perturbation expansion based on the following equation:³⁰

$$\left(\hat{H}^{(0)} + \lambda \hat{V}\right) \Psi_{AB} = E_{AB} \Psi_{AB} \quad (2.1)$$

As the perturbation parameter λ is varied from 0 to 1, the eigenfunction Ψ_{AB} varies from the product of the monomer wavefunctions to the full wavefunction of the dimer. Similarly, the energy varies from the sum of the isolated monomer energies to the energy of the dimer. In this expression, the monomer Hamiltonians \hat{H}_A and \hat{H}_B act only on the electrons of monomers A and B, respectively. This means that each electron is assigned to one monomer and that they are not strictly indistinguishable. This unphysical zeroth-order wavefunction has consequences on the perturbation theory that will be examined later.

Within Rayleigh-Schrödinger perturbation theory, the total energy and wavefunction are expanded as powers of λ :⁶⁶

$$\begin{aligned} E_{tot} &= E^{(0)} + \lambda E^{(1)} + \lambda^2 E^{(2)} + \dots \\ \Psi_{tot} &= \Psi^{(0)} + \lambda \Psi^{(1)} + \lambda^2 \Psi^{(2)} + \dots \end{aligned} \quad (2.2)$$

where $\Psi^{(0)}$ and $E^{(0)}$ correspond to the case where $\lambda = 0$ so that $E^{(0)} = E_A + E_B$ and $\Psi^{(0)} = \Psi_A \Psi_B$. The intermediate normalization condition is used, *i.e.*, each of the wavefunction correction $\Psi^{(n)}$, $n \neq 0$, is chosen to be orthogonal to $\Psi^{(0)}$. The Schrödinger equation is then rewritten:

$$\begin{aligned} &\left(\hat{H}^{(0)} + \lambda \hat{V}\right) \left(\Psi^{(0)} + \lambda \Psi^{(1)} + \lambda^2 \Psi^{(2)} + \dots\right) \\ &= \left(E^{(0)} + \lambda E^{(1)} + \lambda^2 E^{(2)} + \dots\right) \left(\Psi^{(0)} + \lambda \Psi^{(1)} + \lambda^2 \Psi^{(2)} + \dots\right) \end{aligned} \quad (2.3)$$

Gathering all terms with the same power of λ on both sides, multiplying each equation by $\Psi^{(0)}$,

integrating and using the intermediate normalization condition, one obtains equations for each energy correction directly:

$$E^{(0)} = \langle \Psi^{(0)} | \hat{H}^{(0)} | \Psi^{(0)} \rangle \quad (2.4)$$

$$E^{(1)} = \langle \Psi^{(0)} | \hat{V} | \Psi^{(0)} \rangle \quad (2.5)$$

$$E^{(2)} = \langle \Psi^{(0)} | \hat{V} | \Psi^{(1)} \rangle \quad (2.6)$$

The second-order ground state energy correction $E^{(2)}$ is rewritten only in terms of the eigenfunctions and eigenvalues of $\hat{H}^{(0)}$:

$$E^{(2)} = \sum_{n \neq 0} \frac{|\langle \Psi^{(0)} | \hat{V} | \Psi_n^{(0)} \rangle|^2}{E^{(0)} - E_n^{(0)}} \quad (2.7)$$

where the n subscript spans the set of eigenvalues and eigenfunctions of $\hat{H}^{(0)}$, except the lowest one.

One of the great advantages of polarization theory over the supermolecular approach of computing intermolecular interactions is the natural decomposition of the energy into physically meaningful terms, as shown by a simple transformation of the formula for $E^{(1)}$.

$$\begin{aligned} E^{(1)} &= \langle \Psi_A \Psi_B | \hat{V} | \Psi_A \Psi_B \rangle \\ &= \int \int \rho_A^{tot}(\mathbf{r}_1) \frac{1}{r_{12}} \rho_B^{tot}(\mathbf{r}_2) d^3\mathbf{r}_1 d^3\mathbf{r}_2 \end{aligned} \quad (2.8)$$

where

$$\rho_A^{tot}(\mathbf{r}) = \sum_{\alpha} Z_{\alpha} \delta(\mathbf{r} - \mathbf{R}_{\alpha}) - \rho_A(\mathbf{r}) \quad (2.9)$$

the delta function ensures that nuclear charges Z_{α} contribute only at their position \mathbf{R}_{α} and ρ_A is the usual electronic density. A similar definition holds for $\rho_B^{tot}(\mathbf{r})$. Thus, Equation 2.8 contains the electron-electron, electron-nuclei and nuclei-nuclei interactions of the two monomers, and completely describes the electrostatic interactions of A and B.

The second-order energy term can be written

$$E^{(2)} = \sum_{n \neq 0} \frac{|\langle \Psi_A \Psi_B | \hat{V} | (\Psi_A \Psi_B)^{exc} \rangle|^2}{E^{(0)} - E_n^{(0)}} \quad (2.10)$$

so that it contains only the ground and excited states of the isolated monomers, corresponding to the eigenfunctions of $\hat{H}^{(0)}$. The different terms in the sum are grouped according to the excitations occurring within them. If the excitation is localized on a single monomer, *i.e.*, the ket is of the form $\Psi_A^{exc} \Psi_B$ or $\Psi_B^{exc} \Psi_A$, it represents induction energy. A simultaneous excitation of both monomers represents simultaneous electron correlation on both molecules, giving rise to dispersion interactions.

Polarization theory gives access to the electrostatic energy at first order and to the induction and

dispersion energies at second order. Higher-order terms can similarly be interpreted in terms of these simple physical contributions and the coupling between them. Although physically insightful, polarization theory is not of practical use for many-electron systems since it misses an essential physical component of intermolecular interactions.⁶⁷ This can be traced back to the zeroth-order wavefunction $\Psi^{(0)} = \Psi_A \Psi_B$, which is not antisymmetric upon electron exchange between monomers A and B. Consequently, the exchange energy is not explicitly accounted for in polarization theory and can only be recovered with unrealistically large orders of perturbation or analytical techniques.^{68,69} Corrections of polarization theory to yield exchange terms from first order are known as symmetry adaptations.

2.1.2 Symmetry-Adapted Perturbation Theory

To obtain the correct antisymmetric wavefunction from $\Psi^{(0)}$, the antisymmetrizer \mathcal{A} is introduced. This operator acts on the Pauli-violating wavefunction and restores the proper antisymmetry upon electron exchanges between monomers A and B. The antisymmetrizer was used in different ways, and the proposed symmetry adaptations were classified in two categories: weak symmetry forcing, where the antisymmetrizer is used only in the energy expressions, and strong symmetry forcing, where \mathcal{A} enters directly the perturbation equations. The latter considerably complicates the expressions for many-electron systems, and will not be further discussed herein. Although the most successful weak symmetry forcing formalism is now commonly known as SAPT, its original name was Symmetrized Rayleigh-Schrödinger (SRS).^{70,71} As far as the low-order energetic terms are concerned, SRS is very similar to the polarization theory except that the antisymmetrizer \mathcal{A} is now introduced in the energy expressions in the following way:

$$E^{(1)} = \langle \Psi^{(0)} | \hat{V} | \mathcal{A} \Psi^{(0)} \rangle \left(\langle \Psi^{(0)} | \mathcal{A} \Psi^{(0)} \rangle \right)^{-1} \quad (2.11)$$

$$E^{(2)} = \langle \Psi^{(0)} | \hat{V} | \mathcal{A} \Psi^{(1)} \rangle \left(\langle \Psi^{(0)} | \mathcal{A} \Psi^{(1)} \rangle \right)^{-1} \quad (2.12)$$

The antisymmetrizer is written as $\mathcal{A} = 1 + \mathcal{P}$ where \mathcal{P} interchanges at least one electron pair between two monomers. Thus, Equations 2.11 can be decomposed into one term without any new electron exchange and another term containing exchange. The first corresponds to the electrostatics, induction and dispersion terms found in polarization theory, and the second part contains exchange energy as well as exchange-induction and exchange-dispersion. Every term in polarization theory has an exchange counterpart arising from the antisymmetrization of the wavefunction upon electron exchange between monomers A and B.

Up to now, the monomers were treated with a Hartree-Fock wavefunction. To improve the energetics, electronic correlation within monomers should also be included. Perturbation theory was proposed for this purpose, using the Møller-Plesset partitioning of the energy.⁷² The combination of perturbation theory for electron correlation and SAPT yields a double perturbation theory, where both the intermolecular interaction operator and the Møller-Plesset perturbation operator are simultaneously used as perturbations. Practically, this results in an expansion of the electrostatic, induction, dispersion and exchange terms in powers of intramonomer correlation,

written for a general term:

$$E^{(n)} = E^{(n0)} + E^{(n1)} + E^{(n2)} + E^{(n3)} + \dots \quad (2.13)$$

Since two monomers are present in the computation, the order of perturbation theory indicated in the terms above corresponds to the sum of the perturbation order on each monomer. The convergence of the perturbation series 2.13 is quite slow for the exchange term, hence coupled-cluster type expansions were used to obtain the higher-order contributions.⁷³ The monomer electron correlation may alternatively be computed from Density Functional Theory (DFT) so that a double perturbation treatment is not needed.^{74–79} However, the asymptotic behaviour of the chosen density functional has to be corrected using experimental values to achieve the best results.⁸⁰ Treatment of monomer correlation with perturbation theory turns SAPT into a double perturbation expansion, which may be truncated at different orders depending on the desired accuracy. In the most recent implementation of SAPT in the PSI4 software,⁸¹ five different truncation levels are available:

- $E_{SAPT0} = E_{elst}^{(10)} + E_{exch}^{(10)} + E_{ind,resp}^{(20)} + E_{exch-ind,resp}^{(20)} + E_{disp}^{(20)} + E_{exch-disp}^{(20)}$
- $E_{SAPT2} = E_{SAPT0} + E_{elst,resp}^{(12)} + E_{exch}^{(11)} + E_{exch}^{(12)} + {}^tE_{ind}^{(22)} + {}^tE_{exch-ind}^{(22)}$
- $E_{SAPT2+} = E_{SAPT2} + E_{disp}^{(21)} + E_{disp}^{(22)}$
- $E_{SAPT2+(3)} = E_{SAPT2+} + E_{elst,resp}^{(13)} + E_{disp}^{(30)}$
- $E_{SAPT2+3} = E_{SAPT2+(3)} + E_{exch-disp}^{(30)} + E_{ind-disp}^{(30)} + E_{exch-ind-disp}^{(30)}$

The following abbreviations are used: *elst* for electrostatics, *exch* for exchange, *ind* for induction, *resp* when the orbital response is taken into account, *disp* for dispersion. The *t* superscript indicates that the corresponding term has been modified to avoid double counting of the orbital response. A detailed study of the accuracy of the different truncations has recently been published.³¹ The highest level, SAPT2+3, includes selected third-order terms and is as accurate as the gold standard of computational chemistry, CCSD(T). In recent years, the implementation of SRS has benefited from numerous improvements: density fitting approximations, Cholesky decomposition⁸² or Laplace transformation techniques⁸³ have been used to speed-up evaluations of the terms, and the costly $E_{disp}^{(22)}$ second-order dispersion term can now be approximated both efficiently and accurately using MP2 natural orbitals.⁸⁴ All of these improvements are implemented in the program package PSI4,⁸¹ which makes it the most efficient software for SAPT computations.

In summary, the computation of intermolecular interactions by perturbation theory has a long history. Polarization theory uses isolated monomers as a starting point and adds the intermolecular interactions at different orders, however, it misses a fundamental component of electronic interaction, the exchange energy, arising from the indistinguishability of the electrons. Upon this realization, different attempts were undertaken to properly symmetrize perturbation theory.

The most successful attempt was amongst the simplest: in the energy expressions from perturbation theory, the product of the monomer wavefunctions is replaced by its antisymmetrized counterpart. This Symmetrized Rayleigh-Schrödinger (SRS) theory is now commonly referred to as SAPT, and benefits from numerous improvements, both from the theoretical and computational perspectives. As a result, it now reaches the accuracy of CCSD(T) interaction energies and can routinely be applied to medium-sized molecules. However, it is inherently limited to intermolecular energy computations. In **Chapter 3**, the first steps toward an intramolecular version of SAPT are presented. For this purpose, the concepts of the CHA approach introduced next are essential.

2.2 The Chemical Hamiltonian

The concept of atoms in molecule is intuitive and natural to all chemists. However, quantum chemistry describes molecular systems as an ensemble of particles, including delocalized electrons. Thus, the identification of atoms and of the transferable functional groups well known to the experimental chemist is not trivial. The CHA approach was originally developed as a way to restore the concept of atoms and transferable functional groups in molecules within a rigorous quantum mechanical treatment. In CHA, the partitioning of energetic terms relies on the basis functions employed to describe the orbitals, consequently atom-centered basis sets are mandatory. The partitioning naturally gives rise to different energy decomposition schemes that will be described in Section 2.2.2. Although CHA has been rigorously derived at the level of the Hamiltonian itself in the second quantized formalism,³³ we here restrict the discussion to the energy expression for a single Slater determinant, *i.e.*, to the Hartree-Fock energy expression E_{HF} .

$$\begin{aligned}
 E_{HF} &= \sum_{IJ} \frac{Z_I Z_J}{R_{IJ}} + \sum_{\mu\nu} D_{\mu\nu} \langle \chi_\nu | \hat{h} | \chi_\mu \rangle \\
 &+ \frac{1}{2} \sum_{\mu\rho\nu\tau} \left(D_{\mu\nu} D_{\rho\tau} - P_{\rho\nu}^\alpha P_{\mu\tau}^\alpha - P_{\rho\nu}^\beta P_{\mu\tau}^\beta \right) \langle \chi_\nu \chi_\tau | \chi_\mu \chi_\rho \rangle
 \end{aligned}
 \quad (2.14)$$

where $\hat{h} = -\sum_I \frac{Z_I}{R_{Ij}} + \hat{T}$ contains the nuclear potential and the kinetic energy operator, $D_{\mu\nu} = P_{\mu\nu}^\alpha + P_{\mu\nu}^\beta$ and $P_{\mu\nu}^\alpha = \sum_i^{occ,\alpha} C_{\mu i} C_{\nu i}$ is the usual spin density matrix. The different energy terms in Equation 2.14 are partitioned by interpreting differently the bra and the ket of the electronic integrals. The ket contains the physical interaction induced by the one- or two-electron operator, and the bra contains the projection of this operator onto the basis set. As an example, consider the integral

$$\langle \chi_\mu | \hat{h} | \chi_\nu \rangle
 \quad (2.15)$$

The operator \hat{h} acts onto the function $|\chi_\nu\rangle$ to give a new function $\hat{h}|\chi_\nu\rangle$ representing the physical action of \hat{h} on an electron in χ_ν , then projected on basis function χ_μ .³³ Similar considerations apply to two-electron integrals.

2.2.1 Application to the BSSE problem

The CHA interpretation of the integrals allows one to identify simply the terms responsible for the BSSE in intermolecular interaction energy computations.³³ The formalism derived by Mayer for this purpose, introduced in the following, bears similarities with the derivation of the zeroth-order wavefunction that will be presented in Section 3.2, although the goal and the energetic partitioning employed are different.

In the case of two monomers A and B, the total energy of the dimer also contains the internal energies of the monomers. Let \hat{h}_A denote the one-electron operator of monomer A, containing both the potential from its nuclei and the kinetic energy. If the index μ is associated with a basis function localized on A (*i.e.*, $\mu \in A$), then the function $\hat{h}_A \chi_\mu$ represents an intramonomer interaction. Basis sets employed in practical computations are not saturated, hence $\hat{h}_A \chi_\mu$ has components that lie outside the basis set of monomer A. These components are responsible for the artificial lowering of the energy when the monomer A is in proximity of the monomer B, *i.e.*, they are responsible for the basis set superposition error. Similarly, the function $\frac{1}{r_{12}} \chi_\mu \chi_\nu$ with $\mu, \nu \in A$ is an intramonomer quantity whose expansion in the monomer basis set is usually incomplete. To eliminate the BSSE from a dimer computation, all the components of the intramonomer interactions which cannot be expressed in the corresponding monomer basis should be removed.^{85,86} These terms can be written explicitly in the case of the Hartree-Fock total energy:

$$\begin{aligned} E_{BSSE} = & \sum_{\nu} \sum_{\mu}^{\mu \in A} D_{\mu\nu} \langle \chi_\nu | (1 - \hat{P}_A) \hat{h}_A | \chi_\mu \rangle + \sum_{\nu} \sum_{\mu}^{\mu \in B} D_{\mu\nu} \langle \chi_\nu | (1 - \hat{P}_B) \hat{h}_B | \chi_\mu \rangle \\ & + \frac{1}{2} \sum_{\mu\rho}^{\mu, \rho \in A} \sum_{\nu\tau} K_{\mu\nu\rho\tau} \left\langle \chi_\nu \chi_\tau | (1 - \hat{P}_A)(\mathbf{r}_1)(1 - \hat{P}_A)(\mathbf{r}_2) \frac{1}{r_{12}} | \chi_\mu \chi_\rho \right\rangle \\ & + \frac{1}{2} \sum_{\mu\rho}^{\mu, \rho \in B} \sum_{\nu\tau} K_{\mu\nu\rho\tau} \left\langle \chi_\nu \chi_\tau | (1 - \hat{P}_B)(\mathbf{r}_1)(1 - \hat{P}_B)(\mathbf{r}_2) \frac{1}{r_{12}} | \chi_\mu \chi_\rho \right\rangle \end{aligned} \quad (2.16)$$

where $K_{\mu\nu\rho\tau} = D_{\mu\nu} D_{\rho\tau} - P_{\rho\nu}^\alpha P_{\mu\tau}^\alpha - P_{\rho\nu}^\beta P_{\mu\tau}^\beta$, and the projector \hat{P}_A on the basis functions of monomer A is defined as

$$\hat{P}_A = \sum_{\gamma\delta \in A} |\chi_\gamma\rangle (\mathbf{S}^{(A)})_{\gamma\delta}^{-1} \langle \chi_\delta| \quad (2.17)$$

and $(\mathbf{S}^{(A)})_{\gamma\delta}^{-1}$ are elements of the inverse overlap matrix of basis functions on monomer A. A similar definition holds for \hat{P}_B . The notation $(1 - \hat{P})(\mathbf{r}_1)$ indicates that the orthogonal complement of the projector \hat{P} is acting only on the coordinates of the first electron.

The BSSE-free total energy is then expressed as $E_{phys} = E_{HF} - E_{BSSE}$. Since the bra and the ket are not treated symmetrically in this formalism, the corresponding Hamiltonian is non-hermitian. Consequently, the variational principle cannot be invoked to optimize the orbitals in E_{phys} . A generalization of the Brillouin theorem provides a solution by imposing⁸⁷

$$\langle \Psi_0 | \hat{H}_{phys} | \Psi_i^a \rangle = 0 \quad (2.18)$$

where Ψ_0 is the ground-state Slater determinant built from the optimized orbitals, Ψ_i^a the excited determinant obtained by replacing the occupied orbital i by a virtual orbital a and \hat{H}_{phys} the non-Hermitian Hamiltonian free of the BSSE terms. \hat{H}_{phys} may be written using second quantization for non-orthogonal orbitals.⁸⁵ The resulting orbital optimization condition reads

$$\mathbf{C}_{virt}^\dagger \mathbf{F} \mathbf{C}_{occ} = 0 \quad (2.19)$$

where \mathbf{F} is the non-hermitian Fock matrix, \mathbf{C}_{virt} and \mathbf{C}_{occ} are the coefficient matrices of the virtual and occupied orbitals, respectively. Note that Equation 2.19 bears similarity with the Brillouin theorem since matrix elements of the Fock operator between virtual and occupied orbitals are required to vanish. The Chemical Hamiltonian Approach Self-Consistent Field (CHA-SCF) method optimizes the orbitals using Equation 2.19 and obtains the energy with the corresponding non-hermitian Fock matrix. The solution to Equation 2.19 was originally obtained by an iterative diagonalization procedure of \mathbf{F} . The non-hermiticity of \mathbf{F} implies that eigenvalues and eigenvectors are not necessarily real. However, since \mathbf{F} is real, the eigenvalues and eigenvectors are either real or in complex conjugate pairs, in which case the density matrix and the energy are still real (if the pair is either in the virtual or in the occupied space).⁸⁵

The usual method for suppressing the BSSE in intermolecular interactions is the Boys and Bernardi method⁵⁶ to compute the energy of the monomers in the dimer basis set, sometimes referred to as the counterpoise correction. The direct application of the CHA-SCF method on simple systems revealed a very different behaviour from that of the Boys and Bernardi correction to the BSSE.⁸⁸ Computing the BSSE from the CHA-SCF energies indicated that the error could be both over and underbinding, in contrast with the common understanding of the BSSE which should always artificially stabilize the dimer and hence overbind, as is observed with the Boys and Bernardi correction. Careful analysis of the different available BSSE corrections on simple analytical models^{34,89} revealed that the orbitals should be optimized with CHA-SCF and the energy computed with the conventional expression, which is realized in the CHA/CE method. The analytical model revealed several details of the available methods:

- CHA-SCF does not contain any BSSE contribution, but does not lead to the correct energy expression, except if exact eigenfunctions of both systems can be obtained.
- the CHA-SCF energy is not necessarily real⁸⁹ and thus the CHA/CE method should be preferred.
- Boys and Bernardi correction excludes pure BSSE effects, but only when the different electronic integrals in the system obey a defined mathematical relationship.
- Boys and Bernardi correction contains spurious terms related to delocalization between occupied orbitals and still contains the interferences between the BSSE and the true interaction.
- CHA/CE always excludes the pure BSSE effects, but still contains the interferences between BSSE and the true interaction.

CHA/CE is thus expected to be close or superior to the Boys and Bernardi correction, which is confirmed by numerical tests on small molecules.

Finally, the CHA/CE approach was simplified further when it was realized that a non-hermitian Fock matrix was not needed. Actually, Equation 2.19 concerns only the virtual-occupied block of the Fock matrix, hence it is possible to apply a hermitization procedure.⁹⁰ The occupied-virtual block of the original, non hermitian Fock matrix \mathbf{F} is replaced by the transposed virtual-occupied blocks. The diagonal blocks are entirely deleted and replaced by the corresponding part of the conventional Fock matrix \mathbf{F}_{CE} . The hermitian matrix obtained \mathbf{F}_{herm} can be diagonalized by conventional methods and, at convergence, the off-diagonal blocks will be zero and Equation 2.19 satisfied. Moreover, the same matrix can be used to evaluate the energy since the diagonal blocks are the conventional ones.

The CHA approach allowed the derivation of the CHA/CE method which naturally suppresses the most important BSSE effects in intermolecular energy computations. CHA/CE may be easily applied to the case of more than two interacting monomers,⁵⁷ where its conceptual and practical advantage over Boys and Bernardi scheme is most obvious. The extension of the CHA/CE concepts to strong interactions, *i.e.*, to suppress the intramolecular BSSE, revealed some deficiencies of the method which are negligible in intermolecular interactions. A correction based on transformations of the relevant quantities to the MO basis was devised and the new scheme termed CHA/FS.⁹¹ The CHA approach is very general and has been applied to Kohn-Sham wavefunctions in the framework of density functional theory⁹² and to obtain BSSE-free MP2 energies.⁹³ The CHA-MP2 method implies to use perturbation theory on quite unconventional non-orthogonal and possibly complex orbitals and benefited from a specific implementation.⁹⁴

2.2.2 Energy partitioning schemes

As mentioned earlier, since the CHA approach allows the identification and interpretation of the different energetic terms in the Hamiltonian, it can also be used to devise energy decomposition schemes for the Hartree-Fock total energy. Only three variants of these methods will be detailed below: E^1 , E^2 and the exact Chemical Energy Component Analysis (CECA).

The E^1 energy partitioning scheme was introduced in the spirit of the Mulliken population analysis⁹⁵ by dividing each one- and two-electron integral between the different centers involved and using their symmetry to shorten the notation. For two atoms A and B, intraatomic energy elements E_A^1 and interatomic elements E_{AB}^1 are defined as:

$$\begin{aligned} E_A^1 &= \sum_{\mu \in A} \sum_{\nu} D_{\mu\nu} h_{\nu\mu}^A + \frac{1}{2} \sum_{\mu, \rho \in A} \sum_{\nu\tau} (D_{\mu\nu} D_{\rho\tau} - P_{\rho\nu}^\alpha P_{\mu\tau}^\alpha - P_{\rho\nu}^\beta P_{\mu\tau}^\beta) \langle \chi_\nu \chi_\tau | \chi_\mu \chi_\rho \rangle \\ E_{AB}^1 &= \frac{Z_A Z_B}{R_{AB}} - \sum_{\mu \in A} \sum_{\nu} D_{\mu\nu} \left\langle \chi_\nu \left| \frac{Z_B}{r_B} \right| \chi_\mu \right\rangle - \sum_{\mu \in B} \sum_{\nu} D_{\mu\nu} \left\langle \chi_\nu \left| \frac{Z_A}{r_A} \right| \chi_\mu \right\rangle \\ &+ \sum_{\mu \in A} \sum_{\rho \in B} \sum_{\nu\tau} (D_{\mu\nu} D_{\rho\tau} - P_{\rho\nu}^\alpha P_{\mu\tau}^\alpha - P_{\rho\nu}^\beta P_{\mu\tau}^\beta) \langle \chi_\nu \chi_\tau | \chi_\mu \chi_\rho \rangle \end{aligned} \quad (2.20)$$

where $h_{\nu\mu}^A = \langle \chi_\nu | \hat{h}^A | \chi_\mu \rangle$ and $\hat{h}^A = -\frac{Z_A}{r_A} - \frac{1}{2}\Delta$ is the one-electron operator of atom A. In E^1 , the kinetic energy is treated entirely as an intraatomic quantity. The present energy decomposi-

tion analysis derived from the CHA approach aims at inter- and intraatomic energy components transferable and of chemical relevance. The term E_{AB}^1 contains only electrostatic and exchange energy contributions in agreement with the original view of covalent bonding.⁹⁶ This perspective was challenged by the seminal work of Ruedenberg⁹⁷ who stressed the importance of the kinetic energy terms. Nowadays, no general consensus has been found on the Hamiltonian term responsible for covalent bond formation, and the question is still being actively debated.^{98–105} Acknowledging that the kinetic energy is considered to play a major role in the covalent bond formation, another energy partitioning scheme (E^2)¹⁰⁶ was designed where the kinetic energy is partitioned as an interatomic quantity.

$$\begin{aligned}
 E_A^2 &= \sum_{\mu, \nu \in A} D_{\mu\nu} T_{\nu\mu} - \sum_{\mu \in A} \sum_{\nu} D_{\mu\nu} \left\langle \chi_\nu \left| \frac{Z_A}{r_A} \right| \chi_\mu \right\rangle \\
 &+ \frac{1}{2} \sum_{\mu, \rho \in A} \sum_{\nu, \tau} (D_{\mu\nu} D_{\rho\tau} - P_{\rho\nu}^\alpha P_{\mu\tau}^\alpha - P_{\rho\nu}^\beta P_{\mu\tau}^\beta) \langle \chi_\nu \chi_\tau | \chi_\mu \chi_\rho \rangle \\
 E_{AB}^2 &= 2 \sum_{\mu \in A} \sum_{\nu \in B} D_{\mu\nu} T_{\nu\mu} - \sum_{\mu \in A} \sum_{\nu} D_{\mu\nu} \left\langle \chi_\nu \left| \frac{Z_B}{r_B} \right| \chi_\mu \right\rangle - \sum_{\mu \in B} \sum_{\nu} D_{\mu\nu} \left\langle \chi_\nu \left| \frac{Z_A}{r_A} \right| \chi_\mu \right\rangle \\
 &+ \sum_{\mu \in A} \sum_{\rho \in B} \sum_{\nu, \tau} (D_{\mu\nu} D_{\rho\tau} - P_{\rho\nu}^\alpha P_{\mu\tau}^\alpha - P_{\rho\nu}^\beta P_{\mu\tau}^\beta) \langle \chi_\nu \chi_\tau | \chi_\mu \chi_\rho \rangle + \frac{Z_A Z_B}{R_{AB}} \quad (2.21)
 \end{aligned}$$

where $T_{\nu\mu} = \langle \chi_\nu | -\frac{1}{2} \Delta | \chi_\mu \rangle$ is a matrix element of the kinetic energy operator. The E^1 and E^2 energy partitionings yield to rather different results. E^1 has very large atomic energies, and very low diatomic energy terms, much lower than the accepted numbers for covalent bonds. Due to the reattribution of the kinetic energy term, E^2 balances both terms: the atomic energies are lower, and the diatomic components are much closer to bond dissociation energies. In both E^1 and E^2 , distant atoms exhibit interaction energies close to zero, and nearby atoms attractive or repulsive interactions. Bond orders cannot distinguish bonding and anti-bonding situations, thus the energy partitionings provide useful information.¹⁰⁷ E^2 seems to be the preferred method as far as stationary points are concerned. However, examination of both schemes upon bond elongation reveals that E^1 behaves better than E^2 . Due to the inclusion of the kinetic energy, E_{AB}^2 decreases (*i.e.*, the bond becomes stronger) as the atoms are separated. E_{AB}^1 exhibits the opposite behaviour and indicates a weaker interaction as the bond is stretched. Consequently, neither E^1 nor E^2 is an ideal energy decomposition analysis.¹⁰⁸

To overcome this shortcoming, Mayer again studied analytically a simple system,³⁵ the H_2 molecule in a minimal basis with the MNDO method¹⁰⁹ to design a better decomposition. The new energy decomposition scheme had to obey two conditions. First, no approximation should be introduced in the decomposition; second, the intraatomic energy of H in H_2 in a minimal basis set must be the same as the energy of the isolated atom. To achieve these two conditions, two modifications were made to scheme E^1 . The first is to transfer the so-called basis extension

terms from the intraatomic term to the interatomic one. The energies then become:³⁵

$$\begin{aligned} E_A^{1'} &= E_A^1 - \sum_{B \neq A} \delta_{AB} \\ E_{AB}^{1'} &= E_{AB}^1 + \delta_{AB} + \delta_{BA} \end{aligned} \quad (2.22)$$

where

$$\begin{aligned} \delta_{AB} &= \sum_{\mu \in A} \sum_{\nu \in B} D_{\mu\nu} \langle \chi_\nu | (1 - \hat{P}_A) \hat{h}^A | \chi_\mu \rangle \\ &+ \frac{1}{2} \sum_{\mu, \rho \in A} \sum_{\nu, \tau \in AB} (D_{\mu\nu} D_{\rho\tau} - P_{\rho\nu}^\alpha P_{\mu\tau}^\alpha - P_{\rho\nu}^\beta P_{\mu\tau}^\beta) \\ &\times \left\langle \chi_\nu \chi_\tau | (1 - \hat{P}_A)(\mathbf{r}_1) (1 - \hat{P}_A)(\mathbf{r}_2) \frac{1}{r_{12}} | \chi_\mu \chi_\rho \right\rangle \end{aligned} \quad (2.23)$$

where \hat{P}_A and \hat{P}_B have been defined in Equation 2.17. δ_{AB} contain similar terms as the BSSE energy defined in Equation 2.16, representing the part of the intra-atomic interactions that cannot be represented in the basis of the atom, hence related to the basis extension. Equation 2.23 introduces a further restriction in that the basis extension is only on the basis functions of the partner atom B. The energy scheme $E^{1'}$ corresponds to an exact version of CECA.¹¹⁰ CECA introduced approximations to represent three- and four-center integrals by, at most, two-center ones, and had a similar energetic behaviour as E^1 with depressed diatomic energy value and a correct distance dependence.

The second modification is more extensive, and we here expose only the general ideas. Detailed formulae are available in the original article by Mayer.³⁵ The analysis of the H_2 system revealed that the two electrons occupying a bonding orbital extend on both atomic partners, and hence give a contribution to their intraatomic electron repulsion. However, this electronic repulsion should be attributed to the interatomic energy terms, since it originates from the electron sharing between the two atoms. The amount of electronic repulsion that should be transferred to the interatomic term depends on how localized the electrons of the bond are on each atom. For this purpose, different sets of localized orbitals are determined for each atom in order to derive from them effective atomic orbitals,^{111,112} and compute a valence index. The valence index indicates how localized the electrons are on the atom, and $E_A^{1'}$ and $E_{AB}^{1'}$ are adjusted accordingly. The improved scheme has much lower interatomic energy components, although they are still far from the usual bond dissociation energies. The correct distance dependence for the E^1 and $E^{1'}$ decompositions is preserved.

In summary, the chemical hamiltonian approach³³ allows interpretation of the different terms in the Hamiltonian as intra- or interatomic quantities. The one- and two-electron integrals are interpreted in an asymmetric manner, the ket containing the physical part of the interaction and the bra being its projection on basis set functions. From CHA, the major terms causing the BSSE in intermolecular energy computations could be identified⁸⁹ and successfully eliminated in CHA/CE.³⁴ CHA/CE results are usually close to the classical method of Boys and Bernardi but are easier to transfer to the case of many interacting monomers. CHA/CE also empirically

demonstrates that energy expressions based on non-hermitian operators may lead to converging orbital optimization, a feature of importance in Section 3.2. The CHA approach was also employed to obtain energy decomposition schemes in intra- and interatomic terms. Inclusion of the kinetic energy as an interatomic term yields appealing bond energy values, however these quantities decrease as the atoms are separated. An improved scheme was derived by keeping the kinetic energy an intraatomic value but adding correction terms for the fraction of bonding electrons localized on atoms. This improved scheme is the starting point for the derivation of a zeroth-order energy in Section 3.2.1.

2.3 Strict orbital localization

Localized orbitals are usually obtained with a minimization or maximization procedure of a suitable functional by a unitary transformation of the canonical orbitals. Different functionals have been proposed, among them maximization of the Mulliken charge on the atoms for each orbital¹¹³ (Pipek-Mezey method), maximization of separation of the orbital centroids¹¹⁴ (Boys method) or maximization of orbital self-repulsion energy¹¹⁵ (Edmiston-Ruedenberg method). Localized orbitals obtained in this way are orthogonal and possess orthogonalization tails, meaning that basis functions on the entire molecule are needed to express them, although the largest contributions arise from a small number of centers.

2.3.1 Fundamental equations

Strictly localized orbitals (SLOs) do not have orthogonalization tails, since they are constrained to have non-zero coefficients on a small number of basis functions. The original equations to obtain strictly localized orbitals self-consistently were derived by Stoll³⁶ in 1980 and are summarized below. Let

$$|\varphi_{ix}\rangle = \sum_{\mu \in x} C_{\mu ix} |\chi_{\mu}\rangle \quad (2.24)$$

where x is a fragment, $|\varphi_{ix}\rangle$ denote a strictly localized orbital, $C_{\mu i}$ the associated coefficients and $|\chi_{\mu}\rangle$ a basis function. The coefficients of $|\varphi_{ix}\rangle$ are set to zero on all basis functions not belonging to fragment x . The orbitals localized on different fragments have to be non-orthogonal, hence the total HF energy expression has to be slightly modified:

$$E_{tot} = \frac{1}{2} \sum_{ix}^{occ} \langle \varphi_{ix} | \hat{h} + \hat{F} | \tilde{\varphi}_{ix} \rangle \quad (2.25)$$

where the reciprocal or biorthogonal orbitals $|\tilde{\varphi}_{ix}\rangle$ are defined as:

$$|\tilde{\varphi}_{ix}\rangle = \sum_{jy}^{occ} |\varphi_{jy}\rangle S_{jy,ix}^{-1} \quad (2.26)$$

and S^{-1} is the inverse overlap matrix of the occupied orbitals. The SLOs are optimized so that they lead to the lowest possible energy, similar to the Hartree-Fock molecular orbitals. Varying

the energy with respect to the occupied SLO $|\varphi_{ix}\rangle$ leads to

$$\delta_{(ix)} E_{tot} = 2 \langle \delta \varphi_{ix} | (1 - \hat{\rho}) \hat{F} | \tilde{\varphi}_{ix} \rangle \quad (2.27)$$

where $\hat{\rho}$ is the projector on the occupied subspace, defined by

$$\hat{\rho} = \sum_{ix} |\varphi_{ix}\rangle \langle \tilde{\varphi}_{ix}| = \sum_{ix} |\tilde{\varphi}_{ix}\rangle \langle \varphi_{ix}| \quad (2.28)$$

Equation 2.27 is transformed to obtain the variation of the energy with respect to the orbital coefficient:

$$\frac{\partial E_{tot}}{\partial C_{\mu ix}} = 2 \langle \chi_{\mu} | (1 - \hat{\rho}) \hat{F} | \tilde{\varphi}_{ix} \rangle \quad (2.29)$$

The lowest energy is obtained when the gradient 2.29 vanishes

$$\langle \chi_{\mu} | (1 - \hat{\rho}) \hat{F} | \tilde{\varphi}_{ix} \rangle = 0 \quad (2.30)$$

In the original Stoll paper, two methods are described to realize the gradient condition. The first transforms Equation 2.30 into an eigenvalue equation, which can then be solved by iterative diagonalization, and the second approximates the hessian of the orbital coefficients to allow for a direct minimization. To transform Equation 2.30 into an eigenvalue equation, a projector on the subspace of fragment x is defined:

$$\hat{\rho}^{(x)} = \sum_i |\tilde{\varphi}_{ix}\rangle \langle \varphi_{ix}| \quad (2.31)$$

Equation 2.30 is rewritten using properties of $\hat{\rho}^{(x)}$

$$\langle \chi_{\mu} | \tilde{F}^{(x)} - \varepsilon_{ix} | \varphi_{ix} \rangle = 0 \quad (2.32)$$

with $\varepsilon_{ix} = \langle \tilde{\varphi}_{ix} | \hat{F} | \tilde{\varphi}_{ix} \rangle$ and $\tilde{F}^{(x)}$ is the transformed Fock matrix

$$\tilde{F}^{(x)} = \left(1 - \hat{\rho} + \hat{\rho}^{(x)T} \right) \hat{F} \left(1 - \hat{\rho} + \hat{\rho}^{(x)} \right) \quad (2.33)$$

Diagonalization of $\tilde{F}^{(x)}$ for each fragment x yields new strictly localized orbitals φ_{ix} , which are used to build new biorthogonal orbitals $\tilde{\varphi}_{ix}$ and new projected Fock matrices $\tilde{F}^{(x)}$. The process is repeated iteratively to self-consistency.

Very similar equations have been derived by Gianinetti et al. in matrix form^{38,116} and by Nagata et al.^{37,117} The difference between the three versions resides in the definition of the fragment projection operator and in the final form of the equations, as shown by the clear summary of Khaliullin et al.⁴¹ Although they have slightly different computational costs, the three different final equations all give the same result.

The second method to optimize the orbitals to satisfy Equation 2.30 is to directly vary the orbital coefficients. The total energy is a function of these coefficients and one applies a multidimen-

sional direct minimization procedure without any diagonalization. The gradient of the orbital coefficients is already available, however efficient minimization algorithms require at least an approximation to the matrix of second derivatives, *i.e.*, an approximation to the Hessian.¹¹⁸ Moreover, the orthogonalization constraints of the orbitals should be properly handled,¹¹⁹ for example by using an appropriate variable transformation¹²⁰ or techniques inspired from geometric considerations.¹²¹

2.3.2 Applications of SLOs

The previous section introduces the equations to optimize SLOs. At least three different versions of eigenvalue equations for SLOs exist, and SLOs themselves exist and are used under different terminologies: Locally Projected Self-Consistent Field for Molecular Interactions (LP-SCF MI),^{37,38} Extremely Localized Molecular Orbitals (ELMO),³⁹ Block-Localized Wavefunction (BLW),⁴⁰ Absolutely Localized Molecular Orbitals (ALMO)⁴¹ or Non-Orthogonal Localized Molecular Orbitals (NOLMO).⁴² Strictly-Localized Molecular Orbitals (SLMO)¹²² are similar in spirit but are expressed in terms of a few atomic hybrid functions¹²³ whose relative contributions are optimized and, hence, they do not obey the equations of the previous section and were originally designed for semi-empirical methods.¹²⁴ The original definition of SLOs permit a basis function to be shared between different orbitals.^{39,125}

The SCF for Molecular Interaction (SCF MI) method was originally developed to suppress the BSSE in interaction energy computations.³⁸ Because of the strict localization imposed on the SLOs, it is clear that BSSE is absent from these computations, however since fewer variational parameters are used than in a HF wavefunction, the energy must be substantially higher. This is indeed the case, and physically important terms were shown to be suppressed in the SCF MI approach by Hamza et al.¹²⁶ Moreover, it can be shown analytically that the strict localization of the orbitals implies a zero charge transfer in the Mulliken sense.³⁷ The deficiency of the charge transfer term can be corrected by expanding the energy using perturbation theory and including only single excitations. The corrected LP-SCF-MI method then reproduces results of the Boys and Bernardi correction. Independently, a similar correction was devised for the ELMO method.¹²⁷ Instead of using perturbation theory, singly excited determinants are explicitly included in the wavefunction to obtain a Valence Bond-like expansion. The coefficients in front of each determinant are then optimized.

The missing charge transfer term in SLO computations is convenient in energy decomposition analysis. In the spirit of Kitaura-Morokuma (KM) analysis,¹²⁸ the wavefunction of isolated monomers may be computed and relaxed progressively to yield physically meaningful energies. The first of these SLO-based energy decomposition schemes was the Block-Localized Wavefunction Energy Decomposition (BLW-ED).¹²⁹ Four different energetic terms were defined. The electrostatic energy corresponds to the interaction of the two frozen monomer wavefunctions with no further antisymmetrization, and the exchange energy corresponds to the effect of adding the antisymmetrization. Electrostatic and exchange terms are obtained in the same way in the Kitaura-Morokuma energy decomposition.¹²⁸ Polarization is the energetic effect of relaxing the antisymmetrized monomer wavefunctions in the field of the partner molecule, preventing orbital delocalization by using SLOs. Since orbitals do not delocalize, charge transfer effects are ab-

sent from polarization by definition. Finally, charge transfer is the energetic effect of completely relaxing the total wavefunction by allowing orbital delocalization. The charge transfer energy is corrected for the BSSE. The same energy decomposition scheme was rederived in the framework of the ALMO method a few years later.¹³⁰ In the ALMO-EDA scheme, charge transfer is further decomposed into forward/backward donation and higher-order terms. Finally, the addition of a density-dependent pairwise dispersion correction⁵⁰ to the final wavefunction yields the dispersion contribution to the interaction energy.¹³¹ Although the KM analysis is very similar to these SLO-based EDA, there is one major difference: in the KM analysis, the polarization and charge transfer terms are determined separately. Polarization represents the effect of relaxing the occupied orbitals of one monomer in the virtual space of the same monomer, and charge transfer the effect of relaxing the occupied orbitals in the virtual space of the partner monomer. Since the virtual spaces of the two monomers are generally overlapping, polarization and charge transfer overlap in the KM analysis, and an additional non-physical "mixing" term is added to correct for the remaining error.

In summary, strictly localized orbitals are expressed only using a fraction of the basis functions of a system and thus are perfectly localized. SLOs can be optimized in the sense that they variationally lead to the lowest possible energy with the imposed constraint. When applied to the interaction of two monomers, SLOs suppress the BSSE and the physically important charge transfer term. Corrections to recover the charge transfer exist, however the Boys and Bernardi or the CHA/CE approaches are more efficient in providing BSSE-free energies. The missing charge transfer term allows energy decomposition analysis to be derived from SLOs, including electrostatic, exchange, polarization and charge transfer. Empirical dispersion corrections then provide the missing dispersion term. Strictly localized orbitals have hence found many different applications, such as insight into physical terms of interacting systems,^{129–132} the role of electronic delocalization in rotational barriers,^{42,133–136} resonance effects,¹³⁷ applications in QM/MM methods¹³⁸ or efficient approximations to electronic densities.¹³⁹ In Section 3.2.2, their properties are exploited to localize electrons on specific molecular fragments.

3 Exploration of Zeroth-Order Wavefunctions and Energies for Intramolecular Symmetry-Adapted Perturbation Theory

3.1 Introduction

Molecular interactions play a fundamental and omnipresent role in chemistry and biology. Their decomposition into physically meaningful energy terms is not only essential to our understanding of most chemical processes but also emphasizes the predicting power of theoretical methods. Many different methods were developed for the analysis of intermolecular interactions. In the early seventies, Kitaura and Morokuma¹²⁸ designed their well-known energy decomposition scheme which leads to electrostatics, exchange, polarization and charge transfer components for a molecular dimer. Since then, many related schemes have been devised, based on strict orbital localization,^{129,130} on variations and extensions of the original Kitaura-Morokuma^{140–146} and on natural orbitals.^{147,148} These methods use constraints on the wavefunction optimization to obtain energy differences related to the physical term desired. The electrostatic energy is usually obtained as the interaction of frozen monomer wavefunctions, the exchange energy by allowing the same interaction and antisymmetrizing the wavefunction properly. The next terms are usually computed by allowing the wavefunction to relax in a controlled manner.

A slightly different philosophy exploits specific orbital pairwise interactions^{134,149,150} rather than wavefunctions to obtain intermolecular energies. In this case, orbitals should be localized in a way that attributes interactions to specific bonds or functional groups inside a molecule. The interaction between the orbitals is computed by perturbation theory or by modifying their coupling. Localization of the orbitals is obtained by constraining them to have non-zero coefficients on a subspace of the full basis only. The orbitals are then forced to extend over certain atoms or group of atoms only. Strict localization of orbitals was used under many different terminologies, as was already mentioned in Section 2.3.2: Locally Projected Self-Consistent Field for Molecular Interactions (LP-SCF MI),³⁷ Extremely Localized Molecular Orbitals (ELMO),¹³³ Block-Localized Wavefunction (BLW),⁴⁰ Absolutely Localized Molecular Orbitals (ALMO)...⁴¹ All of these methods ultimately lead to the same orbitals, although the optimization algorithm varies.

Chapter 3. Exploration of Zeroth-Order Wavefunctions and Energies for Intramolecular Symmetry-Adapted Perturbation Theory

Other intermolecular energy decomposition schemes relied on different criteria: the use of molecular symmetry to separate energetic contributions,¹⁵¹ partitionings of the Hamiltonian itself,^{33,35,152} or real-space partitionings of the electronic density.¹⁵³ Among them, the Chemical Hamiltonian³³ (CHA)-based schemes are of particular relevance in the present context. By using the second-quantized formalism for non-orthogonal atomic orbitals and projection operators, CHA partitions the Hamiltonian into intra- and interatomic terms as summarized in Section 2.2. Different energy decompositions are then derived from this partitioning (see Section 2.2.2).

Alternatively, linear-scaling fragment approaches^{154–158} naturally decompose the total intermolecular interaction energy into different physical terms. The form of the different physical contributions often originates from one of the others above mentioned energy decomposition schemes. In particular, the Local MP2 method provides access to dispersion interactions between different fragments¹⁵⁸ by decomposing the MP2 correlation energy.

Since most of the schemes described previously are based on a decomposition of Hartree-Fock or Kohn-Sham energies, they do not account for dispersion contributions. This is not the case of the perturbational family of intermolecular decomposition schemes.^{159,160} Among them, the most successful is probably the Symmetry-Adapted Perturbation Theory (SAPT).³⁰ Starting from monomer wavefunctions, this scheme derives the total dimer interaction energy by perturbation theory, whereby the different physical terms such as electrostatics, exchange, induction and dispersion arise naturally.

The numerous schemes mentioned up to here are primarily devised for analysing intermolecular interactions. Some of them could be applied to intramolecular interactions, but currently only in two ways. The first alternative uses fragment-based methods by partitioning the molecule and computing the interaction between the fragments, using for example the Fragment Molecular Orbital (FMO) method^{155,161} or SLOs. Covalent bonds then must be broken, hence the interaction is computed between an ensemble of radicals and not between intramolecular fragments. The second approach relies upon the analysis of the molecular wavefunction. In the Natural Bond Orbital (NBO) method,¹⁴⁹ the wavefunction is decomposed in terms of natural localized orbitals and donor-acceptor interactions between them. Alternatively, the Interacting Quantum Atoms (IQA)¹⁶² decomposition fractions the molecular density in real space basins and computes their pairwise interactions. However, analysis of the molecular wavefunction is likely to lead to poor induction and dispersion energies since it automatically excludes the wavefunction relaxation effects from the intramolecular interaction energy. Hence, the tools to analyze intramolecular interactions are rather scarce as compared to their intermolecular congeners. Yet, intramolecular interactions are equally important, as illustrated by their role in enzymatic activity,¹⁶³ energetic differences of structural isomers,¹⁶⁴ design of optical materials,^{165,166} conformations of metal complexes¹⁶⁷ or peptides,¹⁶⁸ to quote only a few examples.

The present chapter describes the first step toward an energy decomposition scheme specifically designed for the analysis of non-covalent intramolecular interactions. Desired character-

istics of the developed theoretical model include high accuracy and the possibility of including dispersion interactions. SAPT fits these criteria³⁰ for intermolecular interaction computations. After decades of development, efficient implementation of high-order SAPT terms^{84,169} allows very accurate computation and decomposition of intermolecular energies.^{170–173} An intramolecular version of SAPT thus would fit our target. The first step, fundamental to the derivation of any perturbation theory correction, is the definition of a zeroth-order wavefunction, the subject of the present chapter.

Recently, Yamada and Koga^{174,175} developed the space-restricted wavefunction (SRW) formalism to obtain variationally determined electronic states allowing for the computation of intramolecular interactions. Their approach is similar to the generalized¹²⁵ BLW⁴⁰ method: different subspaces of the full basis set are defined, and orbitals have non-zero coefficients only on basis functions belonging to one subspace. Moreover, basis functions may share different subspaces. The SRW formalism differs from general BLW by defining an occupied and a virtual space for each basis function subspace, and allowing orbitals to vary only within these occupied and virtual spaces. Instead of basing their subsequent energy decomposition analysis (EDA) on perturbation theory, Yamada and Koga use the Kitaura-Morokuma philosophy, by allowing their space-restricted Hartree Fock wavefunction to relax to the canonical Hartree-Fock wavefunction in different steps corresponding to the addition of different interactions. The first step is then to obtain a zeroth-order electronic state, denoted subspace-isolated Hartree-Fock (SIHF), where all subspaces are isolated from each other. In principle, such a state would be convenient as a zeroth-order wavefunction for SAPT. However, although the SIHF state is mentioned, the authors show no wavefunction or energetic results for this state, and details of SIHF orbital optimization are awaiting publication at this time. Since no details on how the SIHF state would be obtained are available, a comparison with the present work is impossible.

Section 3.2 defines the zeroth-order energy and wavefunction, on top of which the intramolecular version of SAPT will be built in future work. We first introduce the zeroth-order energy based on the Chemical Hamiltonian concepts⁵⁷ as well as the scheme to optimize the orbitals. Then, the possibility to strictly localize the electrons on the different molecular fragments will be discussed and the corresponding equations formulated. Finally, the failure of simpler and more intuitive formalisms will be briefly mentioned. Section 3.3 presents results for prototype systems. Issues of basis set dependence, reproduction of well-known chemical trends and application to non-equilibrium geometries are investigated, along with the influence and energetic consequences of the electronic localization. Intramolecular hydrogen bonds and intermolecular systems serve to assess the relevance of the derived absolute energies. The formalism and the results are summarized in Section 3.4. The wavefunction is shown to be successfully optimized, and the chemical trends qualitatively reproduced. Possible improvements toward better quantitative energetics are finally discussed.

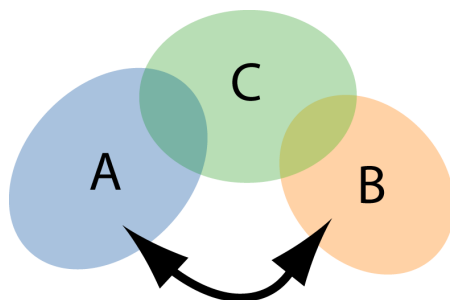


Figure 3.1: Scheme of the molecular partitioning. The interaction of interest between fragments A and B is symbolized by a black arrow. Fragment C contains all atoms not included in fragments A and B. Covalent bonds between fragments are symbolized by overlap of their colors.

3.2 Zeroth-order wavefunction from non-hermitian operators

As mentioned in **Chapter 2**, intermolecular SAPT uses the energies and wavefunctions of isolated monomers as a starting point. Perturbation theory then corrects for the modifications induced by the intermolecular interactions. This section introduces a zeroth-order wavefunction $\Psi^{(0)}$ suitable for prospective development of intramolecular SAPT. Although for intermolecular interactions, the zeroth-order wavefunction is easily constructed from monomer wavefunctions, the intramolecular $\Psi^{(0)}$ is much more challenging since the wavefunction should exclude interactions between the two fragments of interest, but preserve the molecular structure. For this purpose, one considers a hypothetical molecular system, that is composed of N_{nuc} nuclei, N electrons and M basis functions. The system is divided into three fragments: the interacting fragments A and B, and fragment C containing all the other atoms in the molecule (see Figure 3.1). Fragments A and B can correspond to any single atom or group of atoms within a molecule, under the condition that no covalent bond exists between A and B.

3.2.1 Chemical Hamiltonian partitioning

The CHA concept was introduced in Section 2.2, thus only the essential points are repeated here. CHA introduces a partitioning of the Hamiltonian into intra- and interatomic terms, allowing a derivation of energy decomposition schemes (see Section 2.2.2). The zeroth-order wavefunction we intend to derive in this chapter requires identification of the interaction energy terms between fragments A and B, which is achieved through the CHA-based energy decomposition analysis described below.

To obtain the zeroth-order wavefunction, we derive an energy expression excluding any interaction between fragments A and B. The best available CHA-based energy decomposition analysis is the ideal starting point, but it contains orbital-dependent corrections as described in the end of Section 2.2.2. Since orbitals are optimized in the zeroth-order wavefunction, an orbital-independent energy decomposition is desirable, hence the orbital-dependent correction is removed from the energy partitioning, and the corresponding equations for the intra- and

3.2. Zeroth-order wavefunction from non-hermitian operators

interatomic energies are equivalent to Equations 2.22 describing $E^{1'}$:

$$\begin{aligned} E_A^{1'} &= E_A^1 - \sum_{B \neq A} \delta_{AB} \\ E_{AB}^{1'} &= E_{AB}^1 + \delta_{AB} + \delta_{BA} \end{aligned} \quad (3.1)$$

where

$$\begin{aligned} \delta_{AB} &= \sum_{\mu \in A} \sum_{\nu \in B} D_{\mu\nu} \langle \chi_\nu | (1 - \hat{P}_A) \hat{h}^A | \chi_\mu \rangle \\ &+ \frac{1}{2} \sum_{\mu, \rho \in A} \sum_{\nu, \tau \in AB} (D_{\mu\nu} D_{\rho\tau} - P_{\rho\nu}^\alpha P_{\mu\tau}^\alpha - P_{\rho\nu}^\beta P_{\mu\tau}^\beta) \\ &\times \left\langle \chi_\nu \chi_\tau | (1 - \hat{P}_A) (\mathbf{r}_1) (1 - \hat{P}_A) (\mathbf{r}_2) \frac{1}{r_{12}} | \chi_\mu \chi_\rho \right\rangle \end{aligned} \quad (3.2)$$

$$\begin{aligned} E_A^1 &= \sum_{\mu \in A} \sum_{\nu} D_{\mu\nu} h_{\nu\mu}^A + \frac{1}{2} \sum_{\mu, \rho \in A} \sum_{\nu\tau} (D_{\mu\nu} D_{\rho\tau} - P_{\rho\nu}^\alpha P_{\mu\tau}^\alpha - P_{\rho\nu}^\beta P_{\mu\tau}^\beta) \langle \chi_\nu \chi_\tau | \chi_\mu \chi_\rho \rangle \\ E_{AB}^1 &= \frac{Z_A Z_B}{R_{AB}} - \sum_{\mu \in A} \sum_{\nu} D_{\mu\nu} \left\langle \chi_\nu | \frac{Z_B}{r_B} | \chi_\mu \right\rangle - \sum_{\mu \in B} \sum_{\nu} D_{\mu\nu} \left\langle \chi_\nu | \frac{Z_A}{r_A} | \chi_\mu \right\rangle \\ &+ \sum_{\mu \in A} \sum_{\rho \in B} \sum_{\nu\tau} (D_{\mu\nu} D_{\rho\tau} - P_{\rho\nu}^\alpha P_{\mu\tau}^\alpha - P_{\rho\nu}^\beta P_{\mu\tau}^\beta) \langle \chi_\nu \chi_\tau | \chi_\mu \chi_\rho \rangle \end{aligned} \quad (3.3)$$

and the different quantities have been defined in Section 2.2.

For the energy partition $E^{1'}$ to be suitable for orbital optimization, it was necessary to introduce two modifications. First, fragments A and C are covalently bound, as are fragments B and C. These covalent bonds should be maximally preserved during orbital optimization, and for this purpose the projectors \hat{P}_A and \hat{P}_B are replaced by \hat{P}_{AC} and \hat{P}_{BC} in Equation 3.2, projecting on the pair of fragments AC or BC. \hat{P}_{AC} is defined as

$$\hat{P}_{AC} = \sum_{\gamma\delta \in AC} |\chi_\gamma\rangle (\mathbf{S}^{(AC)})_{\gamma\delta}^{-1} \langle \chi_\delta| \quad (3.4)$$

where $\mathbf{S}^{(AC)}$ is the overlap matrix of the basis functions on A and C, and a similar definition holds for \hat{P}_{BC} . Then, three- and four-center integrals, which were not partitioned in Mayer's original work,³⁵ are also submitted to projection on AC or BC according to their kets. Although three- and four-center integrals have negligible values in the energy decomposition, justifying Mayer's choice, a better convergence behaviour of the zeroth-order wavefunction was observed

Chapter 3. Exploration of Zeroth-Order Wavefunctions and Energies for Intramolecular Symmetry-Adapted Perturbation Theory

upon their inclusion. The zeroth-order energy is then written as:

$$\begin{aligned}
 E^{(0)} = & \sum_{I,J \notin AB} \frac{Z_I Z_J}{R_{IJ}} + \sum_{\mu\nu} D_{\mu\nu} \langle \chi_\nu | \hat{V}_C | \chi_\mu \rangle + \sum_{\mu \in A} \sum_{\nu}^M D_{\mu\nu} \langle \chi_\nu | \hat{P}_{AC} \hat{h}_A | \chi_\mu \rangle \\
 & + \sum_{\mu \in B} \sum_{\nu}^M D_{\mu\nu} \langle \chi_\nu | \hat{P}_{BC} \hat{h}_B | \chi_\mu \rangle + \sum_{\mu \in C} \sum_{\nu}^M D_{\mu\nu} \langle \chi_\nu | \hat{V}_A + \hat{V}_B + \hat{T} | \chi_\mu \rangle \\
 & + \frac{1}{2} \sum_{\mu, \rho \in A} \sum_{\nu\tau}^M K_{\mu\nu\rho\tau} \left\langle \nu\tau | \hat{P}_{AC}(\mathbf{r}_1) \hat{P}_{AC}(\mathbf{r}_2) \frac{1}{r_{12}} | \mu\rho \right\rangle \\
 & + \frac{1}{2} \sum_{\mu, \rho \in B} \sum_{\nu\tau}^M K_{\mu\nu\rho\tau} \left\langle \nu\tau | \hat{P}_{BC}(\mathbf{r}_1) \hat{P}_{BC}(\mathbf{r}_2) \frac{1}{r_{12}} | \mu\rho \right\rangle \\
 & + \frac{1}{2} \sum_{\mu, \rho \notin \{AB\}} \sum_{\nu\tau}^M K_{\mu\nu\rho\tau} \langle \nu\tau | \mu\rho \rangle
 \end{aligned} \tag{3.5}$$

where the notation $\mu, \rho \notin \{AB\}$ means that at least μ or ρ belongs to C, and the notation $I, J \notin AB$ means that if $I \in A$, then $J \notin B$ and vice-versa. Equation 3.5 can be rewritten simply as

$$E^{(0)} = \sum_{I,J \notin AB} \frac{Z_I Z_J}{R_{IJ}} + \frac{1}{2} \sum_{\mu\nu} P_{\mu\nu}^\alpha (F_{\nu\mu}^\alpha + h_{\nu\mu}) + \frac{1}{2} \sum_{\mu\nu} P_{\mu\nu}^\beta (F_{\nu\mu}^\beta + h_{\nu\mu}) \tag{3.6}$$

where the one-electron \mathbf{h} matrix is defined as

$$h_{\nu\mu} = \langle \chi_\nu | \hat{V}_C | \chi_\mu \rangle + \begin{cases} \langle \chi_\nu | \hat{P}_{AC} \hat{h}_A | \chi_\mu \rangle & \text{if } \mu \in A \\ \langle \chi_\nu | \hat{P}_{BC} \hat{h}_B | \chi_\mu \rangle & \text{if } \mu \in B \\ \langle \chi_\nu | \hat{V}_A + \hat{V}_B + \hat{T} | \chi_\mu \rangle & \text{if } \mu \in C \end{cases} \tag{3.7}$$

and the Fock matrix \mathbf{F}^σ where σ can be either α or β :

$$F_{\nu\mu}^\sigma = h_{\nu\mu} + \begin{cases} D_{\rho\tau} \left\langle \nu\tau | \hat{P}_{AC} \hat{P}_{AC} \frac{1}{r_{12}} | \mu\rho \right\rangle - P_{\rho\tau}^\sigma \left\langle \nu\tau | \hat{P}_{AC} \hat{P}_{AC} \frac{1}{r_{12}} | \rho\mu \right\rangle & \text{if } \mu, \rho \in A \\ D_{\rho\tau} \left\langle \nu\tau | \hat{P}_{BC} \hat{P}_{BC} \frac{1}{r_{12}} | \mu\rho \right\rangle - P_{\rho\tau}^\sigma \left\langle \nu\tau | \hat{P}_{BC} \hat{P}_{BC} \frac{1}{r_{12}} | \rho\mu \right\rangle & \text{if } \mu, \rho \in B \\ D_{\rho\tau} \langle \nu\tau | \mu\rho \rangle - P_{\rho\tau}^\sigma \langle \nu\tau | \rho\mu \rangle & \text{if } \mu, \rho \notin \{AB\} \end{cases} \tag{3.8}$$

Since the bra and the kets are not treated in the same way, the Fock matrix is non-hermitian. Orbital optimization based on non-hermitian Fock matrices was detailed earlier in this thesis in the context of the CHA application to the BSSE problem in Section 2.2.1. Although a non-hermitian Fock matrix is formally not associated with physical quantities, the CHA/CE method⁵⁷ demonstrates that orbitals are still successfully optimized, resulting in reasonable energies. Our orbital optimization resorts to similar techniques, with a modification of the hermitization step of the Fock matrix. Instead of using the diagonal blocks of the full Fock matrix (which would restore interaction between A and B), the lower triangular part of the block is copied to the upper triangular one. Although formally similar to CHA/CE, our method does use only one energy expression for orbital optimization and energy evaluation, and eliminates a physical interaction from the Hamiltonian.

3.2.2 Electron localization

The definition of the molecular fragments is straightforward at the nuclear level, however the distribution of the electrons among fragments deserves special attention. If the wavefunction is a Slater determinant, then each electron is assigned to a spin-orbital. Hence they are usually delocalized over the whole system, including the two fragments A and B. Localizing sets of electrons on each fragment is more appealing since each particle can be attributed to a fragment easily. Moreover, such a localization is similar to intermolecular SAPT, where each electron is associated with one monomer. This localization is achieved using strictly localized orbitals, as detailed in Section 2.3. The density matrix in terms of SLOs is written:³⁶

$$\mathbf{P}^\sigma = \mathbf{C}^\sigma \mathbf{V}^{\sigma-1} \mathbf{C}^{\sigma\dagger} \quad (3.9)$$

where $\mathbf{V}^\sigma = (\mathbf{C}^{\sigma\dagger} \mathbf{S} \mathbf{C}^\sigma)$ is the overlap matrix of the occupied orbitals, \mathbf{C} contains the orbital coefficients and σ can be α or β spin. The Fock matrix is transformed prior to the hermitization procedure according to Section 2.3.1, where x is an arbitrary fragment:

$$\tilde{F}^{(x)} = \left(1 - \hat{\rho} + \hat{\rho}^{(x)T}\right) \hat{F} \left(1 - \hat{\rho} + \hat{\rho}^{(x)}\right) \quad (3.10)$$

where $\hat{\rho}$ is the projector on the occupied space

$$\hat{\rho} = \sum_{ix} |\varphi_{ix}\rangle \langle \tilde{\varphi}_{ix}| = \sum_{ix} |\tilde{\varphi}_{ix}\rangle \langle \varphi_{ix}| \quad (3.11)$$

and $\hat{\rho}^{(x)}$ the projector on fragment x space

$$\hat{\rho}^{(x)} = \sum_i |\tilde{\varphi}_{ix}\rangle \langle \varphi_{ix}| \quad (3.12)$$

$\tilde{F}^{(x)}$ is then hermitized and diagonalized to yield strictly localized orbitals on fragment x . As already noted, Equations 2.19 and 2.30 can both be related to the Brillouin theorem, which validates the use of SLOs within a non-hermitian formalism. This partitioning of electrons among fragments using localized orbitals is denoted MO-partitioning in the following.

Since SLOs extend only over one fragment, interfragment bonds must be broken. The resulting radical fragments are still interacting through their singly occupied orbitals, to which electrons of opposite spins are attributed. If the two singly occupied orbitals are denoted $|\varphi^X\rangle$ and $|\varphi^Y\rangle$, each bond is described by the product

$$|\varphi^X \varphi^Y\rangle (\alpha\beta) \quad (3.13)$$

Since $|\varphi^X\rangle$ and $|\varphi^Y\rangle$ have different spatial parts, function 3.13 is not a spin eigenfunction. A correct description of the bonds should make use of a spin-coupling scheme similar to those used in Valence Bond theory.¹⁷⁶ Each pair of bonding functions is then multiplied by a proper

Chapter 3. Exploration of Zeroth-Order Wavefunctions and Energies for Intramolecular Symmetry-Adapted Perturbation Theory

singlet spin function

$$\frac{1}{\sqrt{2}}|\varphi^X\varphi^Y\rangle(\alpha\beta - \beta\alpha) \quad (3.14)$$

In this description, four Slater determinants are introduced if two interfragment bonds are broken. Given that the purpose of the present implementation is to assess the validity of the approach chosen for the zeroth-order wavefunction, spin-coupling is not yet introduced in the code, and importance of spin-contamination is evaluated by computing the expectation value of the spin \hat{S}^2 operator.

The MO-partitioning of the electrons through the SLOs may provide a more physical picture of the non-interacting system, but it also suppresses charge transfer between fragments A and C, and between fragments B and C, which are still expected to fully interact. Consequently, the interaction energy probed when using the SLOs (*vide infra*) has a different meaning and magnitude than if using a canonical reference. For comparison, we also investigate an alternative electron partitioning using delocalized orbitals. The attribution of electrons to fragments is then based on the Mulliken gross AO populations:⁹⁵ the population of a basis function is attributed to its central atom. The resulting partitioning is denoted AO-partitioning, and does not suffer from spin problems since bonding orbitals are not broken. Density matrices are then defined as:

$$\mathbf{P}_{\mu\nu}^{\sigma} = \sum_i^{occ} \mathbf{C}_{\mu i}^{\sigma} \mathbf{C}_{\nu i}^{\sigma} = (\mathbf{C}^{\sigma} \mathbf{C}^{\sigma\dagger})_{\mu\nu} \quad (3.15)$$

where \mathbf{C} contains the orbital coefficients and σ can be α or β spin. Both the AO-partitioning and the MO-partitioning are applied and compared in this chapter.

3.2.3 Relevance of the non-hermitian formalism

The zeroth-order wavefunction introduced above is not the only possible formalism to eliminate the interaction between two molecular fragments. Prior to discussing our results using the non-hermitian scheme, we provide a brief summary of our previous attempts. Two other families of zeroth-order wavefunctions were also tried: approximations based on localized orbitals from a Hartree-Fock wavefunction, and a hermitian formalism symmetrically interpreting the electronic integrals to selectively eliminate them.

The first attempt to obtain SAPT-like energies for the intramolecular case was very simple. Localized orbitals were computed from the molecular Hartree-Fock wavefunction using three localization methods, *i.e.*, Pipek-Mezey,¹¹³ Boys¹¹⁴ and Natural Localized Molecular Orbitals (NLMOs).¹⁴⁹ Localized orbitals were simply inserted into the intermolecular SAPT first-order formula for electrostatics. Such a crude method is likely to be inaccurate as it neglects orbital relaxation. The magnitude of the error was assessed by application of the scheme to intermolecular systems and comparison with the canonical SAPT results. Localized orbitals and electrostatic contribution $E_{pol}^{(1)}$ were then computed for a dimer. Results are presented below for the water and the methane dimers. The geometries are taken from the S22 database,¹⁷⁷ and the cc-pVDZ¹⁷⁸ basis set is used.

3.2. Zeroth-order wavefunction from non-hermitian operators

Table 3.1: $E_{pol}^{(1)}$ (in kcal/mol) for intermolecular and intramolecular SAPT. Orbitals optimized with the standard Hartree-Fock procedure.

$E_{pol}^{(1)}$ in kcal/mol	SAPT inter ^a	Boys ^b	Pipek ^b	NLMOs ^b
(H ₂ O) ₂	-9.10	-22.80	-21.69	-22.41
(CH ₄) ₂	-0.13	-0.68	-0.64	-0.62

^aResults obtained with intermolecular SAPT.

^bResults obtained with intramolecular SAPT and SCF orbitals localized with the indicated method.

As expected, we observe large errors in the interaction energy components. Their origin can in part be attributed to the localization tails of the orbitals. Truncation of the tails and appropriate reorthogonalization improved the energetics for water, but worsened them significantly for the methane dimer. Use of strictly localized orbitals projected from the HF wavefunction¹⁷⁹ was equally unsuccessful.

The second attempt aimed to define a zeroth-order wavefunction, similar to the present work. For this purpose, we chose a symmetric (*i.e.*, Hermitian) interpretation of the electronic integrals to identify those involved in the interaction between fragments A and B. $\langle \mu | \hat{V} | \nu \rangle$ then represents the interaction of an electron delocalized on μ and ν with the potential in \hat{V} , and $\langle \nu \tau | \mu \rho \rangle$ the interaction of an electron delocalized on μ and ν with an electron delocalized on ρ and τ . Integrals were then divided into different classes depending on which center the basis functions are localized. Some integral classes should obviously be kept, like $\langle AC | AC \rangle$ since it represents the interaction of an electron on A with an electron on C, and some others should obviously be deleted like $\langle AB | AB \rangle$, which represents the interaction of an electron on A with an electron on B. Whether to keep or delete some other integral classes may be ambiguous, like $\langle AB | CC \rangle$ representing the interaction of an electron on AC with an electron on BC.

Different choices gave rise to different variants of the zeroth-order wavefunction that we implemented. Further variants were obtained by modifying the wavefunction antisymmetry to suppress all electron exchanges between fragments A and B. All of these Hermitian variants led to undesired energy behaviour upon optimization. Frequently, the energy did not converge and became excessively negative, several thousands Hartree below the Hartree-Fock energy, which was interpreted as a variational collapse. Some combinations of basis sets and systems converged yet led to excessive energy values of hundreds or thousands of kcal/mol for non-covalent interactions, casting doubt on their physical meaning. Corrections by *ad hoc* modifications of the algorithm, *i.e.*, freezing orbitals or deleting selected energy terms from the orbital optimization, were not satisfactory.

All Hermitian variants had reasonable total energies for the guess orbitals, with problematic characteristics only occurring upon optimization. It would be extremely useful to be able to predict the convergence behaviour of trial energy functions in quantum methods, however this seems unfeasible at present, and the only possible validation was implementation and numerical experiments. From the experience acquired by implementing different energy expressions,

Chapter 3. Exploration of Zeroth-Order Wavefunctions and Energies for Intramolecular Symmetry-Adapted Perturbation Theory

convergence is possible only when a rigorous balance between the different physical terms is achieved. This balance is quite challenging to achieve, partially because of the overlap of the basis functions: eliminated integrals may be partially described by those kept in the energy expression. However, more detailed studies are needed to confirm this hypothesis.

3.3 Results and discussion

The zeroth-order energy expression derived in Section 3.2.1 leads to the zeroth-order wavefunction $\Psi^{(0)}$ upon orbital optimization. $\Psi^{(0)}$ allows the computation of the intramolecular interaction energy by comparison of $E^{(0)}$ with the total energy of the appropriate reference wavefunction. In the case of the AO-partitioning, this reference is simply the canonical Hartree-Fock energy, since both wavefunctions use delocalized orbitals. The MO-partitioning uses SLOs, hence the zeroth-order energy in this case is compared to the energy of the SLO wavefunction with all interactions included, but orbitals strictly localized in both cases. The computed intramolecular interaction energy contains contributions from electrostatics, exchange and induction, but no electron correlation (hence no dispersion) since it is based on a single-determinantal wavefunction in all cases.

The method developed herein is completely general and can be applied to any non-covalent intramolecular interactions. Once perturbation theory developments allow the computation of intramolecular dispersion, detailed investigations of many intramolecular phenomena will be possible. These include dispersion-driven isomerism^{180,181} whereby large acenes and alkanes adopt open or closely packed conformations, study of intramolecular halogen bonds,¹⁸² conformational analysis,¹⁸³ intramolecular hydrogen bonds¹⁸⁴ and alkane branching. This last interaction motivated the following application.

Since the 1930s, scientists have known^{185,186} that branched alkanes such as neopentane or isobutane are more stable than their linear counterparts, *n*-pentane and *n*-butane. However, the rationalization of this fact is still actively debated in the literature, particularly between two families of explanations as recently summarized by Schleyer.¹⁸⁷ The first postulates a global increase of attractive energy terms upon branching. The origin of this increase is greater electronic correlation upon branching for one part, as advanced early by Pitzer and Catalano,¹⁸⁸ and hyperconjugative interactions for the other part, either C-C-C geminal hyperconjugation¹⁸⁹ or delocalization between C-H to C-C bonds.^{190,191} The second family of explanations considers that alkane branching induces a lowering of repulsive terms. Originating in the work of Bartell in the 1960s,^{192–194} this explanation was defended most notably by Gronert^{195,196} in series of articles disputing the attractive model.^{197,198} In this context, a new, electron correlation based view of alkane branching stabilization was formulated by Wodrich et al.:¹⁹⁹ the protobranching model. Protobranching considers stabilizing 1,3-alkyl-alkyl interactions as the origin of the branching stabilization. Consequently, such interactions are also present in all linear alkanes, except ethane and methane.

Protobranching was strongly criticized by Gronert,²⁰⁰ notably on the missing origin of the attractive interaction. This point was studied in detail recently by Grimme²⁰¹ and Schleyer,¹⁸⁷

Table 3.2: Intramolecular interaction energy results for the two methyl groups in propane. Geometry optimized with HF/6-31G*. $\Delta E = E_{ref} - E^{(0)}$, all values in kcal/mol. The value of $\langle \hat{S}^2 \rangle$ is given in parentheses.

Basis set	AO-partitioning	MO-partitioning
	ΔE	ΔE
6-31G*	14.4	14.0 (0.94)
def2-SVP	11.7	17.1 (0.94)
cc-pVDZ	9.5	16.2 (0.87)
cc-pVTZ	18.4	19.1 (0.60)
6-311G(d,p)	12.0	16.3 (0.90)
6-311+G(d,p)	6.6	13.9 (0.87)

decomposing the correlation energies of branched alkanes into pairwise orbital contributions. In agreement with the protobranching model, an increase in electron correlation contributions from 1,3-alkyl-alkyl interactions plays an important role in stabilizing branched alkanes. To complete these studies, intramolecular SAPT would be an ideal tool providing a more exhaustive decomposition of the energy into physical terms. Consequently, propane is chosen as our main example to test the zeroth-order wavefunction derived above. The two fragments used for computing the interaction are the two terminal methyl groups, constituting a protobranch. In contrast to previous studies, the effect of wavefunction relaxation upon switching on the interaction is considered herein. Note however that the role of attractive dispersion interactions will not be elucidated at this stage as dispersion is an electron correlation effect arising only at second order in SAPT, and not in $\Psi^{(0)}$.

3.3.1 Basis set dependence

Since both the AO- and MO-partitionings of the electrons depend on the atomic character of the basis functions, we tested the basis set dependence of the intramolecular interaction energy for the case of the 1,3 methyl-methyl interaction in propane. Moreover, regarding the previous convergence difficulties encountered with the hermitian formalism (see Section 3.2.3), convergence properties with various basis sets are of interest. The molecular geometry of propane was optimized with HF/6-31G* and the intramolecular interaction energy was obtained with the specified partitioning and the 6-31G*,^{202,203} def2-SVP,^{204,205} cc-pVDZ,¹⁷⁸ cc-pVTZ,¹⁷⁸ 6-311G(d,p)²⁰⁶ and 6-311+G(d,p)^{206,207} basis sets. The use of diffuse functions in a method relying on the atomic character of the basis functions is expected to slightly deteriorate the results. Intramolecular interaction energies for the AO- and the MO-partitionings are presented in Table 3.2.

All basis sets presented here lead to convergence of the total energy. Computations were also performed with aug-cc-pVDZ, but in this case the AO-partitioning did not converge. Note, however, that no convergence accelerator is used, and an appropriate scheme could improve the situation.

The basis set dependence of the AO partitioning is undoubtedly significant, as the intramolecular

Chapter 3. Exploration of Zeroth-Order Wavefunctions and Energies for Intramolecular Symmetry-Adapted Perturbation Theory

interaction energy varies between 7 and 18 kcal/mol. Even basis sets of similar sizes give rise to variations of up to 6 kcal/mol. As expected, the introduction of diffuse functions also results in a significant variation of 6 kcal/mol, the origin of which is attributed to the lack of atomic character of the basis. The basis set dependence of the MO-partitioning is smaller: basis sets of similar size differ by 2-3 kcal/mol in the intramolecular interaction energy. The inclusion of diffuse functions again lowers the interaction energy, but not as dramatically. The weak effect of diffuse functions can be understood by considering that ΔE is computed using the energy of an SLO wavefunction as a reference. Consequently, fragment localization is comparable between the zeroth-order wavefunction and the SLO-based reference wavefunction, and only a minor additional error is included in the interaction. Note, however, that the aug-cc-pVDZ basis set gives an interaction energy of 35.1 kcal/mol, which arises from its more diffuse character in comparison to 6-311+G(d,p). The addition of polarization functions on H (*i.e.*, by going from 6-31G* to def2-SVP or cc-pVDZ) influences the energy much less than in the AO-partitioning case. This small basis set dependence of strictly localized orbitals was already observed in BLW.²⁰⁸

Finally, although all interactions are repulsive, no conclusion can be drawn regarding the protobranching model. First, the current model inherently lacks electron correlation, and second, the AO-partitioning energies likely are shifted by a constant repulsive amount, as discussed below. The MO-partitioning suffers less from this problem but it does not include hyperconjugation between fragments and it may underestimate the attractive energy terms in these cases. Nevertheless, the zeroth-order wavefunction applied to propane gives very encouraging results. Convergence was obtained for all cases in the MO-partitioning, with only one problematic case for the AO-partitioning. Moreover, all numbers obtained are of the same order and display values much lower than a C-C covalent bond dissociation energy, which was not the case for the previous attempts with hermitian schemes (see Section 3.2.3). The spin contamination of the MO-partitioning is quite significant, halfway between pure singlet and pure triplet value for all molecules. This is actually positive, since interaction energies are likely to be significantly improved by including the appropriate spin-coupling. These conclusions regarding spin coupling are valid for the following computations as well.

3.3.2 Chemical trends

Although the value itself of the intramolecular interaction is of interest to, for example, describe the repulsive or attractive nature of the interaction, the relative trends between different molecules are also of importance for chemistry. As an example, a series of substituted propanes $\text{CH}_3\text{CH}_2\text{X}$ (where X may be CH_3 , F, Cl, Br, CF_3 , CCl_3 or CBr_3) is considered, all geometries being optimized with HF/def2-SVP and the intramolecular energy computed for the 1,3-interaction between X and CH_3 .

Table 3.3 summarizes the results. Once again, for the cases studied, all energies converge and are on a reasonable chemical scale. Two factors determine relative intramolecular interaction energies in this studied series: the halogen size, which increases in the order $\text{F} < \text{Cl} < \text{Br}$, and the local dipoles of the halogen-carbon bonds, whose strength decreases in the order $\text{F} > \text{Cl} >$

Table 3.3: Intramolecular interaction results for the interaction between -X and -CH₃ in derivatives of propane. Geometry optimized and energies computed with HF/def2-SVP. $\Delta E = E_{ref} - E^{(0)}$, all values in kcal/mol. The value of $\langle \hat{S}^2 \rangle$ is given in parentheses.

-X group	AO-partitioning	MO-partitioning
	ΔE	ΔE
-CH ₃	11.7	17.1 (0.94)
-F	12.0	10.5 (1.22)
-Cl	12.9	10.3 (1.16)
-Br	13.7	10.4 (1.16)
-CF ₃	7.0	17.9 (0.95)
-CCl ₃	12.8	18.2 (0.96)
-CBr ₃	13.5	18.7 (0.97)

Br. Overall, the interaction energy is expected to be more and more repulsive going down the periodic table, as observed with both partitionings. The magnitude of the variation is smaller in the MO-partitioning, and for X=Cl, F, and Br the energy varies by only 0.2 kcal/mol, hence all three halogen atoms are considered to have roughly equal interactions. Inclusion of dispersion energies would likely change these trends.

The AO- and MO-partitionings are based on different orbitals and this is reflected in the results obtained, mainly on the relative interaction between CH₃...CH₃ and F...CH₃. The AO-partitioning predicts the interaction with F to be slightly more repulsive than with CH₃, whereas the MO partitioning predicts more attraction for F than for CH₃. Chemical intuition is more in line with the MO-partitioning results: an F atom is smaller than C, and thus also smaller than a methyl group. Moreover, the induced bond dipole should further reduce the repulsion. The AO-partitioning also predicts that replacing a single halogen atom by its trihalomethyl group does not increase repulsion, and even decreases it for fluorine. Overall, the AO-partitioning seems to enhance attractive effects of bond dipoles. Again, this seems counter-intuitive and favors the MO-partitioning and localization of each electron on only one fragment.

The performance of both partitioning schemes is also assessed based on an intuitively attractive hydrogen bonded (H-bonded) system. The interaction between the two OH groups in pentane-2,4-diol was computed and compared to intermolecular interaction energies in the water and methanol dimers. Pentane-2,4-diol and the methanol dimer were optimized at the HF/6-31G* level of theory, whereas the water dimer was frozen to reproduce the relative conformations of the two OH groups of pentane-2,4-diol. The two additional H atoms were fixed at a H-O bond distance of 0.95 Å, and a H-O-H bond angle near 110°. The two additional H atom form a dihedral angle H-O-O-H of -10°. The intermolecular interaction energies were computed by subtracting the energies of the monomers from the energy of the dimer, without applying corrections for the BSSE.

The intermolecular test cases on the water and methanol dimers all indicate an attractive interaction, in agreement with expectations for H-bonds. Surprisingly, the AO-partitioning predicts the

Chapter 3. Exploration of Zeroth-Order Wavefunctions and Energies for Intramolecular Symmetry-Adapted Perturbation Theory

Table 3.4: Intramolecular interaction results for representative H-bonded systems. Methanol and water dimer interaction energies computed with HF/6-31G*, no BSSE correction. Geometry optimized with HF/6-31G* except for the frozen water dimer. All values in kcal/mol. The value of $\langle \hat{S}^2 \rangle$ is given in parentheses.

	pentanediol		(MeOH) ₂	(H ₂ O) ₂
	AO-partitioning	MO-partitioning		
ΔE	10.6	-3.9 (1.24)	-5.5	-2.8

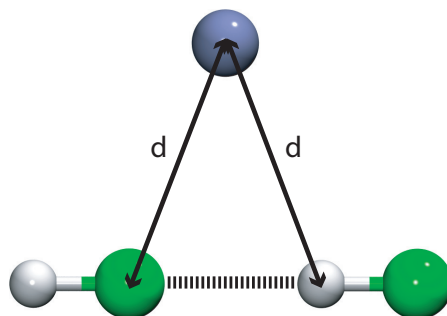


Figure 3.2: The (HF)₂He system used for benchmarking. The distance d is 2.7 Å, 1.6 Å or 1.2 Å. F in green, He in blue and H in white.

intramolecular hydrogen bond to be repulsive by 10.6 kcal/mol, whereas it was overestimating attraction for the halogenated derivatives of propane. As before, the MO-partitioning once again gives the best results for this interaction, an attractive value of 4 kcal/mol, in agreement with the intermolecular test cases.

To further investigate the origin of the excessive repulsion predicted by the AO-partitioning, it is desirable to obtain energies directly comparable with an intermolecular case. For this purpose, the method was applied to the interaction of two HF molecules. Because of the strength of the HF...HF hydrogen bond, the use of the equilibrium geometry is not mandatory to be in the attractive part of the potential energy surface. Atomic positions could be chosen to facilitate further geometric modifications. Thus, the HF bond distance was selected to be 1.00 Å and the H-bond distance 2.00 Å. To account for the effect of the spectator fragment C in the intramolecular energy computations, a He atom was added to the system, on an axis perpendicular to the H-bond axis at the midpoint between the two geometric centers of the HF molecules. The distance between He and the H-bond axis was varied in order to tune its effect on the H-bond as desired (see Figure 3.2). Since He is a small rare gas atom, its effect on the H-bond should be minor, facilitating easy comparison with the isolated HF dimer. Three different He...HF distances (to the closest atom) were used: 2.7 Å, where no interaction is expected, 1.6 Å, and 1.2 Å. The distance of 1.6 Å is typical of a covalent bond distance between fragments. Since He is smaller and has fewer basis functions than second-row atoms, the interfragment distance of 1.2 Å is a better model of the interfragment overlap present in larger molecules.

Table 3.5: Comparison of intramolecular (AO-partitioning) and intermolecular energies for (HF)₂He. 6-31G* was used throughout, all intermolecular energies computed with the Hartree-Fock method and in the trimer basis set. The three-body contribution to the intermolecular interaction energy is given in parentheses.

All results in kcal/mol	2.7 Å	1.6 Å	1.2 Å
Intermolecular ΔE	-4.4 (0.0)	-4.4 (0.8)	-4.4 (-0.7)
AO-partitioning ΔE	-5.2	-3.3	3.6

At each distance, the interaction between the two HF molecules (*i.e.*, fragments A and B) was computed using the AO-partitioning while the He atom is attributed to fragment C. The reference intermolecular energy is computed for the isolated HF dimer. The effect of the He atom on the H-bond energy is neglected, and this approximation is validated by the computation of the three-body contribution $\Delta\epsilon^{(3)}$ to the total interaction energy of the trimer. All intermolecular energy computations were performed in the full system basis set and are thus BSSE-free. The three-body effects are computed as the difference between the total trimer interaction energy and the sum of the three dimer interaction energies.

$$\Delta\epsilon^{(3)} = E_{ABC}^{int} - E_{AB}^{int} - E_{BC}^{int} - E_{AC}^{int} \quad (3.16)$$

$\Delta\epsilon^{(3)}$ measures the maximum variation of the H-bond energy inside the trimer compared to its isolated value.

At the largest distance, the AO-partitioning reproduces the interaction energy reasonably well, with an error of only 0.8 kcal/mol. As He is brought to the medium distance, the disagreement increases to reach 1.1 kcal/mol. Since a maximum three-body effect of 0.8 kcal/mol is computed, the AO-partitioning value is still within reasonable bounds. However, at the shortest distance corresponding to the He-H and He-F distances of 1.17 Å, the error of the AO-partitioning method is 8 kcal/mol. This largely exceeds $\Delta\epsilon^{(3)}$, hence the error is an artifact of the method. As fragment C approaches fragments A and B, the interfragment overlap increases and the intramolecular interaction energy deviates from the expected value. The exact origin of this error still needs to be clarified, however, the fact that the MO-partitioning leads to an attractive H-bond in pentane-2,4-diol may indicate that orbital delocalization plays a role. An examination of the orbitals in the (HF)₂He system is in agreement with this hypothesis, and future development of the MO-partitioning implementation will make direct numerical tests possible, in addition to spin-coupling corrections.

3.3.3 Geometry dependence

Until now, all intramolecular interaction computations were performed at a single geometry. To validate whether the proposed zeroth-order wavefunction leads to intuitive results upon geometric distortion, a geometric scan was performed for propane. The CCC bond angle was varied between 72 and 172 degrees at 10-degree intervals. All other degrees of freedom were optimized

Chapter 3. Exploration of Zeroth-Order Wavefunctions and Energies for Intramolecular Symmetry-Adapted Perturbation Theory

with HF/6-31G*, and the intramolecular energies were computed at the final geometry using the same basis set.

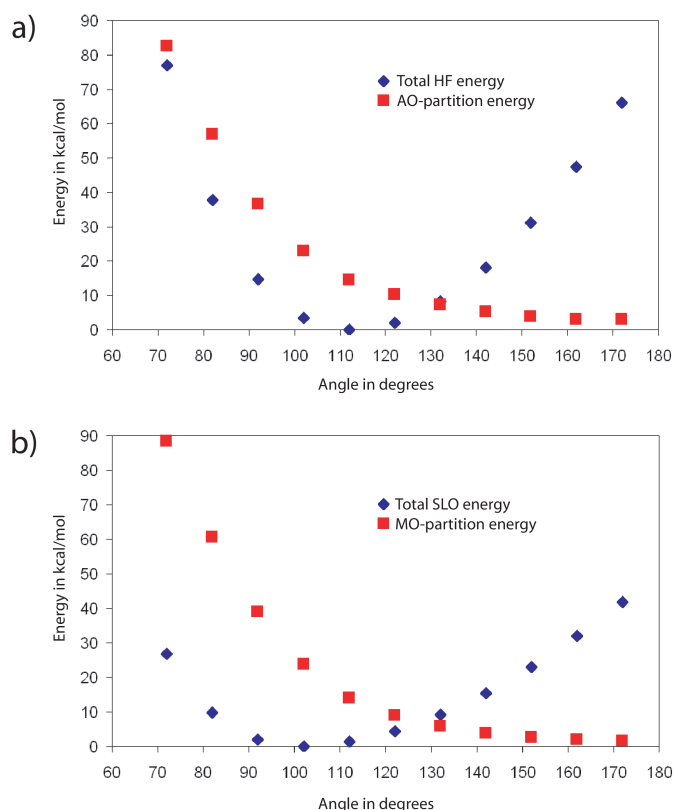


Figure 3.3: Scan of the CCC angle in propane. Top: AO-partitioning, intramolecular interaction energy in red and HF total energies relative to equilibrium in blue. Bottom: MO-partitioning, intramolecular interaction energy in red and HF SLO wavefunction total energies relative to equilibrium in blue. 6-31G* basis set used throughout.

As expected, the reference energies (HF or fully interacting SLOs) roughly correspond to the familiar parabola, representing an increasing energy upon distortion of a molecule from equilibrium. The intramolecular interaction energies have different behaviours, decreasing to a finite limit as the CCC angle is widened. At 172 degrees, the AO-partitioning limiting value is 2.9 kcal/mol while the MO-partitioning value is 1.6 kcal/mol. Thus, both methods yield a completely intuitive (dispersionless) behaviour for geometric deformation, the intramolecular energy depending monotonically on the distance between the fragments. No convergence problems were observed in spite of the large magnitude of the angles chosen.

3.4 Conclusion

Deriving a zeroth-order wavefunction and energy excluding interaction between two fragments within the same molecule is by no means trivial. Most variants relying on a hermitian formalism resulted in variational collapse, and others in energy values larger than for covalent

bond dissociations. A non-hermitian approach based on CHA and related energy decomposition analysis³⁵ was successful in defining and optimizing a wavefunction leading to zeroth-order energies on a chemical scale. Although non-hermitian, the resulting Fock matrix is symmetrized and can be diagonalized with common methods to lead real-valued orbitals.

Physically, a single electron should not be divided between interacting fragments. Hence, strictly localized orbitals are employed to ensure electron localization on a single fragment, resulting in the MO-partitioning. The effects of electron delocalization and subsequent division on the intramolecular energy were assessed using the alternative AO-partitioning. Results on different test systems showed that the MO-partitioning is preferred over its AO counterpart for several reasons. The AO-partitioning has a larger basis set dependence, less chemically intuitive trends for halogenated derivatives of propane, and predicts repulsive intramolecular hydrogen bonds. Tests on a trimer system confirmed that the AO-partitioning leads to excessive repulsion when fragment C is close to A and B, as is the case in covalently bound systems. In spite of this artifact, both the AO- and the MO-partitionings faithfully reproduce the expected behaviour of the 1,3-methyl-methyl interaction in propane as the CCC bond angle is varied.

The zeroth-order wavefunction derived reproduces expected trends and behaviour in chemical systems, and the orbital optimization converges smoothly in all cases. This is almost surprising given the physical impossibility of a molecule with non-interacting neighbouring fragments, and underlines the power of the CHA approach. The next steps toward the derivation of intramolecular SAPT will include correction of the MO-partitioning by spin-coupling and further testing of the method on intermolecular cases. An adaptation of the method to Kohn-Sham wavefunctions is also of interest for a cheap inclusion of intrafragment correlation. A perturbation expansion of the intramolecular interaction will then lead to a physically meaningful energy partitioning.

4 Branched Alkanes Have Contrasting Stabilities

4.1 Introduction

Detailed knowledge of fundamental processes and interactions within simple hydrocarbons has profound implications for all aspects of organic chemistry. Within this context, significant advancements have been made in the understanding of hydrocarbon thermochemistry since the pioneering works of Rossini and Nenitzescu in the 1930s.^{185,186} A recently developed concept, protobranching,^{199,209} proposes that linear *n*-alkanes are stabilized through similar (although fewer) 1,3-alkyl-alkyl interactions than those present in their more stable branched counterparts.

This concept has shown to be useful in reconciling previously inconsistent values for quantifying energies of organic phenomena (e.g., the resonance energy of benzene); nonetheless, the relevance and interpretation of protobranching interactions remains heavily debated.^{187,195,196,200,201,210–213} The energies associated with protobranching (and other 1,3-nonbonded alkyl-alkyl interactions) provide significant insight into the understanding of alkane stability and behavior. Despite the notion that branched species are more stable than linear alkanes, too much branching can destabilize molecules, manifested in weaker C-C bond energies.^{214,215} For example, the heat of formation of *n*-tridecane (-74.5 kcal/mol) is lower than its highly branched isomer tri-*tert*-butylmethane (-56.2 kcal/mol).²¹⁶ Presumably, the close proximity of bulky methyl groups in highly branched alkanes is responsible for much of this destabilization. In contrast to **Chapter 3**, the present chapter does not rely upon a direct *ab initio* approach to intramolecular interactions. Instead, we manipulate accurate thermochemical data using simpler techniques to assess energetic values of specific interactions. This chapter proceeds along three lines: (i) establishing a reliable and inexpensive computational technique for predicting accurate heats of formation of highly branched alkanes, (ii) probing the (de)stabilizing effects of various branching patterns, and (iii) identifying the pattern causing the destabilization of highly branched alkanes.

Isodesmic bond separation energy (BSE)^{217–219} evaluations are commonly used to determine the total sum of (de)stabilizing interactions within a molecule of interest. In the BSE procedure, all bonds between heavy (non-hydrogen) atoms are split into their simplest (or parent) molecular fragments preserving the heavy atom bond types. Reactions are balanced by inclusion of the necessary number of simple hydrides (methane, ammonia, water, etc.). Isodesmic bond separation reactions are part of a hierarchy⁴³ in which the chemical environment of the

parent molecule is increasingly preserved. Hyperhomodesmotic reactions (highest rank in the hierarchy) preserve the connectivities of each carbon-carbon bond upon fragmentation of the parent molecule, inducing large error compensations when computing the corresponding energy. Positive bond separation energies reflect a stabilizing phenomenon, while negative energies correspond to destabilization. The BSE of propane (Equation 4.1) has been used to quantify the 1,3-methyl-methyl protobranching stabilizing interaction, 2.83 kcal/mol.^{199,209} Here, we employ the BSE as a tool to probe the (de)stabilizing interactions in highly branched alkanes.



4.2 Computational details

Some of the alkanes studied in this chapter have considerable conformational flexibility, essentially because of the high number of dihedral angles. Only the lowest energy conformers were considered in our computations as Boltzmann averaging of the energies was found to be negligible compared to the DFT errors (see Table A.1 in Appendix A.1). Conformational searches were performed using a random atomic search with molecular topology imposed by a MM force field (Dreiding). In more details, the coordinates of all atoms are randomly chosen within some interval,^{220–222} and the molecular geometry roughly reoptimized with the force field. At least 1000 random conformers per structure were generated, classically optimized, and then refined at the B3LYP^{25,49}/6-31G*^{25,49} level. Single-point energies were computed on the global minima using the cc-pVTZ¹⁷⁸ basis set together with SVWN5,^{24,223–225} B3LYP, M06-2X,^{53,54} PBE,²²⁶ PBE-D,²²⁷ PBE-dD10,²²⁸ B2PLYP,²²⁹ B2PLYP-D,²³⁰ density-fitted MP2,²³¹ and spin component scaled df-MP2.²³² Gaussian09,²³³ MOLPRO²³⁴ and deMon-2K²³⁵ were used for computations.

The value of 1,4-alkyl-alkyl interaction energy was estimated by computing the electronic energy difference between relaxed gauche butane and relaxed *n*-butane, using a CCSD(T)-F12²³⁶ extrapolation of cc-pVDZ-F12/cc-pVTZ-F12²³⁷ results with the coefficients recommended by Werner and coworkers.²³⁸

The least-squares fitting were performed with GNUpot (www.gnuplot.info) version 4. Each alkane series was fitted with a different expression. For *n*-alkanes, the BSE *y* was expressed as

$$y = (x - 2)a \quad (4.2)$$

where *x* is the length of the main carbon chain and *a* the fitted parameter representing the CH₃⋯CH₃, CH₃⋯CH₂ and CH₂⋯CH₂ interaction energies. The singly methylated alkane BSEs *y* were fitted to

$$y = 2a + 2(x - 2)b + (x - 4)c \quad (4.3)$$

where *a* is the previously determined parameter, *b* and *c* the fitted parameters associated with CH₃⋯CH(CH₃)R and CH(CH₃)R⋯CH(CH₃)R interactions, respectively. Finally, the perme-

4.3. Determination of Heats of Formation of Branched Alkanes

thylated alkane BSEs y were fitted to

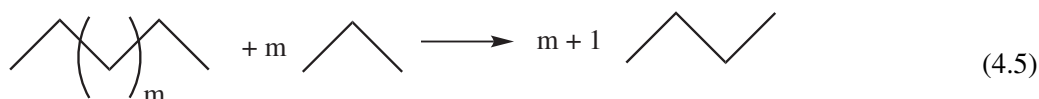
$$y = (2 + x)a + (6x - 18)d + (4x - 10)e + (x - 4)f \quad (4.4)$$

where a is fixed at its previous value, d is a fixed parameter associated with 1,4-alkyl-alkyl interaction energies, e and f are fitted parameters associated with $\text{CH}_3 \cdots \text{C}(\text{CH}_3)_2\text{R}$ and $\text{C}(\text{CH}_3)_2\text{R} \cdots \text{C}(\text{CH}_3)_2\text{R}$ interactions, respectively.

4.3 Determination of Heats of Formation of Branched Alkanes

Because experimental data is unavailable for many highly branched alkanes, it is desirable to employ an accurate, yet inexpensive, scheme for computing heats of formation. Note that these heats of formation may be computed from any reaction when well-established experimental values for all reactants and products, other than the molecule of interest, are known. For instance, the theoretical heat of formation for propane could be computed from Equation 4.1, so long as the experimental heats of formation of both methane and ethane are known. Within this context, Wheeler et al.⁴³ demonstrated the remarkable error-canceling ability of hyperhomodesmotic reactions (e.g., Equation 4.5),^{239,240} which provide good experimental agreement using inexpensive standard DFT methods. In contrast, isodesmic reactions, including bond separation equations, generally require computationally expensive, correlated methods to achieve reasonable experimental agreement. To gauge overall accuracy, two techniques (direct and indirect) for computing bond separation reaction energies have been tested on a set of 16 branched alkanes with experimental data (see Figure A.1 in Appendix A.1).^{216,241} Note that these gas-phase enthalpies of formation are nearly identical to those in the classic text of Stull, Westrum, and Sinke²⁴² (errors ranging from 0.0 to 0.2 kcal/mol for available compounds smaller than $\text{C}_{10}\text{H}_{22}$). The computations are based on lowest energy conformer searches as assessed by the procedure described in Section 4.2.

In the *direct* procedure, computed enthalpies are used to determine the isodesmic bond separation reaction energy of the alkane of interest. The *indirect* alternative uses hyperhomodesmotic equations, derived from the highest rung of Wheeler's hierarchy of homodesmotic equations,⁴³ to determine the theoretical heat of formation. The BSE is then computed on the basis of this value along with the experimental heats of formation of methane and ethane. Figure 4.1 illustrates average and maximum deviations of various theoretical levels (see Section 4.2) between computed and experimental bond separation energies using both the direct and indirect procedures.



As previously reported, standard density functionals give inaccurate BSEs for hydrocarbons.^{164,201,243–247} The average error from experiment for the popular B3LYP^{25,49} and PBE²²⁶ functionals using the direct method are 23.2 and 17.7 kcal/mol, respectively. Specifically parametrized functionals,

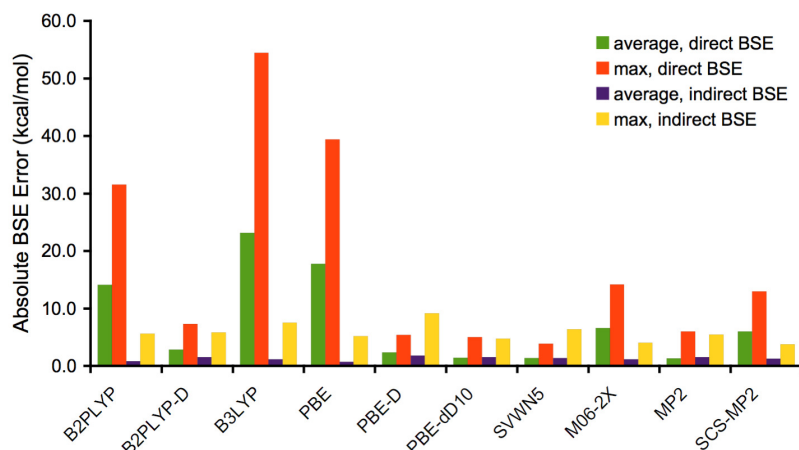


Figure 4.1: Absolute errors of computed bond separation energies from experimental data (in kcal/mol). Indirect BSE uses both experimental and computed heats of formation from hyperhomodesmotic reactions, while direct uses only DFT energies.

such as M06-2X,^{53,54} and those supplemented with an empirical dispersion term (B2PLYP-D,^{229,230} PBE-D,²²⁷ PBE-dD10²²⁸) reduce this value to under 10 kcal/mol. The correlated MP2²³¹ method outperforms all functionals for the direct computations, including SCS-MP2.²³² Using hyperhomodesmotic equations to determine heats of formation significantly reduces the deviation from experiment for BSE reactions (the indirect method). The 23.2 kcal/mol average B3LYP error using the *direct* method is reduced to a mere 1.1 kcal/mol with the *indirect* method. Other functionals, both with and without dispersion corrections, perform remarkably well in the indirect procedure. The PBE functional gives the lowest average error from experiment (0.70 kcal/mol) and, therefore, is used to derive the heats of formation of the highly branched alkanes investigated throughout the remainder of this work. Thus, the indirect procedure allows for determination of remarkably accurate heats of formation of complex molecules using computationally inexpensive DFT methods.

4.4 Quantifying Nonbonded Group Interactions in Branched Alkanes

Having validated a reliable method for computing the heats of formation of highly branched alkanes, we employ bond separation reaction energies to delineate the extent of their destabilization and identify its origin. The BSE of *n*-alkanes (Equation 4.6) show positive values, which increase linearly as the alkane is elongated. Starting from propane, the addition of each methylene group increases the overall stabilization by 2.81 kcal/mol on average (orange set, Figure 4.2). This procedure and quantitative value were previously used to define the energy of a single protobranching interaction.^{199,209} The substitution by a methyl group of one hydrogen

4.4. Quantifying Nonbonded Group Interactions in Branched Alkanes

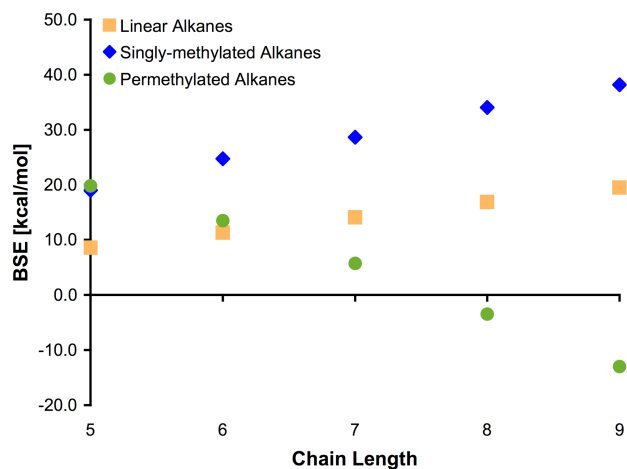


Figure 4.2: Bond separation reaction energies of *n*-, singly methylated, and permethylated alkanes (in kcal/mol).

atom on each methylene leads to the singly methylated alkane series (Equation 4.7). Similar to the *n*-alkanes, the BSEs of the singly methylated species are positive and increase linearly with parent chain lengthening (blue set, Figure 4.2). The increased substitution gives rise to *skew* interactions, *i.e.*, the destabilization arising from the 1,4-methyl-methyl interaction when the groups are separated by a $\pm 60^\circ$ torsion angle, also known as *gauche* interaction. This destabilization is absent in the anti (180°) conformation. Despite the introduction of these energetically unfavorable skew interactions, singly methylated alkanes show a ~ 4.8 kcal/mol BSE increase per $-\text{CH}(\text{CH}_3)-$ moiety added, nearly twice the value of *n*-alkanes (2.81 kcal/mol).

In sharp contrast with both *n*- and singly methylated alkanes, the BSE profile of permethylated alkanes (Equation 4.8) shows an average *destabilization* of 8.2 kcal/mol (green set, Figure 4.2) per motif added. The total bond separation reaction energy even crosses over from positive (representative of stabilization) to negative values (destabilizing) for compounds with a parent chain length larger than seven. This permethylated alkane BSE trend, which opposes *n*- and singly methylated alkanes, is indicative of a dramatically different type of interaction.

As the degree of branching increases, additional 1,3-topologies, not present in simple *n*-alkanes, are introduced (see Figure 4.3). The monomethylation of the methylene groups in *n*-alkane not only results in protobranching-type interactions (between methyl and/or methylene groups) but also gives rise to topological motifs featuring tertiary and primary carbons $[\text{CH}_3 \cdots \text{CH}(\text{CH}_3)\text{R}]$ and $\text{R}(\text{CH}_3)\text{CH} \cdots \text{CH}(\text{CH}_3)\text{R}$, $\text{R} = \text{alkyl}$ as well as 1,4-skew interactions.

Similarly, permethylated species, which have widely spaced conformational energy levels and thus one dominant conformation,²⁴⁸ contain unique 1,3-motifs between primary and quaternary carbon groups $[\text{CH}_3 \cdots \text{C}(\text{CH}_3)_2\text{R}]$ and $\text{R}(\text{CH}_3)_2\text{C} \cdots \text{C}(\text{CH}_3)_2\text{R}$, $\text{R} = \text{alkyl}$. To determine the energetic quantities associated with these various 1,3-alkyl-alkyl substituent patterns (*i.e.*, the number of hydrogen and methyl groups attached to 1,3-disposed carbon atoms) and identify the

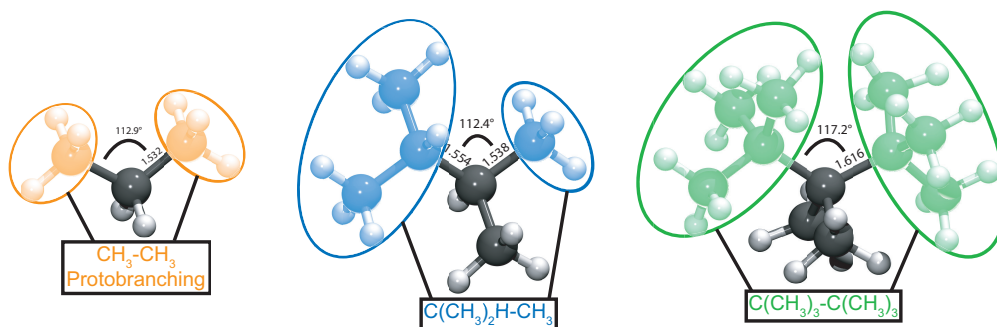
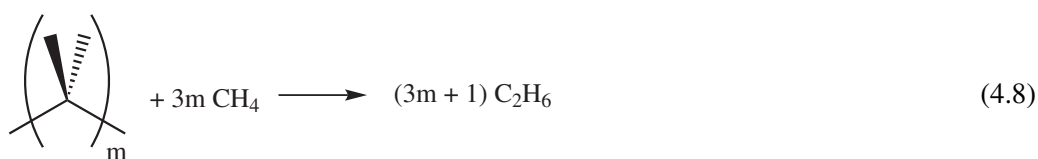
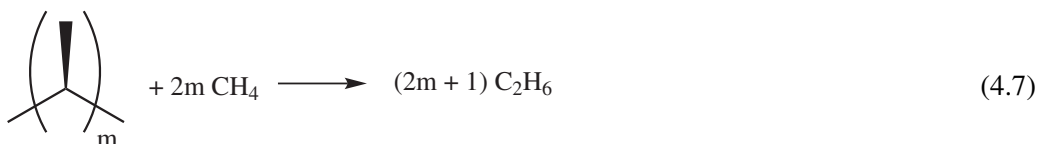
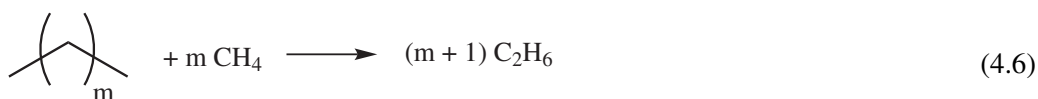


Figure 4.3: Illustration on propane of the different substitutions and 1,3-interactions studied in this work. Bond distances in Å.

origin of destabilization of highly branched alkanes, we dissect the total bond separation energies (Equations 4.6-4.8) into individual motif contributions by using a combination of previously established values and data-fitting procedures.



The energy associated with the methyl(ene)⋯methyl(ene) interaction, taken as 2.81 kcal/mol, is derived from the average BSE of *n*-alkanes. Note that using the attenuated values of proto-branching for singly methylated (2.58 kcal/mol estimated from isobutane) and permethylated alkanes (2.28 kcal/mol estimated from neopentane), respectively, have no effect on general trends. Similarly, a value of -0.67 kcal/mol is derived for the skew interaction (see Section 4.2). Using these predetermined values, best-fit parameters to the Figure 4.2 BSE curves have been established for the interactions associated with the two additional patterns present in singly methylated and permethylated alkanes (see Section 4.2).

Table 4.1 provides a summary of the energetic quantities associated with each interaction type.

Table 4.1: Quantities, kcal/mol, associated with specific types of 1,3 and skew (1,4) patterns

interaction	value (kcal/mol)
$\text{CH}_3 \cdots \text{CH}_3$ (<i>n</i> -alkane like) ^a	2.81
$\text{CH}_3 \cdots \text{CH}(\text{CH}_3)\text{R}^b$	2.53
$\text{CH}_3 \cdots \text{C}(\text{CH}_3)_2\text{R}^b$	2.74
$\text{R}(\text{CH}_3)\text{CH} \cdots \text{CH}(\text{CH}_3)\text{R}^b$	1.72
$\text{R}(\text{CH}_3)_2\text{C} \cdots \text{C}(\text{CH}_3)_2\text{R}^b$	-18.00
skew	-0.67

^aValues of $\text{CH}_3 \cdots \text{CH}_2$ and $\text{CH}_2 \cdots \text{CH}_2$ interactions are taken to be identical with $\text{CH}_3 \cdots \text{CH}_3$ interactions.

^bR = alkyl

Singly methylated alkanes have two new types of 1,3-alkyl-alkyl interactions absent in *n*-alkanes: $\text{CH}_3 \cdots \text{CH}(\text{CH}_3)\text{R}$ and $\text{R}(\text{CH}_3)\text{CH} \cdots \text{CH}(\text{CH}_3)\text{R}$ (R = alkyl), which contribute positively to the BSE by 2.53 and 1.72 kcal/mol, respectively. Although slightly smaller, note that both values are comparable to the original protobranching energy in *n*-alkanes (2.81 kcal/mol). Permethylated alkanes also add two additional 1,3-nonbonded motifs, $\text{CH}_3 \cdots \text{C}(\text{CH}_3)_2\text{R}$ and the very bulky $\text{R}(\text{CH}_3)_2\text{C} \cdots \text{C}(\text{CH}_3)_2\text{R}$. While the value for $\text{CH}_3 \cdots \text{C}(\text{CH}_3)_2\text{R}$ (2.74 kcal/mol) remains close to the protobranching value, the quantity associated with the $\text{R}(\text{CH}_3)_2\text{C} \cdots \text{C}(\text{CH}_3)_2\text{R}$ substitution pattern is dramatically destabilizing (-18.00 kcal/mol). Given the negative slope associated with the BSEs of permethylated alkanes (Figure 4.2), it is clear that a large destabilization is needed to overcome the numerous other stabilizing 1,3-alkyl-alkyl interactions dominating the BSE of singly methylated chains. This destabilization, existing only in highly branched alkanes, is caused by the steric hindrance between 1,5-methyl groups, which manifests itself in highly distorted bond lengths and angles (Figure 4.3). The relationship between strain and C-C bond lengths has already been noticed by previous research.^{214,215} The central CCC bond angle in 2,2,3,3,4,4-hexamethylpentane opens by over 4° and is accompanied by a C-C bond lengthening of nearly 0.1 Å as compared to propane. Similarly, the carbon-carbon geminal distance has increased by 8%, from 2.554 Å in propane to 2.759 Å in 2,2,3,3,4,4-hexamethylpentane.

4.5 Conclusion

In this chapter, we have introduced an efficient scheme for computing heats of formation of large branched alkanes using computationally inexpensive approaches and employed bond separation evaluations to probe the destabilizing interactions associated with branched alkanes. Moreover, we have provided information regarding the magnitude and sign of specific 1,3-alkyl-alkyl interactions arising from various branching patterns. In contrast to **Chapter 3**, which relies upon a rigorous and direct first principle approach, intramolecular interactions are here assessed based on a simple fitting procedure of accurate thermochemical data. While useful, the present method depends on the studied system and is unable to provide insight regarding the physical nature of the interaction. We demonstrated that singly methylated alkanes are characterized by unfavorable skew interactions absent in *n*-alkanes, however, that destabilization is overwhelmed by the greater number of energetically favorable 1,3-interactions. All 1,3-nonbonded alkyl-alkyl

Chapter 4. Branched Alkanes Have Contrasting Stabilities

patterns, except those involving two quaternary carbon atoms, result in a stabilization between 1.7 and 2.8 kcal/mol. However, the presence of $\text{R}(\text{CH}_3)_2\text{C}\cdots\text{C}(\text{CH}_3)_2\text{R}$ bulky motifs destabilizes the permethylated alkanes dramatically (-18.00 kcal/mol). Thus, despite the simplified picture of branched alkane stability presented in many organic chemistry textbooks,^{249,250} these species show widely varying stability trends based on number and location of added methyl groups.

5 π -Depletion as a Criterion to predict π -stacking Ability

5.1 Introduction

The focus of the present chapter shifts from the quantification and characterization of intramolecular interactions (*i.e.*, within molecules) to the identification of the driving force of one type of intermolecular interactions. π -stacking interactions constitute one of the most important classes of non-covalent interactions, which govern a variety of structural and energetic phenomena such as self-assembly processes, protein–drug interactions, and the crystal packing of organic molecules.^{251,252} In the present chapter, π -stacking serve as a driving force for developing a rational design criterion able to rapidly detect tailored polyaromatic molecules exhibiting enhanced π -stacking ability. To proceed, we aimed at increasing favorable interactions by identifying and quantifying the physical underpinnings behind π -stacking. Whereas long-range dispersion effects dominate these interactions,²⁵³ their enhancement, without considering substituent effects,²⁵⁴ has most recently been rationalized by theoreticians in terms of charge penetration^{255,256} (*i.e.*, favorable electrostatic contributions at short distance) and reduction in exchange repulsion by localization of the π -conjugated framework. In particular, Bloom and Wheeler²⁵⁷ proposed that electrons confined to their double bonds can deliver stronger π -stacking interactions than those being delocalized in aromatic systems. This remarkable realization could have a significant impact on the design of receptors, including those anticipated herein. They noted, however, that this trend was not general: the stacking interaction of benzene with the mildly aromatic central ring of triphenylene was more favorable than with hydrogenated derivatives.²⁵⁷ Alternatively, Siegel et al. invoked the reduction of "unfavorable" electrostatic repulsion between electron poor rings based on experiment.²⁵⁸ Nevertheless, a prescription has yet to be provided regarding ways to select a polyaromatic skeleton that ensures stronger π -interactions.

We here introduce a visual and quantitative criterion, LOLIPOP, that characterizes the π -electronic nature of polyaromatic molecules and provides information regarding their π -stacking ability. The trends shown by the LOLIPOP criterion prompted us to reinterpret the origin of the phenomenon identified by Bloom and Wheeler²⁵⁷ by providing evidence that π -depletion, rather than π -localization, enhances π -stacking interactions. The practicality of LOLIPOP is illustrated by using π -depletion as a design principle to screen dyes that can serve as molecular sensors for the fluorimetric detection of caffeine.

5.2 Computational details and methods

All monomer geometries were optimized with B3LYP^{25,49,259}/6-31G*^{202,203} with Gaussian 09.²³³ 2-methylene-1,2-dihydronaphthalene, tetra- and hexahydrotriphenylene were constrained to be planar so that π and σ orbitals could be easily identified. Interacting complexes with benzene were built from frozen monomers, separated by a vertical distance of 3.5 Å except otherwise noted. Interaction energies were computed at the PBE0^{226,260,261}/def2-TZVP,²⁰⁵ PBE0-dDsC^{51,52}/def2-TZVP, HF/def2-TZVP and MP2/def2-TZVP (for molecules of the validation set) levels in a development version of Q-Chem.^{262,263} dDsC^{50–52} is a density-dependent dispersion correction developed in our laboratory that is based on pairwise atomic potentials and a damping function. dDsC corrects for the lack of dispersion interactions in common functionals,²⁶⁴ and its damping function ensures that no correction is made to covalent regions, hence it performs well in both inter- and intramolecular cases. Interaction energies with caffeine were computed with geometries fully relaxed at the PBE0-dDsC/def2-SVP^{204,205} level of theory. To assess the accuracy of the dDsC dispersion correction on these complexes, their interaction energies were also computed at the B97²⁶⁵-dDsC/def2-TZVP, PBE²²⁶-dDsC/def2-TZVP, M06-2X^{53,54}/def2-TZVP, MP2/def2-TZVP and SCS-MP2²³²/def2-TZVP. Johnson et al.^{266,267} showed that meta-GGA functionals like M06-2X²⁶⁸ are particularly sensitive to the integration grid employed, hence a Lebedev²⁶⁹ grid with 99 radial and 590 angular²⁷⁰ points was used. All MP2 computations make use of the RI²⁷¹ approximation to speed up computations, with the cc-pVTZ-RI²⁷² auxiliary basis set. BSSE counterpoise corrections⁵⁶ were applied for all interaction energies, and DFT computations use a Lebedev²⁷³ grid with 75 radial and 302 angular²⁷⁰ points unless otherwise specified.

Energy decomposition analysis was performed on the same geometries and at vertical distances of 3.3 Å, 3.5 Å and 3.7 Å at the SAPT0^{30–32} level using the aug-cc-pVDZ basis set. The resolution of the identity with appropriate auxiliary basis functions was applied to speed up computations.^{82,274}

Nucleus-Independent Chemical Shifts (NICS)²⁷⁵ were computed at the GIAO^{276,277} level with PBE/cc-pVTZ in Gaussian09. The NICS(1)_{zz} variant was chosen because of its good performance in measuring aromaticity of planar systems.²⁷⁸ NICS(1)_{zz} is obtained by taking the negative of the zz component in the chemical shielding tensor, computed 1 Å above the aromatic ring centers.

The LOL function,⁴⁵ on which LOLIPOP is based, relies on the consideration of the electron kinetic energy density $\tau = \sum_i |\nabla \psi_i|^2$:

$$LOL = \frac{1}{1 + \frac{\tau}{D_0}} \quad (5.1)$$

where $D_0 = \frac{3}{5}(6\pi^2)^{2/3}\rho^{5/3}$ is the corresponding kinetic energy density in the uniform electron gas, ρ being the electronic density. Therefore, $LOL > 0.5$ reveals electrons slower (less kinetic energy) than in the uniform electron gas, and $LOL < 0.5$ electrons faster than in the uniform electron gas. Slow electrons are considered to be localized, whereas fast electrons are delocalized, which is confirmed by the orbital interpretation of LOL, associating high values of the

function with stationary points of localized orbitals.⁴⁵

Electronic densities were obtained with Gaussian09²³³ at the PBE²²⁶/cc-pVTZ level and LOL was computed from them in Dgrid²⁷⁹ using all orbitals of π -symmetry, with a grid mesh of 0.05 Bohrs.

In the integration to obtain LOLIPOP, only LOL values above 0.55 are taken into account so that LOLIPOP is proportional to the portion of localized electronic density in space. Moreover, the integration starts at a distance of 0.5 Å from the molecular plane where the most important contributions from the π -bonding basins are present. The chosen integration radius of 1.94 Å corresponds to the average between the C and H radii in benzene but the use of other radii within a small range does not alter the observed trend.

The script to compute LOLIPOP values and detailed instructions to obtain them is available free of charge and without any warranty on our website: <http://lcmd.epfl.ch>.

5.3 The LOLIPOP index

Our approach is based on the Localized Orbital Locator (LOL),⁴⁵ a function of the kinetic energy density very close to its predecessor, the Electron Localization Function (ELF).²⁸⁰ LOL has proven to offer a more intuitive depiction of π -bonds and detailed information on the nature and location of electron pairs.⁴⁶ Figure 5.1 displays LOL isosurfaces computed from the π -density of a series of (poly)aromatic rings. The LOL_π isosurfaces clearly distinguish localized (*i.e.*, double bonds), delocalized (benzene-like) and empty (single bonds) regions. Closer examination of triphenylene and its hydrogenated derivatives (**1–3** in Figure 5.1) reveals that π -depletion around the central ring in **1** (smaller size and number of LOL isosurfaces) results in stronger binding to the benzene probe as compared to the central benzene-like ring of the hexahydrogenated counterpart, **2** (binding energies in green).

This seems to indicate that molecular rings presenting small LOL_π regions, *i.e.*, π -depletion, are prone to bind more easily with benzene. To put this " π -depletion" hypothesis onto quantitative ground and enable a direct correlation with binding energies, we introduce a LOL-based index, LOLIPOP (LOL Integrated Pi Over Plane), that corresponds to the integral of LOL_π values over a 1.94 Å radius cylinder centered in the middle of the chosen molecular ring (see computational details, Section 5.2). In Figure 5.1, the LOLIPOP values (in black) are reflective of the size and number of LOL_π isosurfaces around each ring, providing a good measure of the extent of LOL_π -depletion. The value is the highest for benzene and the lowest for the central ring of coronene (characterized by many empty regions). Alternatively, naphthalene shows a value comparable to that of the outer ring of phenanthrene, which is significantly lower than that for benzene. Less obviously, the intermediate LOLIPOP value of **3** as compared to **1** and **2** is accounted for by the increased LOL_π of the exocyclic double bonds, which are partially comprised in LOLIPOP. These visual inspections thus indicate that LOLIPOP is reflective of the size and number of LOL_π basins. It is worthwhile to mention that LOLIPOP is not an aromaticity criterion and does not correlate with the most popular aromaticity index, *i.e.*, nucleus-independent chemical shift,²⁷⁵ as shown on Figure 5.2. The points obviously do not form a straight line, and an attempt to obtain a linear regression results in an R^2 coefficient of 0.18, indicating no cor-

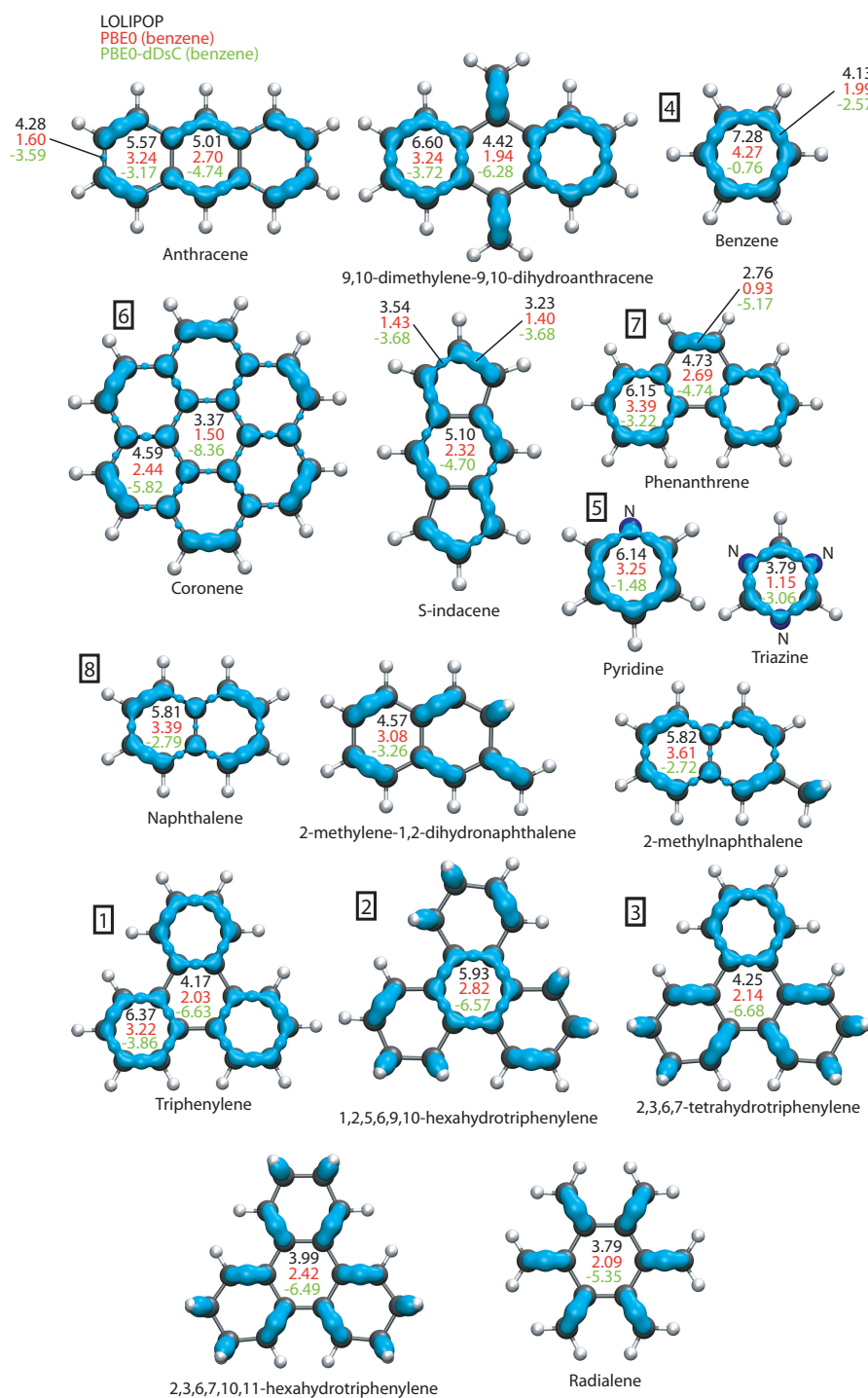


Figure 5.1: LOLIPOP index (black), PBE0 interaction energies in kcal/mol (with benzene) without (red) and with (green) dispersion correction and LOL isovalues of 0.55 obtained from the π -density. Nitrogen atoms are explicitly indicated and values corresponding to stacking on bonds are noted outside molecules.

5.4. The interplay between LOLIPOP and π -stacking energies

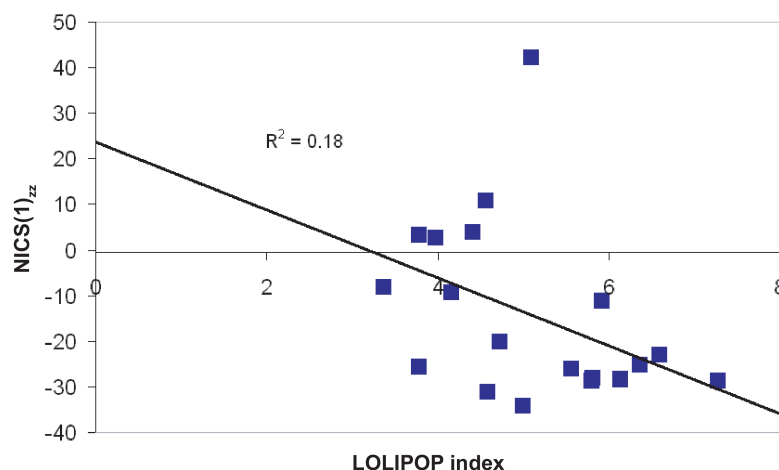


Figure 5.2: NICS(1)_{zz} plotted against LOLIPOP for molecular rings in Figure 5.1. Linear regression and the corresponding R^2 coefficient show no significant correlation between the two indices.

relation. The comparison between naphthalene and benzene is a relevant example as the LOL_π isosurfaces of the two types of rings differ significantly (7.28 and 5.81 for the LOLIPOP index respectively) as compared to their NICS(1)_{zz}²⁷⁸ values (-28.9 for both molecules). The consideration of LOLIPOP together with the visualization of LOL_π isosurfaces constitutes an accurate picture of a ring's π -nature distinct from a magnetic response.

5.4 The interplay between LOLIPOP and π -stacking energies

The correlation between LOLIPOP and the observation of the LOL_π isosurfaces was established in the previous section. A relevant question is how does the LOLIPOP of a series of (poly)aromatic rings correlate with their π -stacking ability? The existence of this relationship can be validated by computing the interaction energy of each ring with a benzene probe located at a distance of 3.5 Å away in a parallel-stacked geometry. Both dispersion-corrected^{51,52} (PBE0-dDsC, green) and non-corrected (red) PBE0^{226,260,261} interaction energies are given in Figure 5.1.

Remarkably, the non-dispersion corrected PBE0 interaction energies reveal good correlation with the LOLIPOP index ($R^2 = 0.79$, Figure 5.3). A similar observation is valid for Hartree-Fock energies, which lack dispersion completely (see Figure 5.4). Despite providing greater accuracy, the PBE0-dDsC (or similarly MP2) interaction energies⁵² are not expected to correlate with LOLIPOP, as the magnitude of the additional (dDsC) density dependent dispersion correction is governed by molecular size and shape. This is due to the form of the dispersion correction as a sum of atomic pairwise terms: more pairs give naturally rise to larger dispersion forces, as is physically observed²⁸¹ (see Figure 5.5). The π -depletion as probed by LOLIPOP depends upon the kinetic energy density⁴⁵ of electrons localized in bonds or lone-pairs (hence slow electrons), which involves shorter range interaction than dispersion. Note that dispersion

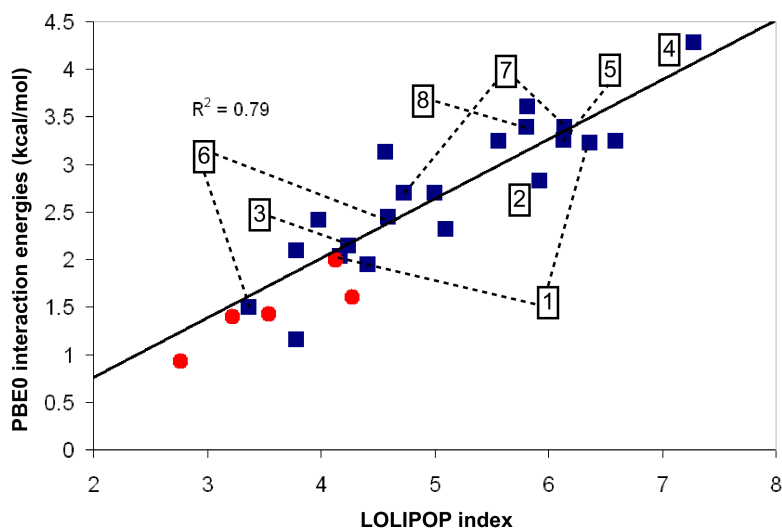


Figure 5.3: PBE0 interaction energies without dispersion correction for parallel stacked (blue squares) and parallel displaced (red circles) geometries of complexes of molecules from Figure 5.1 with benzene plotted against the LOLIPOP index. The linear regression only takes the parallel-stacked geometries into consideration.

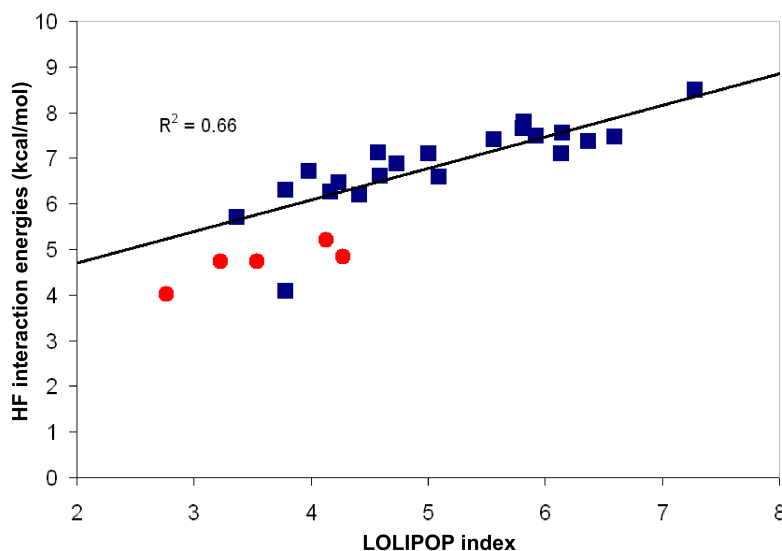


Figure 5.4: HF interaction energies plotted against LOLIPOP index for parallel stacked (blue squares) and parallel displaced (red circles) geometries of complexes of molecules from Figure 5.1 with benzene. Linear regression takes only parallel stacked geometries into account.

5.4. The interplay between LOLIPOP and π -stacking energies

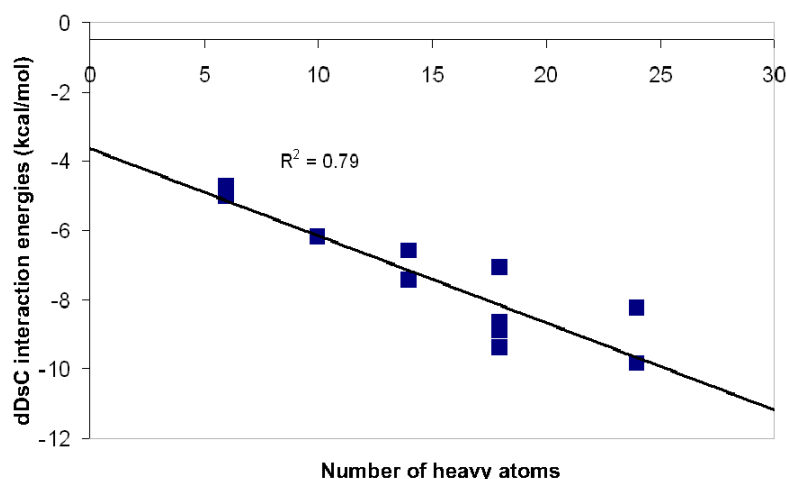


Figure 5.5: dDsC contribution to the interaction energy plotted against the number of heavy atoms for molecules numbered 1-8 in Figure 5.1. Dispersion energies are linked to molecular size.

differences become less important when molecules of similar size and shape are compared, e.g., for the molecular dyes discussed in the forthcoming application section.

In Figure 5.3, the benzene probe interacts more strongly with molecules carrying a LOL_{π} depleted surface, as is seen for molecules **4** and **6**. Similar correlations exist when parallel-displaced geometries (red circles in Figure 5.3), Hartree–Fock energies (see Figure 5.4) or a s-triazine probe are considered (see Figure A.2 in Appendix A.2). Parallel-displaced geometries correspond to stacking benzene above a bond and integrating the LOL values over a cylinder centered at the midbond point. The good correlation indicates that the " π -depletion effect", as quantified through LOLIPOP, is an intrinsic property of the molecule that could estimate trends in the stacking interaction ability, for molecules of similar size, independent of the probe and without computing any binding energies. In addition, the fact that the energy trend persists with a π -depleted probe having a permanent quadrupole moment of opposite sign as benzene (*i.e.*, the s-triazine ring) is supportive of the charge penetration effect.²⁵⁶ This is in line with the model proposed by Cozzi and Siegel²⁵⁸ that electron-poor aromatic rings always experience more favorable interactions than electron-rich ones due to reduced electronic repulsion, a contrasting view with the common Hunter-Sanders model²⁸² where the optimization of quadrupole–quadrupole interactions plays the dominant role.

SAPT provides further support to this view through its decomposition of the interaction energy into physical terms (electrostatic, exchange, polarization/charge transfer, and dispersion components). Energy decomposition analysis based on symmetry-adapted perturbation theory³⁰ was performed on 5 illustrative rings (the two rings of **1**, radialene, benzene and pyridine) for three different intermolecular distances: 3.3, 3.5 and 3.7 Å. The interaction energy components were then plotted against the corresponding LOLIPOP values of these rings (see Figure A.3 in Appendix A.2). A linear regression was computed for each interaction energy component as a function of LOLIPOP. Figure 5.6 gathers the resulting correlation coefficients for all three dis-

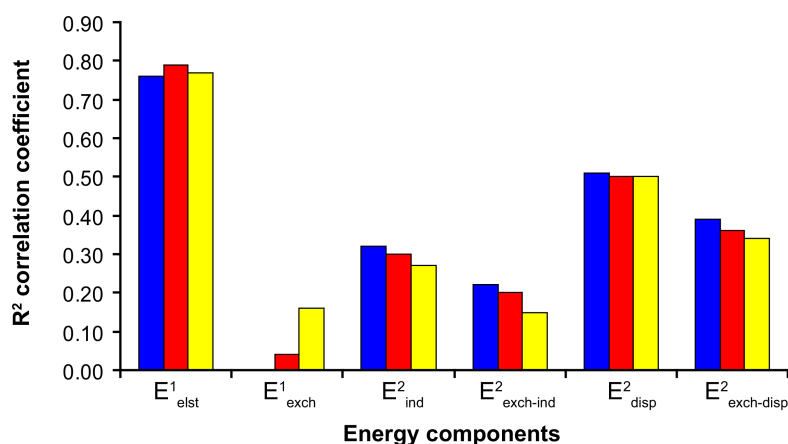


Figure 5.6: R^2 correlation coefficient of linear regressions of SAPT0 energy terms against LOLIPOP values. Intermolecular distances with benzene of 3.3 Å (blue), 3.5 Å (red) and 3.7 Å (yellow).

tances. The best correlation with LOLIPOP arises from the first-order electrostatic term (R^2 of 0.79) indicating that unfavorable classical electrostatic repulsions are reduced or, alternatively, favorable attractions are increased. The tendency persists at shorter (3.3 Å) and at longer (3.7 Å) intermolecular distances.

5.5 Caffeine sensors

The previous section suggests that LOLIPOP can predict the π -stacking ability of molecular sensors through indirect probing of electrostatic effects. In a related context, our laboratory has recently exploited the interaction between trisodium 8-hydroxy-pyrene-1,3,6-trisulfonate (HPTS, in Figure 5.8) and caffeine for sensing caffeine in water²⁸³ in a collaboration with the experimental group of Prof. Kay Severin at EPFL. HPTS was successfully used to quantify caffeine in common beverages and drugs, however, it displays a relatively modest affinity for caffeine ($K_a \sim 250 \text{ M}^{-1}$). These shortcomings prompted us to apply LOLIPOP as a tool for identifying alternative molecular receptors that exhibit enhanced sensitivity compared to HPTS. Our selection of dyes was based on three criteria: (a) incorporation of more polarizable atoms (e.g. sulfur), (b) a conserved large π -stacking surface, and (c) a depleted LOL_π isosurface (especially at the dye center), the latter criterion being quantified through LOLIPOP. With its lowest LOLIPOP value at the center, coronene emerges as an ideal candidate but its large hydrophobic surface prevents good solubility in water. For this reason, we targeted dyes of similar size as the pyrene core. Note that the introduction of sulfonyl groups, mainly for solubility purposes, has no influence on the LOL_π isosurfaces (see Figure 5.7). The structure as well as the LOL_π isosurface and the LOLIPOP of our best candidates are given in Figure 5.8. The central ring of dyes **B** and **C** exhibit the lowest values overall, indicating that the fusion of thiophene with benzenoid rings is a promising structural pattern. Alternatively, fluoranthene (**E**), with three relatively low LOLIPOP values, is also attractive.

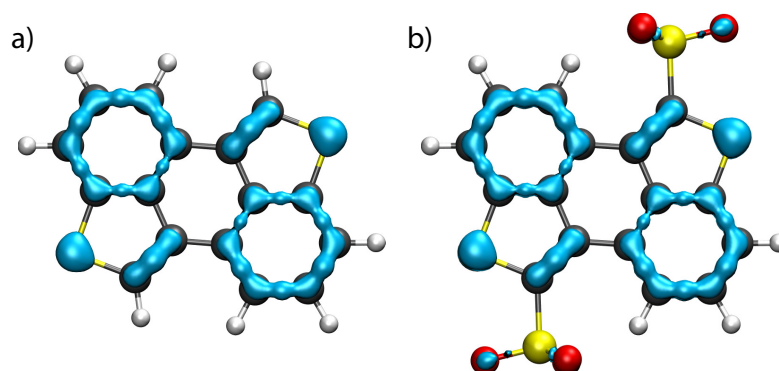


Figure 5.7: LOL isosurfaces (isovalue 0.55) obtained from the π -density for molecules a) C and b) C-dye. The sulfonyl groups do not affect the LOL_π isosurface.

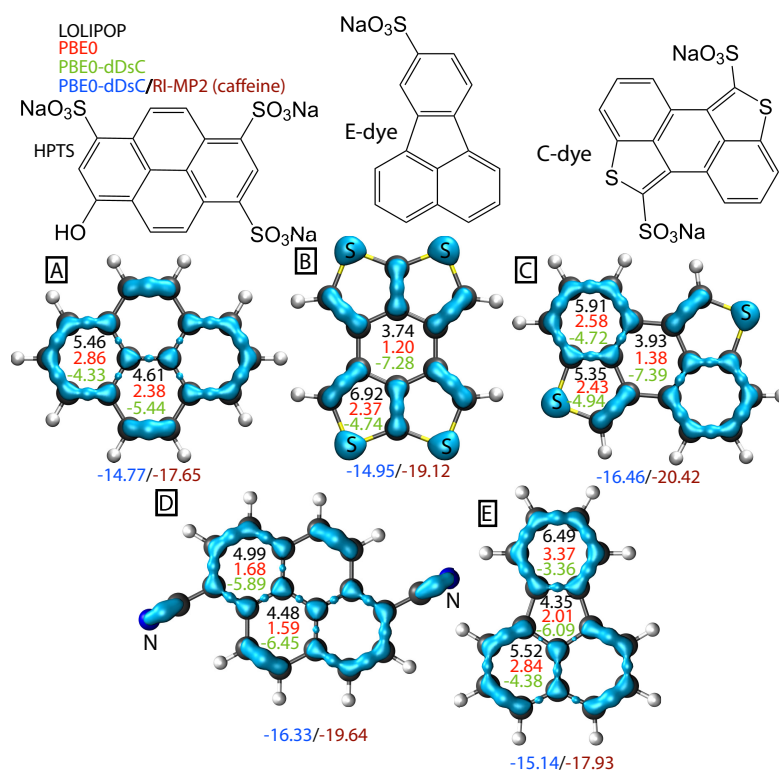


Figure 5.8: LOLIPOP index (black), PBE0 interaction energies in kcal/mol without (red) and with (green) dispersion correction with benzene and LOL_π isosurfaces (isovalue of 0.55) of each aromatic ring. Interaction energies with caffeine (freely optimized geometries) are given in blue/brown for PBE0-dDsC and MP2, respectively.

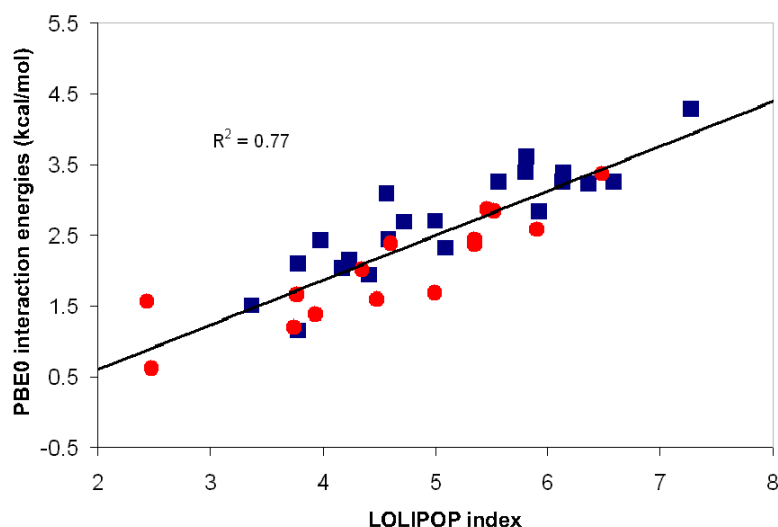


Figure 5.9: PBE0 interaction energies for the validation set (blue squares) and candidate chemosensors (red circles) plotted against LOLIPOP index. Linear regression takes all points into account.

The interaction energy of benzene stacked above each ring of the candidate chemosensors was computed in the same way as for the validation set. Plotting of these energies against the corresponding LOLIPOP values reveals the same correlation as in Figure 5.3. As can be seen on Figure 5.9, the new points fit into the same trendline. Thus, the observed correlation holds for a wide variety of π -extended frameworks. *A priori* identification of sensors exhibiting enhanced π -stacking could rely upon a more global screening index that emphasizes the role played by a dye's central region. Such a global index may be designed as follows: if a candidate's molecular structure contains one (or more) central rings, the average LOLIPOP taken over these rings is considered. For dyes lacking a central ring, the average LOLIPOP values over the rings located at the molecular periphery should be considered.

The global index associated with the carbon skeleton of the four most promising candidates (**B-E** in Figure 5.8) leads to 4.35 for fluoranthene (**E**), 3.93 for **C** and 3.74 for **B** in comparison with 5.03 for the pyrene reference **A** (the aromatic core of the HPTS dye). In line with LOLIPOP, the computed MP2 binding energy of caffeine favors **C** (-20.42 kcal/mol), **B** (-19.12 kcal/mol) and **E** (-17.93 kcal/mol) over **A** (-17.65 kcal/mol). Note that the introduction of electron-withdrawing groups (cyano) into the experimentally exotic dye **D** also leads to a remarkable enhancement of the caffeine binding energy (and lower LOLIPOP), as compared to its parent **A**.

Interaction energies were also computed with B97-dDsC/def2-TZVP, PBE/def2-TZVP, M06-2X/def2-TZVP DFT levels and with SCS-RI-MP2/def2-TZVP (see Table 5.1). Overall, the interaction energies are in the correct range. However, the small interaction energy differences between the candidate chemosensors are beyond DFT(-dDsC) accuracy, all functionals giving

Table 5.1: Interaction energies in kcal/mol of caffeine-candidate complexes computed with B97-dDsC/def2-TZVP, PBE-dDsC/def2-TZVP, M06-2X/def2-TZVP, RI-MP2/def2-TZVP and RI-SCS-MP2/def2-TZVP. All geometries optimized with PBE0-dDsC/def2-SVP.

Interaction energies	B97-dDsC	PBE-dDsC	M06-2X	RI-MP2	SCS-RI-MP2
Candidate A	-13.98	-13.10	-11.91	-17.65	-11.49
Candidate B	-13.77	-13.01	-13.86	-19.12	-12.22
Candidate C	-15.69	-14.48	-14.21	-20.42	-13.39
Candidate D	-15.55	-14.68	-13.20	-19.64	-12.88
Candidate E	-14.53	-13.58	-12.22	-17.93	-11.96

slightly different ordering than (SCS)-MP2.

Disodium 3,4-3'-4'-bibenzo[*b*]thiophene-2,2'-disulfonate (C-dye in Figure 5.8) was synthesized by the group of Prof. Kay Severin (EPFL), who developed a simple test strip for the differentiation of normal from decaffeinated coffee.²⁸⁴ C-dye displays a remarkable sensitivity (apparent binding constant $K_a = 930 \pm 49 \text{ M}^{-1}$) and selectivity towards caffeine in the aqueous phase. Similar experimental studies (in the Severin group) based on sodium fluoranthene-8-sulfonate (E-dye) suggested an even larger apparent binding constant ($K_a = 1100 \pm 100 \text{ M}^{-1}$).

5.6 Conclusion

The preliminary results obtained for caffeine sensors demonstrate that, despite gaps that exist between *in silico* design and "real world" applications, the predictions achieved are experimentally relevant. To further exploit the " π -depletion" trend revealed here, and to go beyond caffeine sensing, our laboratory aims at investigating candidates for chemosensors for 2,4,6-trinitrotoluene (TNT) and to extend the LOLIPOP index to excited states for excimer study. Moreover, the present chapter unravels the short-range electrostatic origin of the observed correlation. The relationship between reduced electronic repulsion and local kinetic energy of electrons should be explored and understood further.

In summary, the recent proposal of Bloom and Wheeler²⁵⁷ motivated us to propose π -depletion as a design principle and introduce a quantitative criterion, LOLIPOP, which offers straightforward insight into the π -stacking ability of organic molecules. The LOL_π isosurfaces and LOLIPOP can, for instance, serve as a prediction tool for screening potential π -stacking candidates in the context of chemosensors.

6 Four-Electron Oxygen Reduction by Tetrathiafulvalene

6.1 Introduction

This chapter focuses on practical applications of computational chemistry methods and emphasises the importance of intermolecular interactions in chemical reactions. More specifically, we here study the reduction of oxygen to water by tetrathiafulvalene. This work was a collaboration with the group of Prof. Hubert Girault (EPFL), hence the most relevant experimental aspects are summarized below. For more details on the experimental setting, the reader is invited to read the original paper⁵⁵ and its supporting information.

The reduction of oxygen to water is a key reaction of the respiratory chain of aerobic organisms.^{48,285,286} It has technological interest as well since it is a key step for the development of efficient fuel cells. In fuel cells, metal catalysts are usually employed for oxygen reduction, but their cost is an incentive for research of cheaper molecular catalysts. Most molecular catalysts to date involve a transition metal complex, with the dioxygen binding to the metal during the reaction.^{48,286–291} Often, the reaction proceeds only to H_2O_2 ,⁵⁵ a strong oxidizer which deteriorates the catalyst. Further reduction to H_2O is achieved through bimetallic catalysts^{48,286–290,292–295} or a careful choice of functional groups tuning the pK_a of dioxygen adducts to promote proton-coupled electron transfer.²⁹⁶ Tetrathiafulvalene (TTF) is a very good electron donor and has been used to enhance dioxygen reduction properties of mesoporous carbon.²⁹⁷ The oxidation of neutral TTF shows two steps: first, the radical cation is formed, and then further oxidation leads to the dication.^{298–304} In the original experimental work,⁵⁵ the oxygen reduction reaction was performed at an interface between two immiscible electrolyte solutions (ITIES). The reaction could also be reproduced in a single organic phase, hence our computational model does not include such interface.

Starting from the experimental data gathered by Olaya et al.,⁵⁵ we investigated aggregates of TTF and TTFH^+ able to provide the electrons and protons needed for the O_2 reduction to water. We postulate the formation of a helical tetramer with two TTF and two TTFH^+ , and compute the barrier for the first H atom transfer to O_2 .

6.2 Computational details

The reaction path was computed using two different density functional approximations: the M06-2X^{53,54} functional, parametrized for improving the description of weak interactions, and

B3LYP-dDsC in which the recently developed dispersion correction, dDsC,^{50–52} is added to B3LYP.^{25,49} The dDsC correction, which uses both density-dependent dispersion coefficients and damping factors (as was already mentioned in Section 5.2), gives highly accurate reaction, conformation, as well as binding energies.^{50–52} The energies were computed at the M06-2X/cc-pVTZ^{178,305}//M06-2X/SVP²⁰⁴ and at B3LYP-dDsC/6-31+G**^{202,203,207,306}//B3LYP-dDsC/6-31G** levels of theory (energy//geometry). All B3LYP-dDsC computations were performed in Q-Chem²⁶² (version 3.2) using a grid with 75 radial points and 302 angular points, roughly corresponding to the default “Fine” grid in Gaussian09.³⁰⁷ B3LYP-dDsC geometries were optimized in the gas phase, and single-point energies were computed with the SM8³⁰⁸ solvation model for 1,2-dichloroethane (note that the current Q-Chem implementation of the SM8 solvation model is compatible with only three basis set types that include 6-31+G**). The M06-2X computations were performed in Gaussian09³⁰⁷ using the “Fine” grid for geometry optimizations in the gas phase and the Ultrafine grid (M06 functionals have been shown to be especially sensitive to the grid^{266–268}) for single-point energy computations in the solvent. 1,2-Dichloroethane was modeled in Gaussian using the IEFPCM implicit solvation.³⁰⁹ The minima and transition states on the potential energy surface were characterized by frequency computations, which were then used to compute zero-point and thermal contributions to single-point energies in order to obtain reaction enthalpies. Note that Gibbs free energies and not enthalpies are experimentally relevant, however the enthalpies are preferred in our case for two reasons: first, no experimental number is available for comparison, and second the entropy contribution to Gibbs free energies is prone to significant errors, especially in the large, flexible assemblies considered here. The unrestricted formalism was employed for all oxygen- or radical-containing species. Stability checks were performed^{310,311} for cases for which closed or open-shell singlet electronic configurations are possible.

In this chapter, interaction enthalpies correspond to enthalpy (at 298 K) differences between a complex and its separated relaxed adducts at their lowest spin state (*i.e.*, triplet for O₂). The energies are corrected for the basis set superposition error using the Boys and Bernardi scheme⁵⁶ on monomers frozen at the complex geometry. Since neither dDsC nor SM8 support ghost atoms in current Q-Chem implementations, B3LYP-dDsC BSSE corrections were approximated by the corresponding B3LYP numbers. The M06-2X BSSE corrections were obtained in the gas phase since the IEFPCM model also does not support ghost atoms.

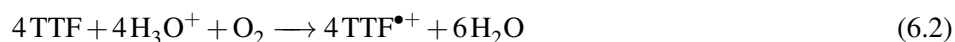
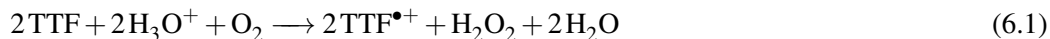
NMR computations at the GIAO^{276,277} B3LYP/6-311+G(2d,p)^{206,207,312,313}//M06-2X/SVP level were referenced to TMS and compared to experiment.

Conformational searches were conducted on the dimers of TTF and the protonated counterpart, TTFH⁺, using a random search procedure^{220–222} to generate different relative orientations of the two monomers.

6.3 Summary of experimental results

The acidification of a solution of TTF under aerobic conditions induces a progressive change of color⁵⁵ from yellow to pink and then progressively dark red. This change of color is in agreement with the formation of the TTF radical cation, TTF^{•+}, suggesting that TTF is reducing O₂. The formation of TTF^{•+} is confirmed spectroscopically both with UV-Vis and voltam-

metry. Comparison of the standard redox potentials of the $\text{O}_2/\text{H}_2\text{O}_2$ and $\text{O}_2/\text{H}_2\text{O}$ couples in 1,2-dichloroethane (1.17 and 1.75 V, respectively, vs Standard Hydrogen Electrode (SHE))³¹⁴ with that of the $\text{TTF}^{\bullet+}/\text{TTF}$ couple (0.56 V vs SHE⁵⁵), it is clear that the oxygen reduction reaction by TTF is thermodynamically feasible. Consequently, the two possible global reactions are written:



UV-Vis spectroscopy of an acidic TTF solution in anaerobic solutions reveals a decrease in the TTF absorbance. Thus, a TTF protonation according to Equation 6.3 is likely to occur.



Kinetic experiments show that the rate of reaction increased with the proton and TTF concentrations, further suggesting that TTFH^+ plays a role in the reduction. UV-Vis spectroscopic results also indicate that $\text{TTF}^{\bullet+}$ forms under anaerobic conditions, but in much smaller quantities. The large amount of $\text{TTF}^{\bullet+}$ observed under aerobic conditions is dependent on the presence of O_2 and probably stems from the reduction reaction. Voltammetric studies confirm the formation of $\text{TTF}^{\bullet+}$ and unravel the dependence of its formation rate on pH, thus supporting the above considerations.

A reduction of O_2 according to Equations 6.1 and 6.2 leads to H_2O_2 and H_2O . An indirect measure of the H_2O_2 concentration at the end of the reaction gives only a 3% yield relative to the initial TTF concentration. The other product of reduction is water, which can be produced through two reaction paths: a direct reduction of O_2 to H_2O by a transfer of four electrons and four protons, or a reduction to H_2O_2 in the first step and a further reduction from H_2O_2 to H_2O . The second path is tested by putting an acidic TTF solution in the presence of H_2O_2 : the formation of $\text{TTF}^{\bullet+}$ is not observed, hence no reduction of H_2O_2 is taking place and TTF performs the four-electron reduction of O_2 to H_2O . Finally, the production of water is tested by NMR spectroscopy of a dried acidic TTF solution in 1,2-dichloroethane in the presence of O_2 . NMR signals consistent with the formation and disparition of TTFH^+ are observed, confirming its role as an intermediate, and the peak corresponding to water increases with time, confirming water formation. NMR spectra of blank solutions without TTF are analyzed at the same times as the reacting mixture. The content of water in the blanks remains constant with time.

In summary, experiments indicated that the reduction of O_2 by TTF results in the formation of $\text{TTF}^{\bullet+}$ and H_2O through a direct four-electron reduction. H_2O_2 does not oxidize TTF to $\text{TTF}^{\bullet+}$ and is not an intermediate in the reaction. Since the reaction rate depends on the pH, protonated TTFH^+ is likely to be an intermediate.

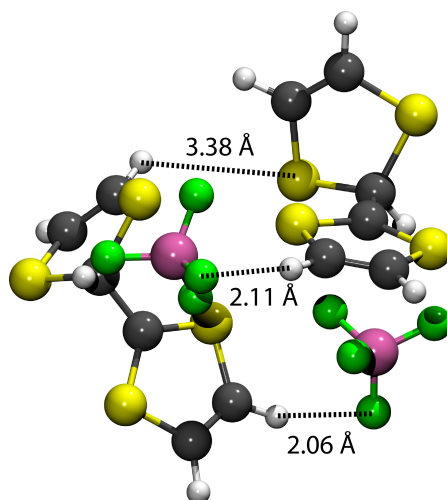


Figure 6.1: Optimized $(\text{TTFH}^+)_2(\text{BF}_4^-)_2$ complex at the M06-2X/SVP level. No specific interaction between the TTFH^+ units is present. Distances between the cation and anion are indicated in Å, as well as the closest cation-cation distance.

6.4 Computational mechanistic investigation

6.4.1 Conformational study

Considering the above data and the fact that TTF alone can transfer at most two electrons, we investigated the aggregation of TTF and TTFH^+ into dimers and tetramers by electronic structure computations. As expected, $(\text{TTFH}^+)_2$ is not bound due to the strong Coulombic repulsion between the two positive charges. In principle, counterions could help overcome this repulsion and favor the dimer formation. However, in 1,2-dichloroethane the protons are associated with a very large anion, tetrakis(pentafluorophenyl)borate (TB^-), which has a very low coordinating power and charge density due to its size. As evidenced by the crystal structure of $(\text{TTFH}^+)(\text{BF}_4^-)^{315}$ obtained from the CSD database,³¹⁶ no specific interactions between two TTFH^+ units could be determined. Counterion-cation $(\text{TTFH}^+)_2(\text{BF}_4^-)_2$ complexes were further analyzed computationally showing that the most stable complex exhibits cation-anion electrostatic interactions rather than direct interactions between the two TTFH^+ units (Figure 6.1). Note that in the presence of the larger and less coordinating TB^- , even less interaction is expected between the TTF units. In contrast, the TTF- TTFH^+ dimer is stabilized by -5.1 kcal/mol (-8.2 kcal/mol) relative to its monomers at the B3LYP-dDsC/6-31+G** (M06-2X/cc-pVTZ) level including continuum solvation (Figure 6.2).

Two such TTF- TTFH^+ dimers can gain an additional 4.0 kcal/mol (5.1 kcal/mol) at B3LYP-dDsC/6-31+G** (M06-2X/cc-pVTZ) with implicit solvation by assembling through their TTF moieties, thereby forming a helical tetramer $[\text{TTF}_4\text{H}_2]^{2+}$ (displayed in Figure 6.3a together with O_2). This tetramer is potentially able to deliver the four electrons needed for the reduction of oxygen to water.

Experimentally, ^1H NMR signals compatible with TTFH^+ were observed: three peaks at $\delta = 6.15$, 6.25 and 8.75 ppm with an integration ratio of 2:1:2, the signals at 8.75 ppm corresponding to

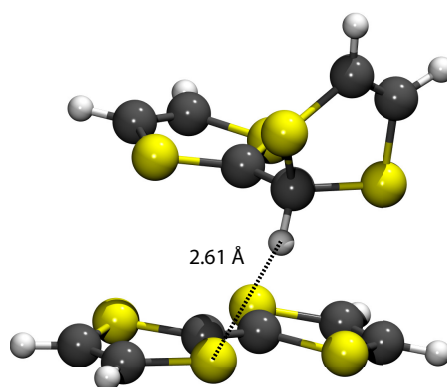


Figure 6.2: TTF-TTFH⁺ dimer geometry and binding enthalpy at 298 K, computed at the B3LYP-dDsC/6-31+G**//B3LYP-dDsC/6-31G** level (M06-2X/cc-pVTZ//M06-2X/SVP number in parentheses) with continuum solvation.

the protons of the charged^{317,318} ring (Equation 6.3). These signals are also compatible with the helical tetramer [TTF₄H₂]²⁺ as supported by computations of chemical shifts at the B3LYP/6-311+G(2d,p) level on the M06-2X/SVP geometry. Three signals in line with experiment are obtained for the TTFH⁺ monomer, namely two protons at 8.6 ppm (from the charged ring), two protons at 6.0-6.1 ppm, and one proton at 6.5 ppm. The spectrum computed for TTFH⁺ in the tetramer reveals essentially the same signals, although slightly shifted at 8.4-8.2 ppm for the charged ring protons, 6.1-6.3 ppm for the neutral ring protons, and 5.3 ppm for the last proton. The signal corresponding to the proton on the central C-C bond shifts from 6.5 ppm in the monomer to 5.3 ppm in the tetramer. This shift could be due to the proximity of the proton to the electron-rich S atoms in the tetramer geometry (Figure 6.3a). These signals disappear progressively with time, confirming that either TTFH⁺ or the helical tetramer is the intermediate in the oxygen reduction reaction; therefore, they support the mechanisms proposed in this work.

6.4.2 Reaction barriers

In the previous section, the conformational space of aggregates of TTF and TTFH⁺ was explored and several assemblies were identified. The reactivity of these assemblies towards O₂ is investigated in the present section.

The potential energy surface of the [TTF₄H₂...O₂]²⁺ complex is very flat as exemplified by the small binding energies computed for the two minima located (conformers A and B, Figure 6.3a, see also Table 6.1). The dioxygen molecule binds weakly to [TTF₄H₂]²⁺ at the M06-2X/cc-pVTZ level (-0.3 to -0.1 kcal/mol) but not at B3LYP-dDsC/6-31+G** for which the complex (Figure 6.3a) is 0.4-1.2 kcal/mol less stable than the optimized isolated monomers. Note that the gas phase electronic energy is actually attractive, and only implicit solvation and basis set superposition corrections make it repulsive (see Table 6.1). The barrier associated with a hy-

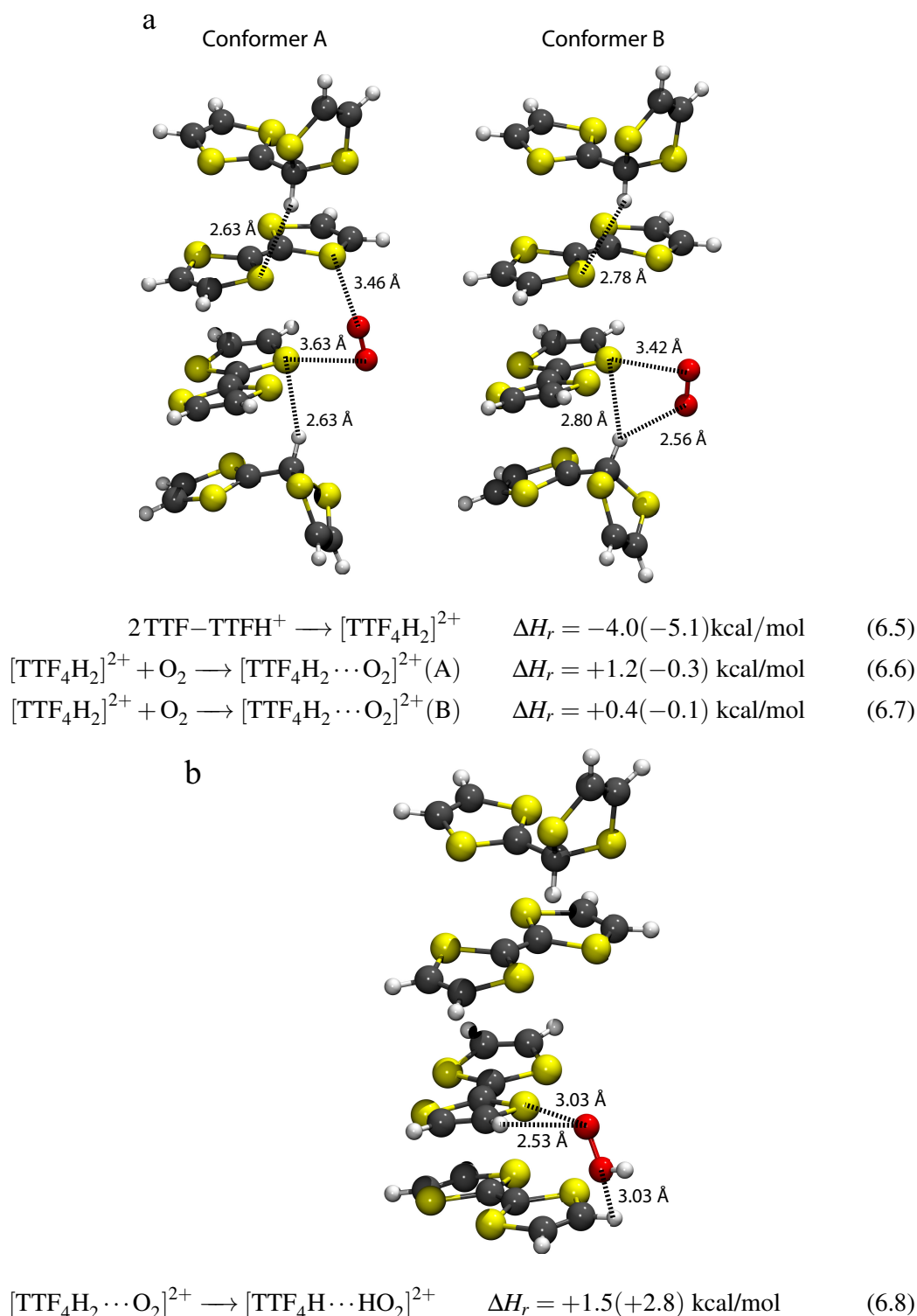


Figure 6.3: (a) $[\text{TTF}_4\text{H}_2 \cdots \text{O}_2]^{2+}$ helical complex geometries A and B; (b) $[\text{TTF}_4\text{H} \cdots \text{HO}_2]^{2+}$ complex geometry. Reaction enthalpies at 298 K computed at the B3LYP-dDsC/6-31+G**//B3LYP-dDsC/6-31G** level (M06-2X/cc-pVTZ//M06-2X/SVP numbers in parentheses) with continuum solvation.

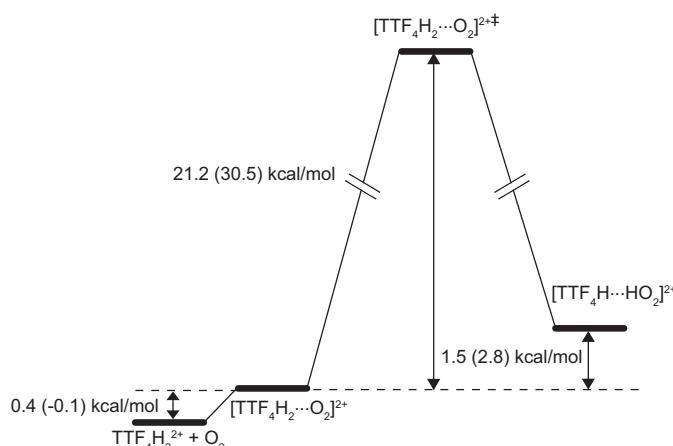


Figure 6.4: The computed reaction pathway, enthalpies at 298 K computed at B3LYP-dDsC/6-31+G**/B3LYP-dDsC/6-31G** (M06-2X/cc-pVTZ/M06-2X/SVP numbers in parentheses) with continuum solvation. Conformer B (Figure 6.3a) is taken as the reference for energy computations. The thermal contribution and BSSE correction is from conformer A.

drogen atom (not a proton) transfer (Figure 6.3b) is 21.2 kcal/mol (30.5 kcal/mol) (Figure 6.4). This relatively high barrier is in agreement with the slow reaction observed experimentally. The associated imaginary frequency is 2085 cm^{-1} , hence tunneling corrections would be of interest to obtain quantitative kinetic rates, which is not the purpose of this study. The complex (triplet electronic state) obtained after the H atom transfer, $[\text{TTF}_4\text{H}\cdots\text{HO}_2]^{2+}$, is only marginally destabilized (1.5 kcal/mol at B3LYP-dDsC/6-31+G** and 2.8 kcal/mol at M06-2X/cc-pVTZ with implicit solvent) as compared to the starting $[\text{TTF}_4\text{H}_2\cdots\text{O}_2]^{2+}$ adduct. It is likely that the highly reactive HO_2^\bullet species reacts further with $[\text{TTF}_4\text{H}]^{\bullet+}$. HO_2^\bullet and the $\text{TTF}^{\bullet+}$ moieties within the tetramer could for instance combine to form a new intermediate (Figure A.4 in Appendix A.3), which could then dissociate from the tetramer and get the needed protons and electrons to form two molecules of water from individual TTFH^+ units in solution. The formation of this intermediate has to proceed on the singlet potential energy surface, whereas the $[\text{TTF}_4\text{H}\cdots\text{HO}_2]^{2+}$ product has a triplet ground state. However, the singlet-triplet energy difference at the M06-2X/cc-pVTZ level with implicit solvent is only 0.02 kcal/mol, making these states quasi-degenerate. From the TTF- HO_2 intermediate, other paths can be envisioned, leading to H_2O_2 or a TTF decomposition. However, there is no experimental evidence supporting those paths.

Chapter 6. Four-Electron Oxygen Reduction by Tetrathiafulvalene

Table 6.1: Reaction energies and barriers for the computed path, with the effects of including a solvation model, thermal, and BSSE corrections

reactions	M06-2X ^a	thermal ^b	solvent ^c	BSSE ^d	dDsC ^e	thermal ^f	solvent ^g	BSSE ^h
reaction 6.4	-24.0	-22.9	-9.2	-8.2	-21.4	-20.2	-7.7	-5.1
reaction 6.5	9.6	10.7	-6.6	-5.1	19.9	21.2	-7.5	-4.0
reaction 6.6	-3.3	-2.6	-1.4	-0.3	-2.2	-2.5	-0.04	1.2
reaction 6.7	-3.4	-2.6	-1.2	-0.1	-2.4	-2.7	-0.9	0.4
barrier ⁱ	34.5	30.7	30.5	30.5	24.1	21.6	21.2	21.2
reaction 6.8 ⁱ	2.8	1.9	2.8	2.8	-1.1	-0.6	1.5	1.5

^aM06-2X/SVP, gas phase.

^bM06-2X/SVP, gas phase with thermal enthalpic corrections.

^cM06-2X/cc-pVTZ with implicit solvation and thermal enthalpic corrections.

^dM06-2X/cc-pVTZ with implicit solvation, thermal enthalpic and BSSE corrections.

^eB3LYP-dDsC/6-31+G**, gas phase.

^fB3LYP-dDsC/6-31+G**, gas phase with thermal enthalpic corrections.

^gB3LYP-dDsC/6-31+G** with implicit solvation and thermal enthalpic corrections.

^hB3LYP-dDsC/6-31+G** with implicit solvation, thermal enthalpic and BSSE corrections.

ⁱEnergies computed with conformer B as a reference, thermal contribution and BSSE correction from conformer A.

6.5 Conclusion

The four-electron reduction of O₂ by TTF was first studied experimentally. Spectroscopic data indicated an oxidation of TTF in acidic solutions under aerobic conditions. No such oxidation was observed in the absence of O₂, supporting the proposed reaction. Spectroscopy, voltammetry, and ¹H NMR analysis show that the reaction proceeds by a fast protonation of TTF followed by the direct four-electron reduction of oxygen to water. On the basis of electronic structure computations, we postulate the formation of stable helical tetramers from dimers between neutral and protonated TTF molecules. A computation of the barrier for the first H atom transfer to O₂ indicates a value consistent with the experimentally observed reaction rate.

The discovery of the aggregates of TTF and TTFH⁺ was possible thanks to proper modeling of intermolecular interactions. In such large systems, the use of post-HF methods is prohibitively expensive and cheaper, reliable methods are needed. M06-2X and B3LYP-dDsC are two such methods, taking weak interactions properly into account through appropriate parametrization or addition of a density-dependent dispersion correction, respectively. Without them, both energetics and obtained geometries would be incorrect, and the entire path to reduce O₂ to H₂O could not be computed reliably. Finally, the barrier for the first H atom transfer is only the first one, and an exploration of the entire reaction path and especially of the O-O bond breaking would be of great interest. The influence of solvation on the geometries may as well be investigated to obtain more reliable energetics.

7 General Conclusions and Outlook

This thesis presents advances in the developments and applications of modern computational approaches that could serve to (i) decompose intramolecular interactions into physically meaningful energy terms and (ii) devise novel techniques to enhance the strength of intermolecular interactions. The proposed schemes serve to improve our understanding of molecular systems and complexes along with identifying relevant structure-property relationships that could be used to achieve new reactions and access targeted properties.

Symmetry-Adapted Perturbation Theory (SAPT) is able to accurately describe intermolecular potentials and their physical contributions, but no intramolecular analogue is currently available. With the perspective of devising an intramolecular SAPT-variant, **Chapter 3** derives and validates a zeroth-order wavefunction able to exclude specific intramolecular interactions. To achieve this goal, we combine three theoretical formalisms that are the chemical Hamiltonian energy decompositions, the strict localization of orbitals and the construction of a wavefunction excluding the interactions between the fragments of interest on which all the SAPT schemes are based. Optimization of such a wavefunction is inherently challenging because it does not correspond to a physical state of the system, and a careful choice of the employed formalism is discussed. Akin to the intermolecular SAPT scheme, our total energy expression also excludes the interactions between the relevant intramolecular fragments.

Numerical applications on propane, halogenated derivatives and intramolecular hydrogen bonds revealed good convergence properties and intuitive energy trends when using strictly localized orbitals. Whereas this first derivation of a zeroth-order wavefunction for intramolecular interaction necessitates a more careful assessment of the resulting energies, the correction for spin contamination along with an improved analytical understanding of the model, the next prospect would be to apply the perturbation expansion and decompose the intramolecular interaction energy into physically meaningful terms.

In spite of its conceptual attractiveness, the *ab initio* approach is not the only alternative to quantify intramolecular information. In **Chapter 4**, those interactions are also quantified through the use of a simpler method based on bond separation reactions and linear regression techniques. We discuss ways to obtain and manipulate accurate heats of formation, which are used to assess (de)stabilizing interactions associated with various 1,3-nonbonded substituent

patterns within highly branched alkanes. While *n*- and singly methylated alkanes show positive bond separation energies (*i.e.*, stabilization), which increase systematically along the series, permethylated alkanes are characterized by decreasing BSEs (*i.e.*, destabilizing interactions). Our quantitative analysis shows that singly methylated alkanes are more stabilized than linear alkane chains and that the unique destabilizing feature of permethylated alkanes arises from the close proximity of bulky methyl groups causing highly distorted geometries along the carbon backbone.

The second objective of this thesis shifts from the development of schemes able to quantify intramolecular interactions to approaches devised for the analysis and enhancement of intermolecular interactions. In **Chapter 5**, we focus on the enhancement of π -interactions, which govern a variety of structural and energetic phenomena such as self-assembly processes, protein–drug interactions, and the crystal packing of organic molecules. We introduce a computational approach, LOLIPOP, which detects π -conjugated frameworks exhibiting enhanced π -stacking ability. We demonstrated that π -depleted polyaromatic molecules present superior π -stacking ability as compared to rich π -electron cores. This realization is quantified using our LOLIPOP criterion, which is based on a function of the kinetic energy density called the Localized Orbital Locator (LOL) as originally proposed by the group of Becke. The connection between the energy trends captured by LOLIPOP and the concept of charge penetration is also discussed. The practical utility of LOLIPOP was then demonstrated by identifying tailored chemosensors presenting enhanced π -stacking ability. In particular, we have designed tailored chemosensors which were experimentally shown to display remarkable sensitivity and selectivity towards caffeine. Despite the gap between simple *in silico* predictions and real-life applications, the experimental relevance of LOLIPOP represents a good example of the predictive power of computations.

Finally, **Chapter 6** emphasizes the importance of intermolecular interactions for stabilizing species responsible for the four-electron reduction of O_2 to H_2O . On the basis of the 1H NMR experimental evidence, we showed that the formation of a non-covalently bond helical tetramer $[TTF_4H_2]^{2+}$ is able to deliver the needed four electrons and protons to convert O_2 into water. The accurate computation of intermolecular interactions and identification of the protonated TTF tetramer was possible thanks to the use of DFT functionals tailored to take weak interactions into account, either by appropriate parametrization or by the inclusion of a density-dependent dispersion correction developed in our laboratory. In this example, standard density functional approximations fail to model the active TTF tetramer assemblies due to their inability to describe weak long-range interactions.

In summary, there exist numerous available methods to achieve an accurate description and quantification of intermolecular interactions. The challenge now lies in their application towards the identification of the most relevant structure-property relationships that could help in the rationalization of chemical trends and in the design of molecules exhibiting tailored properties. In contrast, the quantification of intramolecular interactions is very scarce as the current methods

have not yet reached the same maturity. This situation certainly stimulates the apparition of novel theoretical developments. In this respect, the zeroth-order wavefunction derived in **Chapter 3** opens the way to accurate and insightful intramolecular energies. Our efforts towards better and original approaches have improved the analysis of both inter- and intramolecular interactions. Nevertheless, open questions remain:

Assessment of the zeroth-order wavefunction for SAPT

The preliminary tests performed in this thesis should be extended to ensure the robustness of the derived zeroth-order wavefunction. The origin of the failure of the hermitian formalisms should be determined more accurately, for example by analytical considerations on simple models or by careful decomposition of the different energetic terms on benchmark intramolecular interactions. The $(\text{HF})_2\text{He}$ molecular trimer may be of considerable interest in this context. The effect of spin contamination should be quantified by derivation and implementation of a proper spin coupling scheme.

Intramolecular charge transfer

Since the formalism developed in this thesis indicates that strictly localized orbitals are beneficial to intramolecular interaction energies, intramolecular charge transfer is inherently limited by the spatial overlap of these orbitals. This may be a limitation in some cases like highly polar molecules, and two different solutions exist. The first is to introduce ionic structures into the wavefunction, similarly to Valence Bond theory, restoring charge transfer between the different fragments. The second solution is to include charge transfer in the perturbation expansion of the intramolecular interaction.

Perturbation expansion of intramolecular interaction

The perturbation expansion of the intramolecular interaction is not straightforward for several reasons. First, strictly localized orbitals are not eigenfunctions of a global molecular operator, but only of projected local operators; second, virtual orbitals are more difficult to obtain when spin coupling is introduced; third the operators considered are not hermitian. Future work should focus on these aspects. Non-hermiticity of the operators could be handled by biorthogonal perturbation theory using both their left and right eigenvectors, and virtual orbitals may be obtained through an effective Fock operator. Obviously a simpler hermitian formalism leading to a valid zeroth-order wavefunction would alleviate all these difficulties. Thus it will be important to investigate the current non-hermitian formalism in details.

Tailoring intermolecular properties beyond ground state

The LOLIPOP index based on the π -depletion design criterion was successfully exploited for the design of caffeine sensors soluble in water. Similarly, we can envision the successful application of LOLIPOP to identify other molecular sensors that could detect explosives such as 2,4,6-trinitrotoluene (TNT). More importantly, the construction of similar trends and criteria which could serve to rationalize non-covalent interactions in the excited states is highly relevant. The extension of LOLIPOP beyond ground-state requires the obtention of excited-state orbitals for the computation of the local kinetic energy of the electrons. Fortunately, such orbitals can now be obtained through constricted DFT methods.³¹⁹

The quantification of inter- and intramolecular interactions has been the central theme of this thesis. Our recent efforts and state-of-the-art approaches have provided further understanding of these interactions and set up a basis for future theoretical developments that will serve the objectives of both theoreticians and experimentalists.

A Supplementary Tables and Figures

A.1 Branched Alkanes Have Contrasting Stabilities

Table A.1: Comparisons between computed BSE based on the lowest energy conformer and Boltzmann averaged BSE accounting for all the conformers for an illustrative set of molecules. The error with respect to experiment is also reported. Energies are given in kcal/mol

Conformations	B3LYP/6-31G* BSE	Difference to lowest conformer BSE	Error to experiment
2,2,3-trimethylpentane + 6 CH ₄ → 7 C ₂ H ₆	7.98	0.00	
2,2,3-trimethylpentane 2	6.26	1.72	
2,2,3-trimethylpentane 3	5.00	2.98	
2,2,3-trimethylpentane 4	5.66	2.32	
2,2,3-trimethylpentane 5	5.27	2.71	
2,2,3-trimethylpentane (Boltzmann average)	7.81	0.17	-11.86
2,2,3,3-tetramethylpentane + 7 CH ₄ → 8 C ₂ H ₆	5.07	0.00	
2,2,3,3-tetramethylpentane 2	3.40	1.67	
2,2,3,3-tetramethylpentane 3	2.99	2.09	
2,2,3,3-tetramethylpentane (Boltzmann average)	4.93	0.15	-16.65
2,2,4-trimethylpentane + 6 CH ₄ → 7 C ₂ H ₆	9.57	0.00	
2,2,4-trimethylpentane 2	9.02	0.54	
2,2,4-trimethylpentane 3	5.97	3.60	
2,2,4-trimethylpentane (Boltzmann average)	9.41	0.16	-11.22
2,2,3,4-tetramethylpentane + 7 CH ₄ → 8 C ₂ H ₆	6.76	0.00	
2,2,3,4-tetramethylpentane 2	6.64	0.12	
2,2,3,4-tetramethylpentane 3	6.06	0.70	
2,2,3,4-tetramethylpentane 4	3.62	3.14	
2,2,3,4-tetramethylpentane 5	3.08	3.68	
2,2,3,4-tetramethylpentane 6	2.51	4.25	
2,2,3,4-tetramethylpentane (Boltzmann average)	6.60	0.16	-14.93
2,2,5,5-tetramethylhexane + 8 CH ₄ → 9 C ₂ H ₆	14.78	0.00	
2,2,5,5-tetramethylhexane 2	7.57	7.21	
2,2,5,5-tetramethylhexane (Boltzmann average)	14.78	0.00	-15.98

Continued on next page ...

Appendix A. Supplementary Tables and Figures

Table A.1 - Continued: Comparisons between computed BSE based on the lowest energy conformer and Boltzmann averaged BSE accounting for all the conformers for an illustrative set of molecules. The error with respect to experiment is also reported. Energies are given in kcal/mol

Conformations	B3LYP/6-31G* BSE	Difference to lowest conformer BSE	Error to experiment
2,3,3,4-tetramethylpentane + 7 CH ₄ → 8 C ₂ H ₆	5.65	0.00	
2,3,3,4-tetramethylpentane 2	3.46	2.19	
2,3,3,4-tetramethylpentane 3	3.08	2.57	
2,3,3,4-tetramethylpentane 4	2.54	3.11	
2,3,3,4-tetramethylpentane 5	2.03	3.62	
2,3,3,4-tetramethylpentane (Boltzmann average)	5.55	0.11	-15.76
Tetraethylhexane + 12 CH ₄ → 13 C ₂ H ₆	-11.65	0.00	
Tetraethylhexane 2	-12.00	0.35	
Tetraethylhexane 3	-12.09	0.44	
Tetraethylhexane 4	-12.38	0.73	
Tetraethylhexane 5	-12.54	0.88	
Tetraethylhexane 6	-13.34	1.68	
Tetraethylhexane 7	-13.88	2.23	
Tetraethylhexane 8	-14.01	2.36	
Tetraethylhexane 9	-14.20	2.54	
Tetraethylhexane 10	-14.43	2.77	
Tetraethylhexane 11	-14.57	2.92	
Tetraethylhexane 12	-15.16	3.50	
Tetraethylhexane (Boltzmann average)	-12.06	0.41	-29.68

A.1. Branched Alkanes Have Contrasting Stabilities

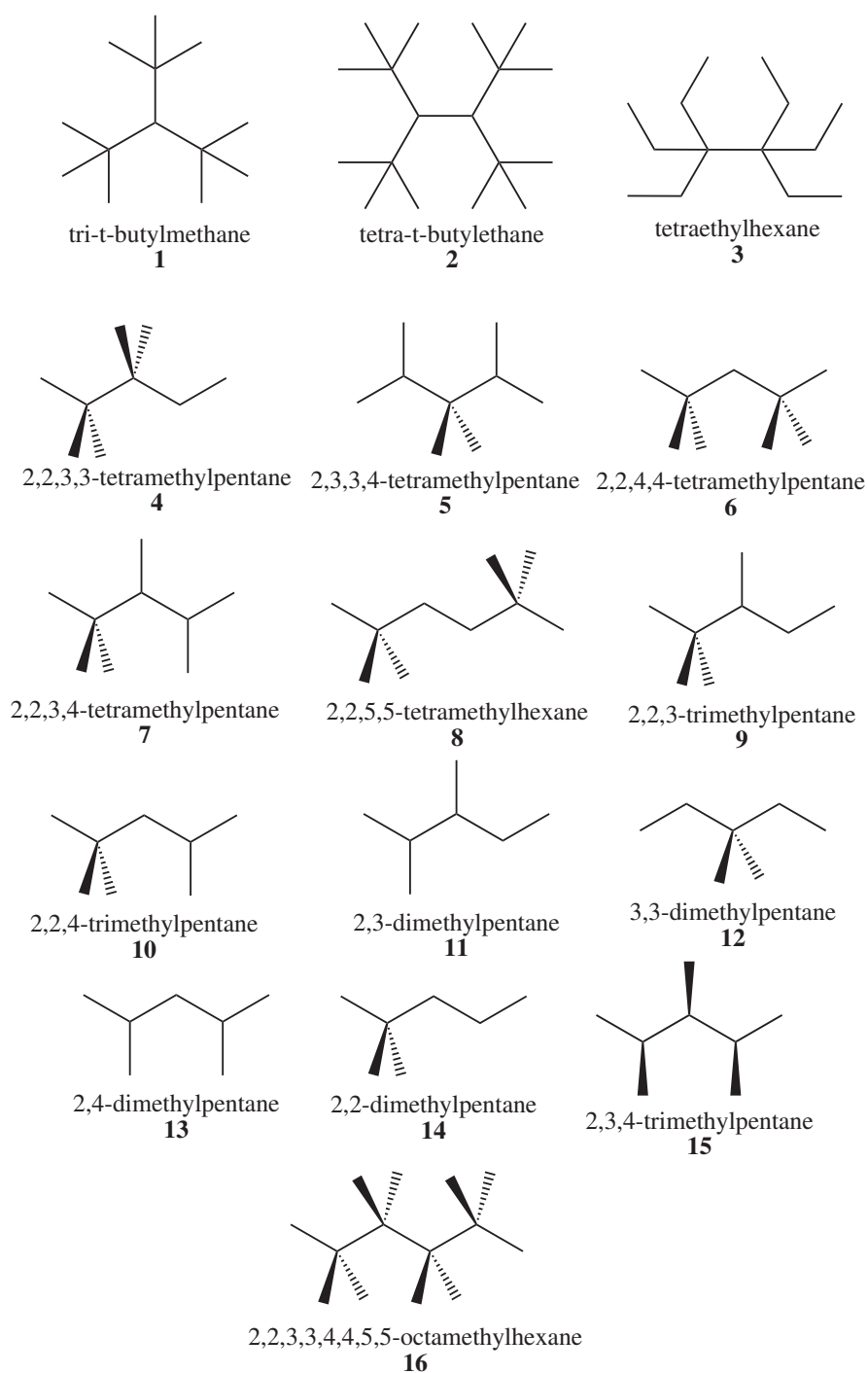


Figure A.1: Sketch of the 16 organic compounds in the test set for hyperhomodesmotic computations.

A.2 π -Depletion as a Criterion to predict π -stacking Ability

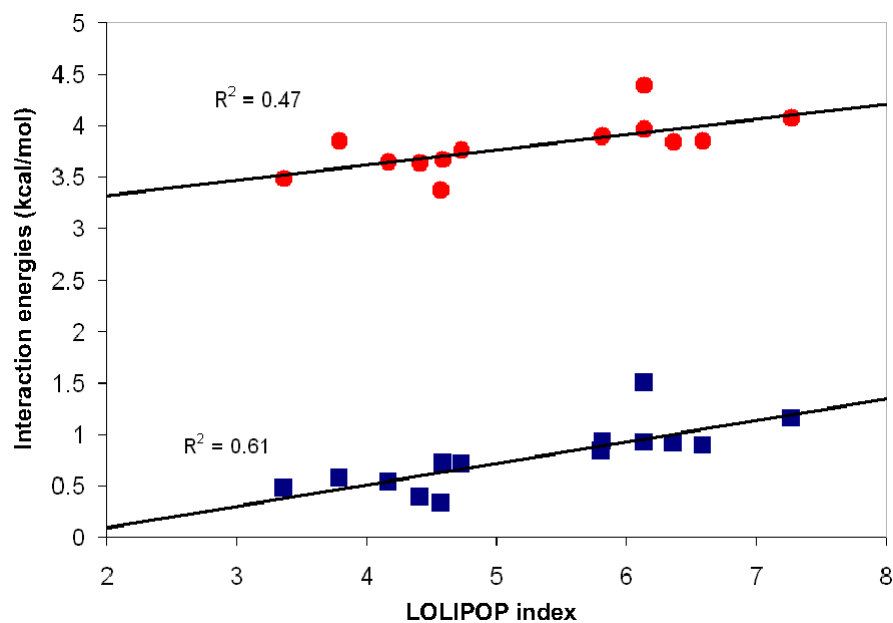


Figure A.2: HF (red circles) and PBE0 (blue squares) interaction energies plotted against LOLIPOP index for parallel stacked triazine geometries.

A.3. Four-Electron Oxygen Reduction by Tetrathiafulvalene

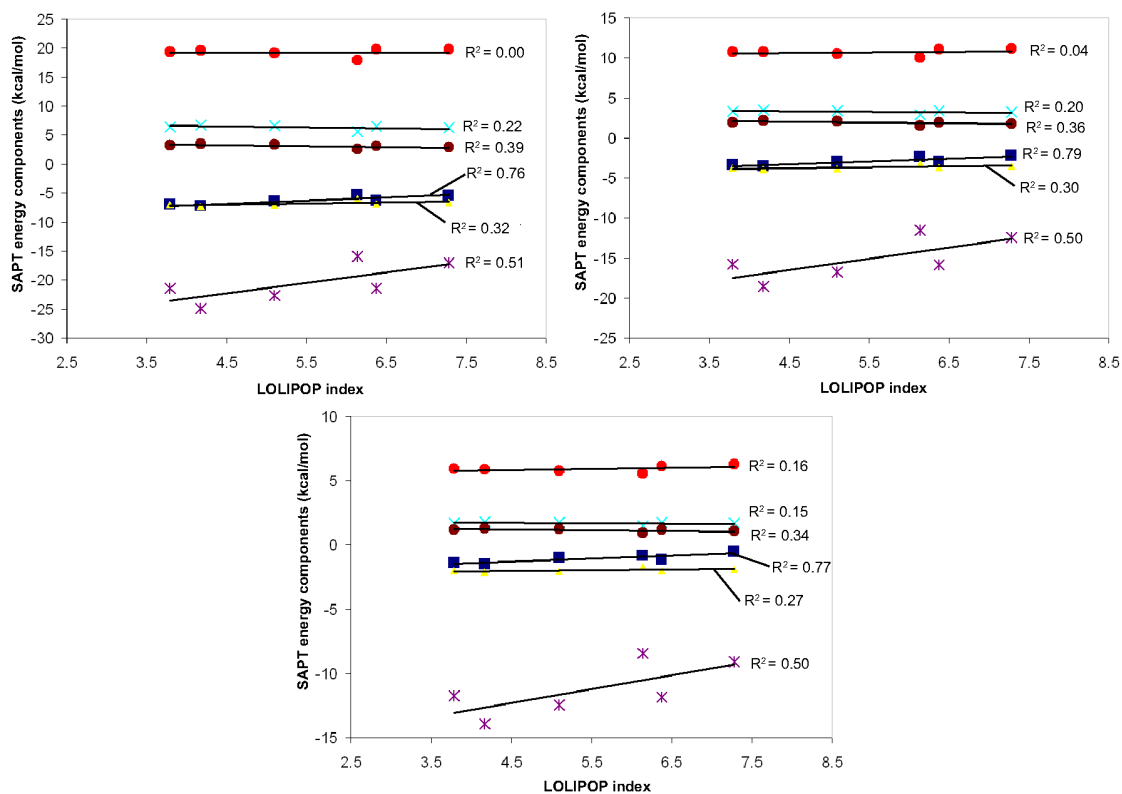


Figure A.3: SAPT0/aug-cc-pVDZ energy components plotted against LOLIPOP index for parallel stacked complexes of benzene: $E_{elst}^{(10)}$ (blue squares), $E_{exch}^{(10)}$ (red circles), $E_{ind}^{(20)}$ (yellow triangles), $E_{exch-ind}^{(20)}$ (light blue crosses), $E_{disp}^{(20)}$ (purple stars) and $E_{exch-disp}^{(20)}$ (brown circles) for vertical distance of 3.3 Å (top left), 3.5 Å (top right) and 3.7 Å (bottom). R^2 values indicate in all cases that the best correlation is between LOLIPOP and $E_{elst}^{(10)}$.

A.3 Four-Electron Oxygen Reduction by Tetrathiafulvalene

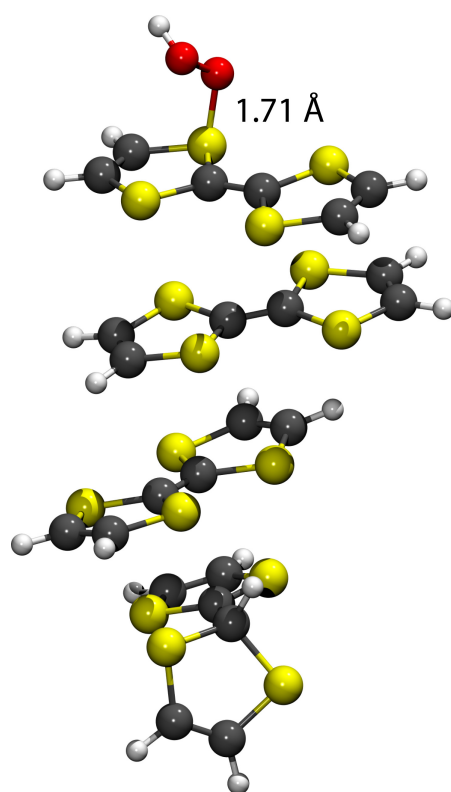


Figure A.4: Computed reaction pathway, enthalpies at 298 K computed at B3LYP-dDsC/6-31+G**//B3LYP-dDsC/6-31G** (M06-2X/cc-pVTZ//M06-2X/SVP numbers in parentheses) with continuum solvation. Conformer B (Figure 6.3a) is taken as the reference for energies computations. Thermal contribution and BSSE correction is from conformer A.

Bibliography

- [1] Moore, G. E. *Electronics* **1965**, April 19, 114–117.
- [2] Schrodinger, E. *Ann. Phys.* **1926**, 384, 361–376.
- [3] Huckel, E. *Z. Phys.* **1933**, 83, 632–668.
- [4] Huckel, E. *Z. Phys.* **1931**, 70, 204–286.
- [5] Huckel, E. *Z. Phys.* **1931**, 72, 310–337.
- [6] Huckel, E. *Z. Phys.* **1932**, 76, 628–648.
- [7] Hartree, D. R. *Proc. Camb. Phil. Soc.* **1928**, 24, 111–32.
- [8] Slater, J. C. *Phys. Rev.* **1930**, 35, 210–211.
- [9] Fock, V. Z. *Phys.* **1930**, 62, 795–805.
- [10] Fock, V. Z. *Phys.* **1930**, 61, 126–148.
- [11] Hartree, D. R.; Hartree, W. *Proc. R. Soc. London, A* **1935**, 150, 9–33.
- [12] Boys, S. F.; Cook, G. B.; Reeves, C. M.; Shavitt, I. *Nature* **1956**, 178, 1207–1209.
- [13] Roothaan, C. C. J. *J. Chem. Phys.* **1958**, 28, 982–983.
- [14] Mulliken, R. S.; Roothaan, C. C. J. *Proc. Natl. Acad. Sci.* **1959**, 45, 394–398.
- [15] Moller, C.; Plesset, M. S. *Phys. Rev.* **1934**, 46, 618–622.
- [16] Hartree, D. R.; Hartree, W.; Swirles, B. *Philos. Trans. R. Soc. London, A* **1939**, 238, 229–247.
- [17] Condon, E. U.; Shortley, G. H. *Phys. Rev.* **1931**, 37, 1025–1043.
- [18] Cizek, J. *J. Chem. Phys.* **1966**, 45, 4256–4266.
- [19] Sinanoglu, O. *J. Chem. Phys.* **1962**, 36, 706–717.
- [20] Bartlett, R. J.; Watts, J.; Kucharski, S.; Noga, J. *Chem. Phys. Lett.* **1990**, 165, 513–522.
- [21] Bartlett, R. J.; Watts, J.; Kucharski, S.; Noga, J. *Chem. Phys. Lett.* **1990**, 167, 60–9.

Bibliography

- [22] Raghavachari, K.; Trucks, G. W.; Pople, J. A.; Head-Gordon, M. *Chem. Phys. Lett.* **1989**, *157*, 479–483.
- [23] Fabian, W. M. F. *Monatsh. Chem.* **2008**, *139*, 309–318.
- [24] Hohenberg, P.; Kohn, W. *Phys. Rev.* **1964**, *136*, B864.
- [25] Becke, A. D. *J. Chem. Phys.* **1993**, *98*, 5648–5652.
- [26] Dykstra, C.; Lisy, J. *J. Mol. Struct. THEOCHEM* **2000**, *500*, 375–390.
- [27] Fukunishi, Y. *OMICS*; CRC Press, 2011; pp 281–292.
- [28] Eisenschitz, R.; London, F. *Z. Phys.* **1930**, *60*, 491–527.
- [29] London, F. *Z. Phys.* **1930**, *63*, 245–279.
- [30] Jeziorski, B.; Moszynski, R.; Szalewicz, K. *Chem. Rev.* **1994**, *94*, 1887–1930.
- [31] Hohenstein, E. G.; Sherrill, C. D. *WIREs Comput. Mol. Sci.* **2012**, *2*, 304–326.
- [32] Szalewicz, K. *WIREs Comput. Mol. Sci.* **2012**, *2*, 254–272.
- [33] Mayer, I. *Int. J. Quantum Chem.* **1983**, *23*, 341–363.
- [34] Mayer, I.; Surján, P. R. *Int. J. Quantum Chem.* **1989**, *36*, 225–240.
- [35] Mayer, I. *Phys. Chem. Chem. Phys.* **2012**, *14*, 337–344.
- [36] Stoll, H.; Wagenblast, G.; Preuss, H. *Theor. Chem. Acc.* **1980**, *57*, 169–178.
- [37] Nagata, T.; Takahashi, O.; Saito, K.; Iwata, S. *J. Chem. Phys.* **2001**, *115*, 3553–3560.
- [38] Gianinetti, E.; Raimondi, M.; Tornaghi, E. *Int. J. Quantum Chem.* **1996**, *60*, 157–166.
- [39] Sironi, M.; Famulari, A. *Theor. Chem. Acc.* **2000**, *103*, 417–422.
- [40] Mo, Y.; Peyerimhoff, S. D. *J. Chem. Phys.* **1998**, *109*, 1687–1697.
- [41] Khaliullin, R. Z.; Head-Gordon, M.; Bell, A. T. *J. Chem. Phys.* **2006**, *124*, 204105–11.
- [42] Smits, G.; Altona, C. *Theor. Chim. Acta* **1985**, *67*, 461–475.
- [43] Wheeler, S. E.; Houk, K. N.; Schleyer, P. v. R.; Allen, W. D. *J. Am. Chem. Soc.* **2009**, *131*, 2547–2560.
- [44] Gonthier, J. F.; Wodrich, M. D.; Steinmann, S. N.; Corminboeuf, C. *Org. Lett.* **2010**, *12*, 3070–3073.
- [45] Schmider, H.; Becke, A. *J. Mol. Struct. THEOCHEM* **2000**, *527*, 51–61.

- [46] Steinmann, S. N.; Mo, Y.; Corminboeuf, C. *Phys. Chem. Chem. Phys.* **2011**, *13*, 20584–20592.
- [47] Gonthier, J. F.; Steinmann, S. N.; Roch, L.; Ruggi, A.; Luisier, N.; Severin, K.; Corminboeuf, C. *Chem. Commun.* **2012**, *48*, 9239–9241.
- [48] Collman, J. P.; Wagenknecht, P. S.; Hutchison, J. E. *Angew. Chem. Int. Ed. Engl.* **1994**, *33*, 1537–1554.
- [49] Lee, C.; Yang, W.; Parr, R. G. *Phys. Rev. B* **1988**, *37*, 78–5.
- [50] Steinmann, S. N.; Corminboeuf, C. *J. Chem. Theory Comput.* **2010**, *6*, 1990–2001.
- [51] Steinmann, S. N.; Corminboeuf, C. *J. Chem. Phys.* **2011**, *134*, 044117–5.
- [52] Steinmann, S. N.; Corminboeuf, C. *J. Chem. Theory Comput.* **2011**, *7*, 3567–3577.
- [53] Zhao, Y.; Truhlar, D. *Theor. Chem. Acc.* **2008**, *120*, 215–241.
- [54] Zhao, Y.; Truhlar, D. G. *Acc. Chem. Res.* **2008**, *41*, 157–167.
- [55] Olaya, A. J.; Ge, P.; Gonthier, J. F.; Pechy, P.; Corminboeuf, C.; Girault, H. H. *J. Am. Chem. Soc.* **2011**, *133*, 12115–12123.
- [56] Boys, S. F.; Bernardi, F. *Mol. Phys.* **1970**, *19*, 553–566.
- [57] Mayer, I. *Int. J. Quantum Chem.* **1998**, *70*, 41–63.
- [58] Mayer, I. *Theor. Chim. Acta* **1987**, *72*, 207–210.
- [59] Jensen, F. *J. Chem. Theory Comput.* **2010**, *6*, 100–106.
- [60] Surjan, P. R.; Mayer, I.; Lukovits, I. *Chem. Phys. Lett.* **1985**, *119*, 538–542.
- [61] Kruse, H.; Grimme, S. *J. Chem. Phys.* **2012**, *136*, 154101–16.
- [62] Ahlrichs, R. *Theor. Chim. Acta* **1976**, *41*, 7–15.
- [63] Hirschfelder, J. *Chem. Phys. Lett.* **1967**, *1*, 325–329.
- [64] Stone, A. J. *The Theory of Intermolecular Forces*; Oxford University Press, Oxford, 1996.
- [65] Freitag, M. A.; Gordon, M. S.; Jensen, J. H.; Stevens, W. J. *J. Chem. Phys.* **2000**, *112*, 7300–7306.
- [66] Szabo, A.; Ostlund, N. S. *Modern quantum chemistry - Introduction to Advanced Electronic Structure Theory*; Dover publications, inc., 1996.
- [67] Chalasinski, G.; Jeziorski, B.; Szalewicz, K. *Int. J. Quantum Chem.* **1977**, *11*, 247–257.
- [68] Cwiok, T.; Jeziorski, B.; Kolos, W.; Moszynski, R.; Rychlewski, J.; Szalewicz, K. *Chem. Phys. Lett.* **1992**, *195*, 67–76.

Bibliography

- [69] Jeziorski, B.; Schwalm, W. A.; Szalewicz, K. *J. Chem. Phys.* **1980**, *73*, 6215–6224.
- [70] Chipman, D. M.; Bowman, J. D.; Hirschfelder, J. O. *J. Chem. Phys.* **1973**, *59*, 2830–2837.
- [71] Jeziorski, B.; Szalewicz, K.; Chalasinski, G. *Int. J. Quantum Chem.* **1978**, *14*, 271–287.
- [72] Szalewicz, K.; Jeziorski, B. *Mol. Phys.* **1979**, *38*, 191–208.
- [73] Moszynski, R.; Jeziorski, B.; Szalewicz, K. *J. Chem. Phys.* **1994**, *100*, 1312–1325.
- [74] Hesselmann, A.; Jansen, G. *Chem. Phys. Lett.* **2002**, *357*, 464–470.
- [75] Williams, H. L.; Chabalowski, C. F. *J. Phys. Chem. A* **2000**, *105*, 646–659.
- [76] Jansen, G.; Hesselmann, A. *J. Phys. Chem. A* **2001**, *105*, 11156–11157.
- [77] Williams, H. L.; Chabalowski, C. F. *J. Phys. Chem. A* **2001**, *105*, 11158–11158.
- [78] Hesselmann, A.; Jansen, G. *Chem. Phys. Lett.* **2002**, *362*, 319–325.
- [79] Hesselmann, A.; Jansen, G. *Chem. Phys. Lett.* **2003**, *367*, 778–784.
- [80] Misquitta, A. J.; Szalewicz, K. *Chem. Phys. Lett.* **2002**, *357*, 301–306.
- [81] Turney, J. M.; Simmonett, A. C.; Parrish, R. M.; Hohenstein, E. G.; Evangelista, F. A.; Fermann, J. T.; Mintz, B. J.; Burns, L. A.; Wilke, J. J.; Abrams, M. L.; Russ, N. J.; Leininger, M. L.; Janssen, C. L.; Seidl, E. T.; Allen, W. D.; Schaefer, H. F.; King, R. A.; Valeev, E. F.; Sherrill, C. D.; Crawford, T. D. *WIREs Comput. Mol. Sci.* **2012**, *2*, 556–565.
- [82] Hohenstein, E. G.; Sherrill, C. D. *J. Chem. Phys.* **2010**, *132*, 184111–10.
- [83] Hohenstein, E. G.; Parrish, R. M.; Sherrill, C. D.; Turney, J. M.; Schaefer, H. F.; III, J. *Chem. Phys.* **2011**, *135*, 174107–13.
- [84] Hohenstein, E. G.; Sherrill, C. D. *J. Chem. Phys.* **2010**, *133*, 104107–7.
- [85] Mayer, I.; Vibok, A. *Chem. Phys. Lett.* **1987**, *136*, 115–121.
- [86] Mayer, I.; Vibok, A. *Chem. Phys. Lett.* **1987**, *140*, 558–564.
- [87] Mayer, I. *J. Mol. Struct. THEOCHEM* **1988**, *165*, 255–272.
- [88] Vibok, A.; Mayer, I. *J. Mol. Struct. THEOCHEM* **1988**, *170*, 9–17.
- [89] Mayer, I.; Turi, L. *J. Mol. Struct. THEOCHEM* **1991**, *227*, 43–65.
- [90] Mayer, I. *Int. J. Quantum Chem.* **2002**, *90*, 89–91.
- [91] Halasz, G.; Vibok, A.; Suhai, S.; Mayer, I. *Int. J. Quantum Chem.* **2002**, *89*, 190–197.
- [92] Kieninger, M.; Suhai, S.; Mayer, I. *Chem. Phys. Lett.* **1994**, *230*, 485–490.

- [93] Mayer, I.; Valiron, P. *J. Chem. Phys.* **1998**, *109*, 3360–3373.
- [94] Salvador, P.; Asturiol, D.; Mayer, I. *J. Comput. Chem.* **2006**, *27*, 1505–1516.
- [95] Mulliken, R. S. *J. Chem. Phys.* **1955**, *23*, 1833–1840.
- [96] Slater, J. C. *J. Chem. Phys.* **1933**, *1*, 687–691.
- [97] Ruedenberg, K. *Rev. Mod. Phys.* **1962**, *34*, 326–376.
- [98] Bacskay, G. B.; Nordholm, S. *J. Phys. Chem. A* **2013**, *117*, 7946–7958.
- [99] Ruedenberg, K.; Schmidt, M. W. *J. Comput. Chem.* **2007**, *28*, 391–410.
- [100] Ruedenberg, K.; Schmidt, M. W. *J. Phys. Chem. A* **2009**, *113*, 1954–1968.
- [101] Nordholm, S.; Eek, W. *Int. J. Quantum Chem.* **2011**, *111*, 2072–2088.
- [102] Bader, R. F. W. *J. Phys. Chem. A* **2011**, *115*, 12667–12676.
- [103] Bader, R. F. *Found. Chem.* **2011**, *13*, 11–37.
- [104] Esterhuysen, C.; Frenking, G. *Theor. Chem. Acc.* **2004**, *111*, 381–389.
- [105] Bader, R. F. W.; Hernandez-Trujillo, J.; Cortes-Guzman, F. *J. Comput. Chem.* **2007**, *28*, 4–14.
- [106] Mayer, I. *Chem. Phys. Lett.* **2003**, *382*, 265–269.
- [107] Mayer, I. *Phys. Chem. Chem. Phys.* **2006**, *8*, 4630–4646.
- [108] Mayer, I. *Faraday Discuss.* **2007**, *135*, 439–450.
- [109] Dewar, M. J. S.; Thiel, W. *J. Am. Chem. Soc.* **1977**, *99*, 4899–4907.
- [110] Mayer, I. *Chem. Phys. Lett.* **2000**, *332*, 381–388.
- [111] Mayer, I. *J. Phys. Chem.* **1996**, *100*, 6249–6257.
- [112] Mayer, I. *Chem. Phys. Lett.* **1995**, *242*, 499–506.
- [113] Pipek, J.; Mezey, P. G. *J. Chem. Phys.* **1989**, *90*, 4916–4926.
- [114] Boys, S. In *Quantum Science of Atoms, Molecules, and Solids*; Löwdin, P., Ed.; Academic Press: New York, 1966.
- [115] Edmiston, C.; Ruedenberg, K. *Rev. Mod. Phys.* **1963**, *35*, 45–7.
- [116] Gianinetti, E.; Vandoni, I.; Famulari, A.; Raimondi, M. *Advances in Quantum Chemistry*; Academic Press, 1998; Vol. 31; pp 251 – 266.
- [117] Nagata, T.; Iwata, S. *J. Chem. Phys.* **2004**, *120*, 3555–3562.

Bibliography

- [118] Baarman, K.; VandeVondele, J. *J. Chem. Phys.* **2011**, *134*, 24410–4.
- [119] Sutcliffe, B. T. *Theor. Chem. Acc.* **1974**, *33*, 201–214.
- [120] VandeVondele, J.; Hutter, J. *J. Chem. Phys.* **2003**, *118*, 436–5.
- [121] Van Voorhis, T.; Head-Gordon, M. *Mol. Phys.* **2002**, *100*, 1713–1721.
- [122] Naray-Szabo, G. *Comput. Chem.* **2000**, *24*, 287–294.
- [123] Pozzoli, S. A.; Rastelli, A.; Tedeschi, M. *J. Chem. Soc., Faraday Trans. 2* **1973**, *69*, 256–261.
- [124] Naray-Szabo, G.; R. Surjan, P. *Chem. Phys. Lett.* **1983**, *96*, 499–501.
- [125] Mo, Y. *Nat. Chem.* **2010**, *2*, 666–671.
- [126] Hamza, A.; Vibok, A.; Halasz, G.; Mayer, I. *J. Mol. Struct. THEOCHEM* **2000**, *501-502*, 427–434.
- [127] Genoni, A.; Sironi, M. *Theor. Chem. Acc.* **2004**, *112*, 254–262.
- [128] Kitaura, K.; Morokuma, K. *Int. J. Quantum Chem.* **1976**, *10*, 325–340.
- [129] Mo, Y.; Gao, J.; Peyerimhoff, S. D. *J. Chem. Phys.* **2000**, *112*, 5530–5538.
- [130] Khaliullin, R. Z.; Cobar, E. A.; Lochan, R. C.; Bell, A. T.; Head-Gordon, M. *J. Phys. Chem. A* **2007**, *111*, 8753–8765.
- [131] Steinmann, S. N.; Corminboeuf, C.; Wu, W.; Mo, Y. *J. Phys. Chem. A* **2011**, *115*, 5467–5477.
- [132] Mo, Y.; Bao, P.; Gao, J. *J. Phys. Chem. Chem. Phys.* **2011**, *13*, 6760–6775.
- [133] Sironi, M.; Genoni, A.; Civera, M.; Pieraccini, S.; Ghitti, M. *Theor. Chem. Acc.* **2007**, *117*, 685–698.
- [134] Mo, Y.; Gao, J. *Acc. Chem. Res.* **2007**, *40*, 113–119.
- [135] Jia, J.-F.; Wu, H.-S.; Mo, Y. *J. Chem. Phys.* **2012**, *136*, 144315–7.
- [136] Mo, Y.; Schleyer, P. v. R.; Wu, W.; Lin, M.; Zhang, Q.; Gao, J. *J. Phys. Chem. A* **2003**, *107*, 10011–10018.
- [137] Mo, Y. *J. Org. Chem.* **2004**, *69*, 5563–5567.
- [138] Fornili, A.; Moreau, Y.; Sironi, M.; Assfeld, X. *J. Comput. Chem.* **2006**, *27*, 515–523.
- [139] Sironi, M.; Ghitti, M.; Genoni, A.; Saladino, G.; Pieraccini, S. *J. Mol. Struct. THEOCHEM* **2009**, *898*, 8–16.

- [140] Chen, W.; Gordon, M. S. *J. Phys. Chem.* **1996**, *100*, 14316–14328.
- [141] Stevens, W. J.; Fink, W. H. *Chem. Phys. Lett.* **1987**, *139*, 15–22.
- [142] Bickelhaupt, F. M.; Nibbering, N. M. M.; Van Wezenbeek, E. M.; Baerends, E. J. *J. Phys. Chem.* **1992**, *96*, 4864–4873.
- [143] Frenking, G.; Wichmann, K.; Fröhlich, N.; Loschen, C.; Lein, M.; Frunzke, J.; Rayón, V. M. *Coord. Chem. Rev.* **2003**, *238-239*, 55–82.
- [144] Ziegler, T.; Rauk, A. *Theor. Chem. Acc.* **1977**, *46*, 1–10.
- [145] Olszewski, K. A.; Gutowski, M.; Piela, L. *J. Phys. Chem.* **1990**, *94*, 5710–5714.
- [146] Bagus, P. S.; Hermann, K.; Bauschlicher, C. W., Jr. *J. Chem. Phys.* **1984**, *80*, 4378–4386.
- [147] Glendening, E. D. *J. Am. Chem. Soc.* **1996**, *118*, 2473–2482.
- [148] Schenter, G. K.; Glendening, E. D. *J. Phys. Chem.* **1996**, *100*, 17152–17156.
- [149] Reed, A. E.; Curtiss, L. A.; Weinhold, F. *Chem. Rev.* **1988**, *88*, 899–926.
- [150] Wei, H.; Hrovat, D. A.; Mo, Y.; Hoffmann, R.; Borden, W. T. *J. Phys. Chem. A* **2009**, *113*, 10351–10358.
- [151] Koster, A. M.; Calaminici, P.; Geudtner, G.; Gomez-Sandoval, Z. *J. Phys. Chem. A* **2005**, *109*, 1257–1259.
- [152] Cardozo, T. M.; Nascimento, M. A. C. *J. Chem. Phys.* **2009**, *130*, 10410–2.
- [153] Salvador, P.; Mayer, I. *J. Chem. Phys.* **2004**, *120*, 5046–5052.
- [154] Day, P. N.; Jensen, J. H.; Gordon, M. S.; Webb, S. P.; Stevens, W. J.; Krauss, M.; Garmer, D.; Basch, H.; Cohen, D. *J. Chem. Phys.* **1996**, *105*, 1968–1986.
- [155] Mochizuki, Y.; Fukuzawa, K.; Kato, A.; Tanaka, S.; Kitaura, K.; Nakano, T. *Chem. Phys. Lett.* **2005**, *410*, 247–253.
- [156] Addicoat, M. A.; Collins, M. A. *J. Chem. Phys.* **2009**, *131*, 10410–3.
- [157] Fedorov, D. G.; Kitaura, K. *J. Phys. Chem. A* **2007**, *111*, 6904–6914.
- [158] Schutz, M.; Rauhut, G.; Werner, H.-J. *J. Phys. Chem. A* **1998**, *102*, 5997–6003.
- [159] Korchowiec, J.; Uchimaru, T. *J. Chem. Phys.* **2000**, *112*, 1623–1633.
- [160] Chalasinski, G.; Szczesniak, M. M. *Chem. Rev.* **1994**, *94*, 1723–1765.
- [161] Fukuzawa, K.; Komeiji, Y.; Mochizuki, Y.; Kato, A.; Nakano, T.; Tanaka, S. *J. Comput. Chem.* **2006**, *27*, 948–960.

Bibliography

- [162] Pendas, A. M.; Blanco, M. A.; Francisco, E. *J. Comput. Chem.* **2007**, *28*, 161–184.
- [163] Gonfloni, S.; Frischknecht, F.; Way, M.; Superti-Furga, G. *Nat. Struct. Mol. Biol.* **1999**, *6*, 760–764.
- [164] Wodrich, M. D.; Jana, D. F.; Schleyer, P. v. R.; Corminboeuf, C. *J. Phys. Chem. A* **2008**, *112*, 11495–11500.
- [165] Goodson, T. G. *Acc. Chem. Res.* **2005**, *38*, 99–107.
- [166] Goodson, T. *Annu. Rev. Phys. Chem.* **2005**, *56*, 581–603.
- [167] Pérez-Galán, P.; Delpont, N.; Herrero-Gómez, E.; Maseras, F.; Echavarren, A. *Chem. Eur. J.* **2010**, *16*, 5324–5332.
- [168] James III, W. H.; Müller, C. W.; Buchanan, E. G.; Nix, M. G. D.; Guo, L.; Roskop, L.; Gordon, M. S.; Slipchenko, L. V.; Gellman, S. H.; Zwier, T. S. *J. Am. Chem. Soc.* **2009**, *131*, 14243–14245.
- [169] Patkowski, K.; Szalewicz, K.; Jeziorski, B. *J. Chem. Phys.* **2006**, *125*, 15410–7.
- [170] Hohenstein, E. G.; Jaeger, H. M.; Carrell, E. J.; Tschumper, G. S.; Sherrill, C. D. *J. Chem. Theory Comput.* **2011**, *7*, 2842–2851.
- [171] Jaeger, H. M.; Schaefer, H. F.; Hohenstein, E. G.; David Sherrill, C. *Comput. Theor. Chem.* **2011**, *973*, 47–52.
- [172] Matczak, P. *J. Phys. Chem. A* **2012**, *116*, 8731–8736.
- [173] van der Avoird, A.; Podeszwa, R.; Szalewicz, K.; Leforestier, C.; van Harrevelt, R.; Bunker, P. R.; Schnell, M.; von Helden, G.; Meijer, G. *Phys. Chem. Chem. Phys.* **2010**, *12*, 8219–8240.
- [174] Yamada, K.; Koga, N. *Theor. Chem. Acc.* **2012**, *131*, 1–17.
- [175] Yamada, K.; Koga, N. *J. Comput. Chem.* **2013**, *34*, 149–161.
- [176] Cooper, D. L.; Karadakov, P. B. *Int. Rev. Phys. Chem.* **2009**, *28*, 169–206.
- [177] Jurecka, P.; Sponer, J.; Cerny, J.; Hobza, P. *Phys. Chem. Chem. Phys.* **2006**, *8*, 1985–1993.
- [178] Dunning, T. H., Jr. *J. Chem. Phys.* **1989**, *90*, 1007–1023.
- [179] Zoboki, T.; Mayer, I. *J. Comput. Chem.* **2011**, *32*, 689–695.
- [180] Ehrlich, S.; Bettinger, H. F.; Grimme, S. *Angew. Chem. Int. Ed.* **2013**, *52*, 10892–10895.
- [181] Luttschwager, N. O. B.; Wassermann, T. N.; Mata, R. A.; Suhm, M. A. *Angew. Chem. Int. Ed.* **2013**, *52*, 463–466.
- [182] Jablonski, M. *J. Phys. Chem. A* **2012**, *116*, 3753–3764.

- [183] Rekken, B. D.; Brown, T. M.; Fettingner, J. C.; Lips, F.; Tuononen, H. M.; Herber, R. H.; Power, P. P. *J. Am. Chem. Soc.* **2013**, *135*, 10134–10148.
- [184] Baranovic, G.; Biliskov, N.; Vojta, D. *J. Phys. Chem. A* **2012**, *116*, 8397–8406.
- [185] Rossini, F. D. *Bur. Stand. J. Res.* **1934**, *13*, 21–35.
- [186] Nenitzescu, C. D.; Chicos, I. *Ber. Dtsch. Chem. Ges.* **1935**, *68*, 1584–1587.
- [187] McKee, W. C.; Schleyer, P. v. R. *J. Am. Chem. Soc.* **2013**, *135*, 13008–13014.
- [188] Pitzer, K. S.; Catalano, E. *J. Am. Chem. Soc.* **1956**, *78*, 4844–4846.
- [189] Kemnitz, C. R. *Chem. Eur. J.* **2013**, *19*, 11093–11095.
- [190] Inagaki, S. In *Topics in Current Chemistry*; Inagaki, S., Ed.; Springer Berlin Heidelberg, 2010; Vol. 289; pp 83–127.
- [191] Ma, J.; Inagaki, S. *J. Am. Chem. Soc.* **2001**, *123*, 1193–1198.
- [192] Jacob, E. J.; Thompson, H. B.; Bartell, L. S. *J. Chem. Phys.* **1967**, *47*, 3736–3753.
- [193] Bartell, L. S. *J. Am. Chem. Soc.* **1959**, *81*, 3497–3498.
- [194] Bartell, L. S. *J. Chem. Phys.* **1960**, *32*, 827–831.
- [195] Gronert, S. *J. Org. Chem.* **2006**, *71*, 1209–1219.
- [196] Gronert, S. *J. Org. Chem.* **2006**, *71*, 9560–9560.
- [197] Gronert, S. *Chem. Eur. J.* **2013**, *19*, 11090–11092.
- [198] Gronert, S. *Org. Lett.* **2007**, *9*, 2211–2214.
- [199] Wodrich, M.; Wannere, C.; Mo, Y.; Jarowski, P.; Houk, K.; Schleyer, P. *Chem. Eur. J.* **2007**, *13*, 7731–7744.
- [200] Gronert, S. *Chem. Eur. J.* **2009**, *15*, 5372–5382.
- [201] Grimme, S. *Angew. Chem. Int. Ed.* **2006**, *45*, 4460–4464.
- [202] Hehre, W. J.; Ditchfield, R.; Pople, J. A. *J. Chem. Phys.* **1972**, *56*, 2257–2261.
- [203] Hariharan, P. C.; Pople, J. A. *Theor. Chem. Acc.* **1973**, *28*, 213–222.
- [204] Schafer, A.; Horn, H.; Ahlrichs, R. *J. Chem. Phys.* **1992**, *97*, 2571–2577.
- [205] Weigend, F.; Ahlrichs, R. *Phys. Chem. Chem. Phys.* **2005**, *7*, 3297–3305.
- [206] Krishnan, R.; Binkley, J. S.; Seeger, R.; Pople, J. A. *J. Chem. Phys.* **1980**, *72*, 650–654.
- [207] Frisch, M. J.; Pople, J. A.; Binkley, J. S. *J. Chem. Phys.* **1984**, *80*, 3265–3269.

Bibliography

- [208] Mo, Y.; Hiberty, P. C.; Schleyer, P. v. R. *Theor. Chem. Acc.* **2010**, *127*, 27–38.
- [209] Wodrich, M. D.; Schleyer, P. v. R. *Org. Lett.* **2006**, *8*, 2135–2138.
- [210] Zavitsas, A. A.; Matsunaga, N.; Rogers, D. W. *J. Phys. Chem. A* **2008**, *112*, 5734–5741.
- [211] Fishtik, I. *J. Phys. Chem. A* **2010**, *114*, 3731–3736.
- [212] Schleyer, P. v. R.; McKee, W. C. *J. Phys. Chem. A* **2010**, *114*, 3737–3740.
- [213] Kemnitz, C. R.; Mackey, J. L.; Loewen, M. J.; Hargrove, J. L.; Lewis, J. L.; Hawkins, W. E.; Nielsen, A. F. *Chem. Eur. J.* **2010**, *16*, 6942–6949.
- [214] Nalin de Silva, K. M.; Goodman, J. M. *J. Chem. Inf. Model.* **2004**, *45*, 81–87.
- [215] Rüchardt, C.; Beckhaus, H.-D.; Hellmann, G.; Weiner, S.; Winiker, R. *Angew. Chem. Int. Ed. Engl.* **1977**, *16*, 875–876.
- [216] Afeefy, H.; Liebman, J.; Stein, S. In *NIST Chemistry WebBook, NIST Standard Reference Database Number 69*; Linstrom, P. J., Mallard, W., Eds.; National Institute of Standards and Technology, Gaithersburg MD, 20899, 2009; Chapter Neutral Thermochemical Data.
- [217] Hehre, W. J.; Ditchfield, R.; Radom, L.; Pople, J. A. *J. Am. Chem. Soc.* **1970**, *92*, 4796–4801.
- [218] Pople, J. A.; Radom, L.; Hehre, W. J. *J. Am. Chem. Soc.* **1971**, *93*, 289–300.
- [219] Hehre, W. J.; Radom, L.; Schleyer, P. v. R.; Pople, J. A. *Ab Initio Molecular Orbital Theory*; John Wiley & Sons, New York, 1986.
- [220] Addicoat, M. A.; Metha, G. F. *J. Comput. Chem.* **2009**, *30*, 57–64.
- [221] Avaltroni, F.; Corminboeuf, C. *J. Comput. Chem.* **2011**, *32*, 1869–1875.
- [222] Saunders, M. *J. Comput. Chem.* **2004**, *25*, 621–626.
- [223] Vosko, S. H.; Wilk, L.; Nusair, M. *Can. J. Phys.* **1980**, *58*, 1200–1211.
- [224] Kohn, W.; Sham, L. J. *Phys. Rev.* **1965**, *140*, A1133.
- [225] Slater, J. C. *The Self-Consistent Field for Molecular and Solids, Quantum Theory of Molecular and Solids*; McGraw-Hill, New York, 1974; Vol. 4.
- [226] Perdew, J. P.; Burke, K.; Ernzerhof, M. *Phys. Rev. Lett.* **1996**, *77*, 386–5.
- [227] Grimme, S. *J. Comput. Chem.* **2004**, *25*, 1463–1473.
- [228] Steinmann, S. N.; Csonka, G.; Corminboeuf, C. *J. Chem. Theory Comput.* **2009**, *5*, 2950–2958.
- [229] Grimme, S. *J. Chem. Phys.* **2006**, *124*, 034108–16.

- [230] Schwabe, T.; Grimme, S. *Phys. Chem. Chem. Phys.* **2007**, *9*, 3397–3406.
- [231] Werner, H.-J.; Manby, F. R.; Knowles, P. J. *J. Chem. Phys.* **2003**, *118*, 8149–8160.
- [232] Grimme, S. *J. Chem. Phys.* **2003**, *118*, 9095–9102.
- [233] Frisch, M. J.; Trucks, G. W.; Schlegel, H. B.; Scuseria, G. E.; Robb, M. A.; Cheeseman, J. R.; Scalmani, G.; Barone, V.; Mennucci, B.; Petersson, G. A.; Nakatsuji, H.; Caricato, M.; Li, X.; Hratchian, H. P.; Izmaylov, A. F.; Bloino, J.; Zheng, G.; Sonnenberg, J. L.; Hada, M.; Ehara, M.; Toyota, K.; Fukuda, R.; Hasegawa, J.; Ishida, M.; Nakajima, T.; Honda, Y.; Kitao, O.; Nakai, H.; Vreven, T.; Montgomery, J. A., Jr.; Peralta, J. E.; Ogliaro, F.; Bearpark, M.; Heyd, J. J.; Brothers, E.; Kudin, K. N.; Staroverov, V. N.; Kobayashi, R.; Normand, J.; Raghavachari, K.; Rendell, A.; Burant, J. C.; Iyengar, S. S.; Tomasi, J.; Cossi, M.; Rega, N.; Millam, J. M.; Klene, M.; Knox, J. E.; Cross, J. B.; Bakken, V.; Adamo, C.; Jaramillo, J.; Gomperts, R.; Stratmann, R. E.; Yazyev, O.; Austin, A. J.; Cammi, R.; Pomelli, C.; Ochterski, J. W.; Martin, R. L.; Morokuma, K.; Zakrzewski, V. G.; Voth, G. A.; Salvador, P.; Dannenberg, J. J.; Dapprich, S.; Daniels, A. D.; Farkas, O.; Foresman, J. B.; Ortiz, J. V.; Cioslowski, J.; Fox, D. J. Gaussian 09 Revision A.2. Gaussian Inc. Wallingford CT 2009.
- [234] Werner, H.-J.; Knowles, P. J.; Lindh, R.; Manby, F. R.; Schütz, M.; Celani, P.; Korona, T.; Mitrushenkov, A.; Rauhut, G.; Adler, T. B.; Amos, R. D.; Bernhardsson, A.; Berning, A.; Cooper, D. L.; Deegan, M. J. O.; Dobbyn, A. J.; Eckert, F.; Goll, E.; Hampel, C.; Heter, G.; Hrenar, T.; Knizia, G.; Köppl, C.; Liu, Y.; Lloyd, A. W.; Mata, R. A.; May, A. J.; McNicholas, S. J.; Meyer, W.; Mura, M. E.; Nicklass, A.; Palmieri, P.; Pflüger, K.; Pitzer, R.; Reiher, M.; Schumann, U.; Stoll, H.; Stone, A. J.; Tarroni, R.; Thorsteinsson, T.; Wang, M.; Wolf, A. MOLPRO, version 2009.1, a package of ab initio programs. 2009; see www.molpro.net.
- [235] Köster, A. M.; Calaminici, P.; Casida, M. E.; Flores-Moreno, R.; Geudtner, G.; Goursot, A.; Heine, T.; Ipatov, A.; Janetzko, F.; del Campo, J. M.; Patchkovskii, S.; Revelles, J. U.; Salahub, D. R.; Vela, A. deMon2k. 2006; deMon developers.
- [236] Adler, T. B.; Knizia, G.; Werner, H.-J. *J. Chem. Phys.* **2007**, *127*, 221106–4.
- [237] Peterson, K. A.; Adler, T. B.; Werner, H.-J. *J. Chem. Phys.* **2008**, *128*, 084102–12.
- [238] Hill, J. G.; Peterson, K. A.; Knizia, G.; Werner, H.-J. *J. Chem. Phys.* **2009**, *131*, 194105–13.
- [239] Hess, B. A.; Schaad, L. J. *J. Am. Chem. Soc.* **1971**, *93*, 305–310.
- [240] Hess, B., Jr.; Schaad, L. *J. Am. Chem. Soc.* **1983**, *105*, 7500–7505.
- [241] Cox, R. D.; Pilcher, G. *Thermochemistry of Organic and Organometallic Compounds*; Academic Press, New York, 1970.

Bibliography

- [242] Stull, D. R.; Westrum, J., Edgar F.; Sinke, G. C. *The Chemical Thermodynamics of Organic Compounds.*; Wiley, 1969.
- [243] Wodrich, M. D.; Corminboeuf, C.; Schleyer, P. v. R. *Org. Lett.* **2006**, *8*, 3631–3634.
- [244] Wodrich, M. D.; Corminboeuf, C.; Schreiner, P. R.; Fokin, A. A.; Schleyer, P. v. R. *Org. Lett.* **2007**, *9*, 1851–1854.
- [245] Schreiner, P. *Angew. Chem. Int. Ed.* **2007**, *46*, 4217–4219.
- [246] Wodrich, M. D.; Corminboeuf, C. *J. Phys. Chem. A* **2009**, *113*, 3285–3290.
- [247] Schreiner, P. R.; Fokin, A. A.; Pascal, R. A.; de Meijere, A. *Org. Lett.* **2006**, *8*, 3635–3638.
- [248] Alder, R. W.; Maunder, C. M.; Guy Orpen, A. *Tetrahedron Lett.* **1990**, *31*, 6717–6720.
- [249] Wade, L. G. In *Organic Chemistry*; River, U. S., Ed.; Prentice Hall, 1999.
- [250] Streitwieser, A.; Heathcock, C. H.; Kosower, E. M. In *Introduction to organic chemistry*; River, U. S., Ed.; Prentice Hall, 1998.
- [251] Salonen, L. M.; Ellermann, M.; Diederich, F. *Angew. Chem. Int. Ed.* **2011**, *50*, 4808–4842.
- [252] Martinez, C. R.; Iverson, B. L. *Chem. Sci.* **2012**, *3*, 2191–2201.
- [253] Sinnokrot, M. O.; Sherrill, C. D. *J. Am. Chem. Soc.* **2004**, *126*, 7690–7697.
- [254] Raju, R. K.; Bloom, J. W. G.; An, Y.; Wheeler, S. E. *ChemPhysChem* **2011**, *12*, 3116–3130.
- [255] Hohenstein, E. G.; Sherrill, C. D. *J. Phys. Chem. A* **2009**, *113*, 878–886.
- [256] Hohenstein, E. G.; Duan, J.; Sherrill, C. D. *J. Am. Chem. Soc.* **2011**, *133*, 13244–13247.
- [257] Bloom, J. W. G.; Wheeler, S. E. *Angew. Chem. Int. Ed.* **2011**, *50*, 7847–7849.
- [258] Cozzi, F.; Cinquini, M.; Annuziata, R.; Siegel, J. S. *J. Am. Chem. Soc.* **1993**, *115*, 5330–5331.
- [259] Becke, A. D. *Phys. Rev. A* **1988**, *38*, 3098–3100.
- [260] Perdew, J. P.; Ernzerhof, M.; Burke, K. *J. Chem. Phys.* **1996**, *105*, 9982–9985.
- [261] Adamo, C.; Barone, V. *J. Chem. Phys.* **1999**, *110*, 6158–6170.

- [262] Shao, Y.; Molnar, L. F.; Jung, Y.; Kussmann, J.; Ochsenfeld, C.; Brown, S. T.; Gilbert, A. T.; Slipchenko, L. V.; Levchenko, S. V.; O'Neill, D. P.; DiStasio Jr, R. A.; Lochan, R. C.; Wang, T.; Beran, G. J.; Besley, N. A.; Herbert, J. M.; Yeh Lin, C.; Van Voorhis, T.; Hung Chien, S.; Sodt, A.; Steele, R. P.; Rassolov, V. A.; Maslen, P. E.; Korambath, P. P.; Adamson, R. D.; Austin, B.; Baker, J.; Byrd, E. F. C.; Dachsel, H.; Doerksen, R. J.; Dreuw, A.; Dunietz, B. D.; Dutoi, A. D.; Furlani, T. R.; Gwaltney, S. R.; Heyden, A.; Hirata, S.; Hsu, C.-P.; Kedziora, G.; Khalliulin, R. Z.; Klunzinger, P.; Lee, A. M.; Lee, M. S.; Liang, W.; Lotan, I.; Nair, N.; Peters, B.; Proynov, E. I.; Pieniazek, P. A.; Min Rhee, Y.; Ritchie, J.; Rosta, E.; David Sherrill, C.; Simmonett, A. C.; Subotnik, J. E.; Lee Woodcock III, H.; Zhang, W.; Bell, A. T.; Chakraborty, A. K.; Chipman, D. M.; Keil, F. J.; Warshel, A.; Hehre, W. J.; Schaefer III, H. F.; Kong, J.; Krylov, A. I.; Gill, P. M. W.; Head-Gordon, M. *Phys. Chem. Chem. Phys.* **2006**, *8*, 3172–3191.
- [263] Krylov, A. I.; Gill, P. M. *WIREs Comput. Mol. Sci.* **2013**, *3*, 317–326.
- [264] Steinmann, S.; Wodrich, M.; Corminboeuf, C. *Theor. Chem. Acc.* **2010**, *127*, 429–442.
- [265] Becke, A. D. *J. Chem. Phys.* **1997**, *107*, 8554–8560.
- [266] Johnson, E. R.; Becke, A. D.; Sherrill, C. D.; DiLabio, G. A. *J. Chem. Phys.* **2009**, *131*, 03411–1.
- [267] Johnson, E. R.; Wolkow, R. A.; DiLabio, G. A. *Chem. Phys. Lett.* **2004**, *394*, 334–338.
- [268] Wheeler, S. E.; Houk, K. N. *J. Chem. Theory Comput.* **2010**, *6*, 395–404.
- [269] Lebedev, V. I.; Skorokhodov, L. *Russian Acad. Sci. Dokl. Math.* **1992**, *45*, 58–7.
- [270] Murray, C. W.; Handy, N. C.; Laming, G. J. *Mol. Phys.* **1993**, *78*, 997–1014.
- [271] Feyereisen, M.; Fitzgerald, G.; Komornicki, A. *Chem. Phys. Lett.* **1993**, *208*, 359–363.
- [272] Weigend, F.; Kohn, A.; Hattig, C. *J. Chem. Phys.* **2002**, *116*, 3175–3183.
- [273] Lebedev, V. I. *Zh. Vychisl. Mat. Mat. Fiz.* **1976**, *16*, 293–306.
- [274] Herbert, J. M.; Jacobson, L. D.; Un Lao, K.; Rohrdanz, M. A. *Phys. Chem. Chem. Phys.* **2012**, *14*, 7679–7699.
- [275] Chen, Z.; Wannere, C. S.; Corminboeuf, C.; Puchta, R.; Schleyer, P. v. R. *Chem. Rev.* **2005**, *105*, 3842–3888.
- [276] Cheeseman, J. R.; Trucks, G. W.; Keith, T. A.; Frisch, M. J. *J. Chem. Phys.* **1996**, *104*, 5497–5509.
- [277] Wolinski, K.; Hinton, J. F.; Pulay, P. *J. Am. Chem. Soc.* **1990**, *112*, 8251–8260.

Bibliography

- [278] Fallah-Bagher-Shaidaei, H.; Wannere, C. S.; Corminboeuf, C.; Puchta, R.; Schleyer, P. v. R. *Org. Lett.* **2006**, *8*, 863–866.
- [279] Kohout, M. *DGrid, version 4.6 Radebeul, 2011*.
- [280] Becke, A. D.; Edgecombe, K. E. *J. Chem. Phys.* **1990**, *92*, 5397–5403.
- [281] Sanders, J. M. *J. Phys. Chem. A* **2010**, *114*, 9205–9211.
- [282] Hunter, C. A.; Sanders, J. K. M. *J. Am. Chem. Soc.* **1990**, *112*, 5525–5534.
- [283] Rochat, S.; Steinmann, S. N.; Corminboeuf, C.; Severin, K. *Chem. Commun.* **2011**, *47*, 10584–10586.
- [284] Luisier, N.; Ruggi, A.; Steinmann, S. N.; Favre, L.; Gaeng, N.; Corminboeuf, C.; Severin, K. *Org. Biomol. Chem.* **2012**, *10*, 7487–7490.
- [285] Decreau, R. A.; Collman, J. P.; Hosseini, A. *Chem. Soc. Rev.* **2010**, *39*, 1291–1301.
- [286] Collman, J. P.; Fu, L.; Herrmann, P. C.; Zhang, X. *Science* **1997**, *275*, 949–951.
- [287] Collman, J. P.; Denisevich, P.; Konai, Y.; Marrocco, M.; Koval, C.; Anson, F. C. *J. Am. Chem. Soc.* **1980**, *102*, 6027–6036.
- [288] Collman, J. P.; Anson, F. C.; Barnes, C. E.; Bencosme, C. S.; Geiger, T.; Evitt, E. R.; Kreh, R. P.; Meier, K.; Pettman, R. B. *J. Am. Chem. Soc.* **1983**, *105*, 2694–2699.
- [289] Collman, J. P.; Hendricks, N. H.; Kim, K.; Bencosme, C. S. *J. Chem. Soc., Chem. Commun.* **1987**, 1537–1538.
- [290] Collman, J. P.; Hutchison, J. E.; Lopez, M. A.; Tabard, A.; Guillard, R.; Seok, W. K.; Ibers, J. A.; L’Her, M. *J. Am. Chem. Soc.* **1992**, *114*, 9869–9877.
- [291] Shi, C.; Steiger, B.; Yuasa, M.; Anson, F. C. *Inorg. Chem.* **1997**, *36*, 4294–4295.
- [292] Durand, R. R.; Bencosme, C. S.; Collman, J. P.; Anson, F. C. *J. Am. Chem. Soc.* **1983**, *105*, 2710–2718.
- [293] Ngameni, E.; Le Mest, Y.; L’Her, M.; Collman, J. P.; Hendricks, N. H.; Kim, K. *J. Electroanal. Chem. Interfacial Electrochem.* **1987**, *220*, 247–257.
- [294] Chang, C. J.; Loh, Z.-H.; Shi, C.; Anson, F. C.; Nocera, D. G. *J. Am. Chem. Soc.* **2004**, *126*, 10013–10020.
- [295] Guillard, R.; Brandes, S.; Tardieux, C.; Tabard, A.; L’Her, M.; Miry, C.; Gouerec, P.; Knop, Y.; Collman, J. P. *J. Am. Chem. Soc.* **1995**, *117*, 11721–11729.
- [296] McGuire Jr., R.; Dogutan, D. K.; Teets, T. S.; Suntivich, J.; Shao-Horn, Y.; Nocera, D. G. *Chem. Sci.* **2010**, *1*, 411–414.

- [297] Ndamani, J. C.; Bo, X.; Guo, L. *The Analyst* **2010**, *135*, 621–629.
- [298] Bigot, J.; Charleux, B.; Cooke, G.; Delattre, F.; Fournier, D.; Lyskawa, J.; Sambe, L.; Stoffelbach, F.; Woisel, P. *J. Am. Chem. Soc.* **2010**, *132*, 10796–10801.
- [299] Sun, W.; Xu, C.-H.; Zhu, Z.; Fang, C.-J.; Yan, C.-H. *J. Phys. Chem. C* **2008**, *112*, 16973–16983.
- [300] Halling, M. D.; Bell, J. D.; Pugmire, R. J.; Grant, D. M.; Miller, J. S. *J. Phys. Chem. A* **2010**, *114*, 6622–6629.
- [301] Guldi, D. M.; Sanchez, L.; Martin, N. *J. Phys. Chem. B* **2001**, *105*, 7139–7144.
- [302] Spruell, J. M.; Coskun, A.; Friedman, D. C.; Forgan, R. S.; Sarjeant, A. A.; Trabolsi, A.; Fahrenbach, A. C.; Barin, G.; Paxton, W. F.; Dey, S. K.; Olson, M. A.; Benitez, D.; Tkatchouk, E.; Colvin, M. T.; Carmielli, R.; Caldwell, S. T.; Rosair, G. M.; Hewage, S. G.; Duclairoir, F.; Seymour, J. L.; Slawin, A. M. Z.; Goddard, W. A.; Wasielewski, M. R.; Cooke, G.; Stoddart, J. F. *Nat. Chem.* **2010**, *2*, 870–879.
- [303] Wudl, F.; Smith, G. M.; Hufnagel, E. J. *J. Chem. Soc. D* **1970**, 1453–1454.
- [304] Ziganshina, A. Y.; Ko, Y. H.; Jeon, W. S.; Kim, K. *Chem. Commun.* **2004**, 806–807.
- [305] Woon, D. E.; Dunning, T. H., Jr. *J. Chem. Phys.* **1993**, *98*, 1358–1371.
- [306] Francel, M. M.; Pietro, W. J.; Hehre, W. J.; Binkley, J. S.; Gordon, M. S.; DeFrees, D. J.; Pople, J. A. *J. Chem. Phys.* **1982**, *77*, 3654–3665.
- [307] Frisch, M. J.; Trucks, G. W.; Schlegel, H. B.; Scuseria, G. E.; Robb, M. A.; Cheeseman, J. R.; Scalmani, G.; Barone, V.; Mennucci, B.; Petersson, G. A.; Nakatsuji, H.; Caricato, M.; Li, X.; Hratchian, H. P.; Izmaylov, A. F.; Bloino, J.; Zheng, G.; Sonnenberg, J. L.; Hada, M.; Ehara, M.; Toyota, K.; Fukuda, R.; Hasegawa, J.; Ishida, M.; Nakajima, T.; Honda, Y.; Kitao, O.; Nakai, H.; Vreven, T.; Montgomery, J. A., Jr.; Peralta, J. E.; Ogliaro, F.; Bearpark, M.; Heyd, J. J.; Brothers, E.; Kudin, K. N.; Staroverov, V. N.; Kobayashi, R.; Normand, J.; Raghavachari, K.; Rendell, A.; Burant, J. C.; Iyengar, S. S.; Tomasi, J.; Cossi, M.; Rega, N.; Millam, J. M.; Klene, M.; Knox, J. E.; Cross, J. B.; Bakken, V.; Adamo, C.; Jaramillo, J.; Gomperts, R.; Stratmann, R. E.; Yazyev, O.; Austin, A. J.; Cammi, R.; Pomelli, C.; Ochterski, J. W.; Martin, R. L.; Morokuma, K.; Zakrzewski, V. G.; Voth, G. A.; Salvador, P.; Dannenberg, J. J.; Dapprich, S.; Daniels, A. D.; Farkas, O.; Foresman, J. B.; Ortiz, J. V.; Cioslowski, J.; Fox, D. J. *Gaussian 09 Revision B.1.* Gaussian Inc. Wallingford CT 2009.
- [308] Marenich, A. V.; Olson, R. M.; Kelly, C. P.; Cramer, C. J.; Truhlar, D. G. *J. Chem. Theory Comput.* **2007**, *3*, 2011–2033.
- [309] Tomasi, J.; Mennucci, B.; Cammi, R. *Chem. Rev.* **2005**, *105*, 2999–3094.
- [310] Seeger, R.; Pople, J. A. *J. Chem. Phys.* **1977**, *66*, 3045–3050.

Bibliography

- [311] Bauernschmitt, R.; Ahlrichs, R. *J. Chem. Phys.* **1996**, *104*, 9047–9052.
- [312] Clark, T.; Chandrasekhar, J.; Spitznagel, G. W.; Schleyer, P. V. R. *J. Comput. Chem.* **1983**, *4*, 294–301.
- [313] McLean, A. D.; Chandler, G. S. *J. Chem. Phys.* **1980**, *72*, 5639–5648.
- [314] Hatay, I.; Su, B.; Li, F.; Mendez, M. A.; Khoury, T.; Gros, C. P.; Barbe, J.-M.; Ersoz, M.; Samec, Z.; Girault, H. H. *J. Am. Chem. Soc.* **2009**, *131*, 13453–13459.
- [315] Giffard, M.; Frere, P.; Gorgues, A.; Riou, A.; Roncali, J.; Toupet, L. *J. Chem. Soc., Chem. Commun.* **1993**, 944–945.
- [316] Allen, F. H. *Acta Crystallogr. Sect. B* **2002**, *58*, 380–388.
- [317] Kobayashi, Y.; Yoshioka, M.; Saigo, K.; Hashizume, D.; Ogura, T. *J. Am. Chem. Soc.* **2009**, *131*, 9995–10002.
- [318] Giffard, M.; Alonso, P.; Garin, J.; Gorgues, A.; Nguyen, T. P.; Richomme, P.; Robert, A.; Roncali, J.; Uriel, S. *Adv. Mater.* **1994**, *6*, 298–300.
- [319] Ziegler, T.; Krykunov, M.; Cullen, J. *J. Chem. Phys.* **2012**, *136*, 124107–10.

Glossary

ALMO Absolutely Localized Molecular Orbitals

AO-partitioning Partitioning of the electrons based on atomic orbitals, using delocalized orbitals in the wavefunction

BLW Block-Localized Wavefunction

BSE Bond Separation Energy

BSSE Basis Set Superposition Error

CECA Chemical Energy Component Analysis,¹¹⁰ one of Mayer's energy decomposition schemes. Projection operators are used to compress all three- and four-center integrals to two-center ones, and the kinetic energy is purely atomic.

CHA Chemical Hamiltonian Approach

CHA/CE Chemical Hamiltonian Approach with Conventional Energy, a method to perform BSSE-free intermolecular energy computations on supermolecular assemblies.

CHA-SCF Chemical Hamiltonian approach to optimize the orbitals self-consistently so that they are BSSE-free

CSD Cambridge Structural Database of molecular structures³¹⁶

counterpoise correction Application of the Boys and Bernardi method to correct for the BSSE.

DFT Density Functional Theory

E¹ One of Mayer's energy decomposition schemes, without a projection operator and with kinetic energy as a purely atomic quantity

Bibliography

E^{1'} An intermediate to the exact CECA energy decomposition analysis³⁵ used as a starting point for the zeroth-order energy in the present work

E² One of Mayer's energy decomposition schemes, similar to E¹ but with partitioning of the kinetic energy between atomic and interatomic terms

EDA Energy Decomposition Analysis

ELMO Extremely Localized Molecular Orbitals

exact CECA Exact version of CECA, where approximations associated with compression of all three- and four-center integrals to two-center ones are corrected.

FMO Fragment Molecular Orbital method¹⁵⁷

HF Hartree-Fock method

IQA Interacting Quantum Atoms method¹⁶²

KM Kitaura-Morokuma¹²⁸

LOL Localized Orbital Locator

LP-SCF MI Locally Projected Self-Consistent Field for Molecular Interactions

MO-partitioning Partitioning of the electrons using strictly localized molecular orbitals, constrained to be expressed only in the basis functions of one fragment

NBO Natural Bond Orbital¹⁴⁹

NLMO Natural Localized Molecular Orbitals¹⁴⁹

NOLMO Non-Orthogonal Localized Molecular Orbitals

SAPT Symmetry-Adapted Perturbation Theory

SE Schrödinger equation

SIHF Subspace-Isolated Hartree-Fock state, one of the electronic states intended to be used with SRW.

SLMO Strictly-Localized Molecular Orbitals

SLO Strictly Localized Orbital

SRW Space-Restricted Wavefunction^{174,175}

Supramolecular approach Computation of intermolecular interactions by subtracting total energies of isolated monomers from the total energy of the complex.

TB⁻ tetrakis(pentafluorophenyl)borate

TNT 2,4,6-trinitrotoluene

TTF Tetrathiafulvalene

Curriculum Vitae

Full name:	Jérôme Florian Gonthier	jerome.gonthier@epfl.ch
Date of birth:	14.03.1986	EPFL SB ISIC LCMD
Marital status:	Single	BCH 5119
Nationality:	French and Swiss	CH-1015 Lausanne
Languages:	French (mother tongue), English (fluent), German (basics)	Tel. +41 21 693 97 53

Education

2009-present : Ph.D. in Theoretical and Computational Chemistry in the Laboratory for Computational Molecular Design, EPFL, Lausanne (Switzerland)

- Advisor: Prof. Clémence Corminboeuf
- Main topic: *Modern computational approaches for quantifying inter- and intramolecular interactions.*

2007-2009 : M.Sc. in Chemistry, EPFL, Lausanne (Switzerland)

- Orientation : Theoretical and Computational Chemistry
- Master Thesis conducted abroad, under the supervision of Prof. Walter Thiel: *Solvation effect on the asymmetric hydrogenation of itaconic acid dimethyl ester catalysed by $[Rh(P(O^iPr)(R-BINOL))_2cod]BF_4$* , Max Planck Institut für Kohlenforschung, Mühleim an der Ruhr, Germany

2004-2007 : B.Sc. in Chemistry and Chemical Engineering, EPFL, Lausanne (Switzerland)

Awards

2013 : Best oral presentation, *General Assembly of the Swiss Chemical Society*, SCS Fall Meeting (September 9th 2013)

2012 : SCNAT/SCS Chemistry travel award from the Swiss Academy of Sciences and the Swiss Chemical Society

Publications

1. Matthew D. Wodrich, Jérôme F. Gonthier, Nicolai Cramer, Clémence Corminboeuf, "Distinguishing Reaction Mechanism Pathways: Beyond Energy Profiles", in preparation.
2. Matthew D. Wodrich, Jérôme F. Gonthier, Clémence Corminboeuf, Steven E. Wheeler, "Reply to Comment on Accurate Thermochemistry of Hydrocarbon Radicals via an Extended Generalized Bond Separation Reaction Scheme", *J. Phys. Chem. A*, **2012**, *116*, 8794
3. Jérôme F. Gonthier, Stephan N. Steinmann, Loïc Roch, Albert Ruggi, Nicolas Luisier, Kay Severin, Clémence Corminboeuf, " π -Depletion as a criterion to predict π -stacking ability", *Chem. Commun.*, **2012**, *48*, 9239
4. Jérôme F. Gonthier, Stephan N. Steinmann, Matthew D. Wodrich, Clémence Corminboeuf, "Quantification of Chemical Concepts: A Computational Perspective", *Chem. Soc. Rev.*, **2012**, *41*, 4671
5. Astrid J. Olaya, Peiyu Ge, Jérôme F. Gonthier, Peter Pechy, Clémence Corminboeuf, Hubert H. Girault, "Four-Electron Oxygen Reduction by Tetrathiafulvalene", *J. Am. Chem. Soc.*, **2011**, *133*, 12115
6. Matthew D. Wodrich, Jérôme F. Gonthier, Stephan N. Steinmann, Clémence Corminboeuf, "How Strained are Carbomeric-Cycloalkanes?", *J. Phys. Chem. A*, **2010**, *114*, 6705
7. Jérôme F. Gonthier, Matthew D. Wodrich, Stephan N. Steinmann, Clémence Corminboeuf, "Branched Alkanes Have Contrasting Stabilities", *Org. Lett.*, **2010**, *12*, 3070

Books

- Basile Curchod, Jérôme Gonthier, Pascal Miéville, Julie Risse, "Introduction à la Chimie", 2012, Editions LEP, Lausanne: General chemistry book for last year of high school and first year university for non-chemists.

Contributed Talks

- SCS Fall Meeting, *General Assembly of the Swiss Chemical Society*, September 9th 2013, Lausanne, Switzerland
Application of the Chemical Hamiltonian to Zeroth-order Wavefunction and Energy for Intramolecular Symmetry-Adapted Perturbation Theory, Jérôme F. Gonthier

Bibliography

- SCS Fall Meeting, *General Assembly of the Swiss Chemical Society*, September 13th 2012, Zürich, Switzerland

Intramolecular Symmetry-Adapted Perturbation Theory, Jérôme F. Gonthier

Poster Presentations

- 7th *Molecular Quantum Mechanics – Electron Correlation: The Many-Body Problem at the Heart of Chemistry*, June 2nd-7th 2013, Lugano, Switzerland
Exploration of Zeroth-order Wavefunction and Energy for Intramolecular Symmetry-Adapted Perturbation Theory, Jérôme F. Gonthier, Clémence Corminboeuf
- *International Congress of Quantum Chemistry*, June 25th-30th 2012, Boulder (CO), USA
Intramolecular Symmetry-Adapted Perturbation Theory, Jérôme F. Gonthier, Clémence Corminboeuf
- *General Assembly of the Swiss Association of Computational Chemists*, February 15th 2012, Bern
Four-electron Reduction of O₂ by Tetrathiafulvalene, Jérôme F. Gonthier, Clémence Corminboeuf
- SCS Fall Meeting, *General Assembly of the Swiss Chemical Society*, September 2011, Lausanne, Switzerland
Four-electron Reduction of O₂ by Tetrathiafulvalene, Jérôme F. Gonthier, Clémence Corminboeuf
- ESQC11, *European Summer School in Quantum Chemistry 2011*, September 2011, Torre Normanna, Italy
Four-electron Reduction of O₂ by Tetrathiafulvalene, Jérôme F. Gonthier, Clémence Corminboeuf
- CUSO 2011 Summer School, August 2011, Villars-sur-Ollon, Switzerland
Four-electron Reduction of O₂ by Tetrathiafulvalene, Jérôme F. Gonthier, Clémence Corminboeuf
- WATOC 2011, *Ninth triennial congress of the World Association of Theoretical and Computational Chemists*, July 2011, Santiago de Compostela, Spain
Four-electron Reduction of O₂ by Tetrathiafulvalene, Jérôme F. Gonthier, Clémence Corminboeuf

- SCS Fall Meeting 2010, *General Assembly of the Swiss Chemical Society*, September 16 2010, Zürich, Switzerland
Predicting heats of formation of highly branched alkanes, Jérôme Gonthier, Stephan Steinmann, Matthew D. Wodrich, Clémence Corminboeuf
- STC 2010, *46th Symposium on Theoretical Chemistry*, September 26-30 2010, Münster, Germany
Branched alkanes have contrasting stabilities, Jérôme F. Gonthier, Matthew D. Wodrich, Stephan N. Steinmann, Clémence Corminboeuf
- ESPA 2010, *Electronic Structure: Principles and Applications*, June 29 - July 2 2010, Oviedo, Spain
Branched alkanes have contrasting stabilities, Jérôme F. Gonthier, Matthew D. Wodrich, Stephan N. Steinmann, Clémence Corminboeuf
- TCC symposium, *International Symposium on Theoretical and Computational Chemistry*, February 28 - March 2 2010, Max Planck Institut für Kohlenforschung, Mühleim an der Ruhr, Germany
Predicting heats of formation of highly branched alkanes, Jérôme Gonthier, Stephan Steinmann, Matthew D. Wodrich, Clémence Corminboeuf

Computer skills

- *Programming and scripting languages*: Fortran 77, Fortran 90, C, Bash, sed, awk, notions of C-shell and Python
- *Scientific software use*: GAMESS, Gaussian, Molpro, Cfour, Psi4, ADF, Q-Chem, CPMD, Maple

Hobbies

- Son Long Quyen Thuat (vietnamese martial art)
- Listening to music